Physics of the Earth and Planetary Interiors

3D Deep Geoelectrical Exploration in the Larderello geothermal sites (Italy)

--Manuscript Draft--

Manuscript Number:	PEPI-D-21-00131R1
Article Type:	Research Paper
Keywords:	Deep Electrical Resistivity Tomography; electrical resistivity; surface-hole acquisition; geothermal site
Corresponding Author:	Enzo Rizzo Universita degli Studi di Ferrara Dipartimento di Fisica e Scienze della Terra Ferrara, Emilia-Romagna ITALY
First Author:	Enzo Rizzo
Order of Authors:	Enzo Rizzo
	Valeria Giampaolo, PhD
	Luigi Capozzoli, PhD
	Gregory De Martino
	Gerardo Romano
	Alessandro Santilano
	Adele Manzella
Abstract:	The paper describes a new experimental deep electrical resistivity acquisition (down to 1600 m) for exploring deep and shallow geothermal systems. The test site is located in the Larderello geothermal area, the oldest geothermal field in the world under exploitation for power production. In this area, many data have been acquired in the frame of previous exploration projects but nowadays several critical issues are still matter of debate: permeability distribution, depth and volume of the magmatic heat source, supercritical fluid condition at depth, and the occurrence of low resistivity anomalies in a dry-steam crystalline and carbonate reservoir. In order to develop new methods for contributing to the hydrothermal reservoir issues, an experimental high resolution 3D Surface-Hole Deep Electrical Resistivity Tomography (SH-DERT) was designed and the Venelle2 well in the Larderello geothermal site, hosted in the crystalline units, was used for the experiment. The design of the in-hole experiment and the results of the deep geoelectrical survey are hereby presented. SH-DERT was properly designed to face extreme conditions at depth characterizing the geothermal well. It provided a 3D resistivity distribution. Transmitting and receiving electrodes were distributed on a large surface (6 km 2) and in the Venelle2 well (down to 1600 m). The in-hole electrical cable was equipped to be able to operate in very high temperature conditions. The experiment represents a challenge and an opportunity for the applied geophysics in geothermal areas, where a lowest resistivity is highlighted in a zone above the reservoir and the resistivity of the reservoir is higher. Moreover, the relationship between temperature, clay alteration and resistivity can define a challenger to enable better prediction of reservoir temperature distribution from resistivity measurements. It is a potential improvement of the reservoir knowledge and a useful success for exploration drilling.
Suggested Reviewers:	Pantelis Soupios, PhD Professor, King Fahd University of Petroleum & Minerals panteleimon.soupios@kfupm.edu.sa
	Aaron Micallef Professor, University of Malta aaron.micallef@um.edu.mt
	Alexis Maineult, PhD Chargé de recherche, Université Pierre et Marie Curie: Sorbonne Universite alexis.maineult@upmc.fr
	Mohamed Mahmoud Gomaa

	Professor, National Research Centre mmmsgomaa@yahoo.com
	Konstantin Titov Dr. Sc., Prof., Saint Petersburg State University Institute of Earth Sciences: Sankt-Peterburgskij gosudarstvennyj universitet Institut nauk o Zemle k.titov@spbu.ru

Response to Reviewers:

Dear Editor,

Thank you for giving us the opportunity to submit a revised draft of our manuscript titled “3D Deep Geoelectrical Exploration in the Larderello geothermal sites (Italy)” to Physics of the Earth and Planetary Interiors journal (Manuscript Number: PEPI-D-21-00131). We appreciate the time and effort that the reviewers have dedicated to providing us valuable feedback on our manuscript.
In the revised manuscript, we were able to incorporate changes to reflect most of the suggestions provided by the reviewers. We have highlighted in red the changes within the manuscript. Moreover, a point-by-point response to the reviewers’ comments and concerns has been submitted.

Best Regards
Enzo Rizzo
Corresponding author

Reviewer #1:
Summary
Authors: Dear Reviewer n.1, we thank you very much for taking the time to assess our manuscript, for your positive feedback and the very useful comments. We have completed our revision, considering all your comments and suggestions, which improved the paper. All changes in the text were marked in red.

General comments
I would recommend to avoid the two many "deep" and shallow" terms given without any number.
Authors: We have revised the text and add a quantitative meaning to "deep" and shallow" terms.

Some short discussion on your objectives is missing. As stated in the manuscript, the Larderello geothermal system has been studied for many years. A lot of geophysical studies have been carried out and published. Could you comment more on the limitation of other geophysical techniques in this environment (MT, CSEM, ..)?
Authors: We expanded the Introduction section by adding a paragraph on the limitation of geophysical techniques in high enthalpy geothermal systems.

I suggest to comment on your perspectives. Can this methodology be applied to other geothermal systems than Larderello, in particular more conventional ones? Can it be used for monitoring?
Authors: Agree. We have revised the Conclusion section to emphasize this point.

For a better understanding of your results, I would suggest to integrate more clearly your different data sets. For example resistivity profiles could be extracted from the 3D resistivity model and compared with temperature profiles (Figure 11) on a same Figure. This would allow a more quantitative interpretation of the results in terms of physical properties, which would fit better with PEPI scopes.
Authors: Thank you for this suggestion. In general, the measured temperature values show a regular increase in depth and some correlation with the electrical resistivity should be observed. Moeover, there is a good correlation between porosity and electrical resistivity along uncasing Venelle2 well portion. Therefore, we improved the manuscript with the new figure n.12 where we compared the resistivity results with the geological information. Moreover, in the same figure we compare the resistivity sections with the temperature and porosity data set. The figure 13 highlights the comparison between the resistivity values and the available well temperature data set, introducing the correlation between the temperature and electrical resistivity.

Some Figures could be improved. The scale is absent or difficult to read in Figures 7-9

and 12.
Authors: As suggested by the reviewer, we have improved all the figures.

What are the red dots on Figure 12?
Authors: Red dots are surface and borehole electrodes in 3D visualization. Figure 12 caption has been updated.

The location of the new 3D deep electrical resistivity model could be shown on Figure 13 for better comparison.
Authors: As suggested by the reviewer, we added the location of the new 3D deep electrical resistivity survey. The Figure 13 is now figure 14 and the captions were updated.

Reviewer #2:

Summary
Authors: Dear Reviewer n.2, we thank you very much for your review and we appreciated your work a lot. We have completed our revision, considering all your comments and suggestions, which improved the paper. All changes in the text were marked in red.

General comments
1. Borehole fluid effects: If I understand correctly, the customized cable with electrode outlets was lowered below the metal casing and was operating in the uncased (open hole) section of the Vanelle2 borehole. To guarantee electrical coupling to the rock formation (and decrease the temperature), a fluid of known electrical conductivity was injected in the borehole. It is well known that conductive borehole fluids can affect ERT images, as they provide a strong electrical contrast close to the electrodes and can result in direct electrical connections between electrodes. In this case, the fluid may also represent an electrical connection to the metal casing. The potentially significant effect of the borehole fluid and potential mitigation techniques (e.g., by incorporating the borehole fluid of known conductivity in the inversion) should be discussed within the paper. Relevant previous work was conducted by Doetsch et al. (2010), who investigate the borehole-fluid effect for different electrode configurations and resistivity contrasts and Wagner et al. (2015), who discuss the effect of borehole filling, electrode shape/size and borehole deviation on ERT monitoring of a CO_2 storage reservoir for example.
Authors: You have highlighted an important point here. According to Doetsch et al. (2010), current channeling phenomena can be favored when the well annulus is filled with highly conductive fluids (resistivity contrasts of 100:1) and borehole diameters of 10 and 20 cm yielded, for a bipole length of 5 m.
In our case, as confirmed by MT, the resistivity contrast between geological formations and injected fluids (1.17 Ωm) is maximum 50:1 while the well diameter is in the range between 30 – 60 cm for a bipole length of 50 m in the borehole and 400 m at surface. For these reasons, we believe that in our case both the borehole - fluid effects can be neglected.
Moreover, considering the small size of well and electrodes respect the mesh elements, it would be anyway computationally prohibitive in our case to use very fine grids to account well filling, electrode shape/size and borehole deviation into the 3D mesh.
Finally, we tried to take in account your consideration in our inversion approach, but the final results highlighted strong artifacts.

2. Synthetic studies: The authors mention spatial resolution and appropriate electrode spacing several times. I was wondering if any synthetic studies were carried out prior to the field experiment to estimate spatial resolution and to find optimum electrode spacings and surface positions beforehand? A synthetic study showing inversion results for the existing geological model would give some insight on what to expect from surface-downhole acquisition in comparison to surface acquisition only.

Authors: Thank you for pointing this out. The first step was the site inspection. We individuated 33 current injection point surrounding the Venelle2 well. They were chosen considering the ease of reaching the place with the geophysical equipment and the absence of any natural and anthropic limits for power cables roll out. Moreover, the Venelle2 well characteristics constrain electrodes array length in the borehole (accessible down to 1.6 km, metallic casing down to 1 km).
Following, taking into account the established surface and borehole electrodes positions, a modelling work phase was performed in order to individuate the best surface and borehole electrical dipoles arrangement and therefore optimize both the geophysical data acquisition time (respecting ENEL directives) and the geophysical result (confidential deliverable of IMAGE fp7 project).
In order to find the best electrodes configuration to replicate at site during the data acquisition phase, a possible scenario was taken into account considering the electrical resistivity distribution at the site, of the first 4 km, coming from previous MT inversion models integrated with geological information.

3. Data processing: While the processing of the acquired time-series is well discussed, the authors assume a 5% error for all data points during the inversion after apparent resistivities have been computed. This estimate seems rather optimistic (also reflected in the higher RMS errors after inversion) and I suspect that the situation will be different for surface and surface-borehole configurations. Were reciprocal measurements acquired? If not, have the authors considered an error estimate depending on the geometric factors?
Authors: Thank you for this question. The reduction in geometric factors increases the probability for better SN levels in measured resistivities. Therefore, following the modeling phase we discharge all quadrupoles with a geometric factor > 1000. However, given the logistic limitations in survey time and electrical current flow through the long borehole cables, it was not possible to realize reciprocal measurements for this experiment.
Due to a general lack of reciprocal measurements in both survey setups (S-DERT and SH-DERT), data were filtered on the basis of the Fourier analysis results.
The choose of 5% data error was a compromise between data error, final RMS e smoothness of the final model. Probably, because of small resistivity contrasts and generally low resistivity values, 3D electrical resistivity tomography inversions using a greater error value (10%) leaded to very smooth results.

4. Comparison to MT Studies: Towards the end, the authors discuss the deep ERT technology in comparison to magnetotelluric studies, which are more common in geothermal exploration and monitoring. Has this comparison been attempted at a quantitative level, e.g. plotting resistivities of both methods at the same location as a function of depth? The ERT results range between 1 and 50 Ohm meters, while the upper colorbar limit of the MT results goes up to 6000 Ohm meters. How can this quantitative agreement be explained? I think this needs to be addressed within the paper.
Authors: You pointed analysis needs some comments. The DERT and MT approach have very different investigation depths and resolutions. The MT results reached high resistive values, generally a depth greater than DERT investigated area. If we give a look on the 2D MT sections, we can observe at the first 2000m resistivity values < 100Ohm*m, that could be associated with the resistivity values indicated in our work (<90 Ohm*m). However, in order to emphasize the point raised by the reviewer, we add the location of the new 3D deep electrical resistivity model on Figure 13 (above the map and MT profiles) for a better comparison between MT and DERT results.

5. Visualization: Many figures have missing, incomplete or overlapping labels and low resolution and should be improved.
Authors: We tried to improve all the figures

6. Linguistic shortcomings: The wording is sometimes a bit confusing (see line-specific comments below) and there are many typos, missing punctuation and several inconsistencies (e.g., British vs. American English). I strongly recommend to carefully proofread the revised manuscript and, if possible, consult native-speaking colleague

	proof reading service. Authors: Spelling and grammatical errors pointed out by the reviewer have been corrected. Moreover, we asked to native-speaking friend to improve our text. Line-specific comments Authors: We rewrote all the indicated highlights, and we thank you for the specific suggestions to help us to improve the manuscript. Therefore, all suggestions have been taken into consideration and all spelling and grammatical errors pointed out by the reviewer have been corrected. References Authors: The indicated works are added into the text and the references were updated.

Università degli Studi di Ferrara
Dipartimento di Fisica e Scienze della Terra

Università degli Studi di Ferrara
Dipartimento di Fisica e Scienze della Terra
Via Saragat 1 • 44122 Ferrara
dip.fisicascienzeterra@unife.it
tel. 0532 0532 97 4728 •
fst.unife.it

January 30, 2022

To: Editors of Journal
Physics of the Earth and Planetary Interiors

Dear Editor,

Thank you for giving us the opportunity to submit a revised draft of our manuscript titled "3D Deep Geoelectrical Exploration in the Larderello geothermal sites (Italy)" to Physics of the Earth and Planetary Interiors journal (Manuscript Number: PEPI-D-21-00131). We appreciate the time and effort that the reviewers have dedicated to providing us valuable feedback on our manuscript.

In the revised manuscript, we were able to incorporate changes to reflect most of the suggestions provided by the reviewers. We have highlighted in red the changes within the manuscript. Moreover, a point-by-point response to the reviewers' comments and concerns has been submitted.

Best Regards
Enzo Rizzo
Corresponding author

Prof. Enzo Rizzo
Professore Associato
Università di Ferrara
Dipartimento di Fisica e
Scienze della Terra
Polo Tecnologico
Via Saragat, 1
44122 Ferrara

Detailed Response to Reviewers

Reviewer #1:

Summary

Authors: *Dear Reviewer n.1, we thank you very much for taking the time to assess our manuscript, for your positive feedback and the very useful comments. We have completed our revision, considering all your comments and suggestions, which improved the paper. All changes in the text were marked in red.*

General comments

I would recommend to avoid the two many "deep" and shallow" terms given without any number.

Authors: *We have revised the text and add a quantitative meaning to "deep" and shallow" terms.*

Some short discussion on your objectives is missing. As stated in the manuscript, the Larderello geothermal system has been studied for many years. A lot of geophysical studies have been carried out and published. Could you comment more on the limitation of other geophysical techniques in this environment (MT, CSEM, ..)?

Authors: *We expanded the Introduction section by adding a paragraph on the limitation of geophysical techniques in high enthalpy geothermal systems.*

I suggest to comment on your perspectives. Can this methodology be applied to other geothermal systems than Larderello, in particular more conventional ones? Can it be used for monitoring?

Authors: *Agree. We have revised the Conclusion section to emphasize this point.*

For a better understanding of your results, I would suggest to integrate more clearly your different data sets. For example resistivity profiles could be extracted from the 3D resistivity model and compared with temperature profiles (Figure 11) on a same Figure. This would allow a more quantitative interpretation of the results in terms of physical properties, which would fit better with PEPI scopes.

Authors: *Thank you for this suggestion. In general, the measured temperature values show a regular increase in depth and some correlation with the electrical resistivity should be observed. Moeover, there is a good correlation between porosity and electrical resistivity along uncasing Venelle2 well portion. Therefore, we improved the manuscript with the new figure n.12 where we compared the resistivity results with the geological information. Moreover, in the same figure we compare the resistivity sections with the temperature and porosity data set. The figure 13 highlights the comparison between the resistivity values and the available well temperature data set, introducing the correlation between the temperature and electrical resistivity.*

Some Figures could be improved. The scale is absent or difficult to read in Figures 7-9 and 12.

Authors*: As suggested by the reviewer, we have improved all the figures.*

What are the red dots on Figure 12?

Authors*: Red dots are surface and borehole electrodes in 3D visualization. Figure 12 caption has been updated.*

The location of the new 3D deep electrical resistivity model could be shown on Figure 13 for better comparison.

Authors*: As suggested by the reviewer, we added the location of the new 3D deep electrical resistivity survey. The Figure 13 is now figure 14 and the captions were updated.*

Reviewer #2:

Summary

Authors: *Dear Reviewer n.2, we thank you very much for your review and we appreciated your work a lot. We have completed our revision, considering all your comments and suggestions, which improved the paper. All changes in the text were marked in red.*

General comments

1. Borehole fluid effects: If I understand correctly, the customized cable with electrode outlets was lowered below the metal casing and was operating in the uncased (open hole) section of the Vanelle2 borehole. To guarantee electrical coupling to the rock formation (and decrease the temperature), a fluid of known electrical conductivity was injected in the borehole. It is well known that conductive borehole fluids can affect ERT images, as they provide a strong electrical contrast close to the electrodes and can result in direct electrical connections between electrodes. In this case, the fluid may also represent an electrical connection to the metal casing. The potentially significant effect of the borehole fluid and potential mitigation techniques (e.g., by incorporating the borehole fluid of known conductivity in the inversion) should be discussed within the paper. Relevant previous work was conducted by Doetsch et al. (2010), who investigate the borehole-fluid effect for different electrode configurations and resistivity contrasts and Wagner et al. (2015), who discuss the effect of borehole filling, electrode shape/size and borehole deviation on ERT monitoring of a CO2 storage reservoir for example.

Authors: *You have highlighted an important point here. According to Doetsch et al. (2010), current channeling phenomena can be favored when the well annulus is filled with highly conductive fluids (resistivity contrasts of 100:1) and borehole diameters of 10 and 20 cm yielded, for a bipole length of 5 m.*

In our case, as confirmed by MT, the resistivity contrast between geological formations and injected fluids (1.17 Ωm) is maximum 50:1 while the well diameter is in the range between 30 – 60 cm for a bipole length of 50 m in the borehole and 400 m at surface. For these reasons, we believe that in our case both the borehole - fluid effects can be neglected.

Moreover, considering the small size of well and electrodes respect the mesh elements, it would be anyway computationally prohibitive in our case to use very fine grids to account well filling, electrode shape/size and borehole deviation into the 3D mesh.

Finally, we tried to take in account your consideration in our inversion approach, but the final results highlighted strong artifacts.

2. Synthetic studies: The authors mention spatial resolution and appropriate electrode spacing several times. I was wondering if any synthetic studies were carried out prior to the field experiment to estimate spatial resolution and to find optimum electrode spacings and surface positions beforehand? A synthetic study showing inversion results for the existing geological model would give some insight on what to expect from surface-downhole acquisition in comparison to surface acquisition only.

Authors: *Thank you for pointing this out. The first step was the site inspection. We individuated 33 current injection point surrounding the Venelle2 well. They were chosen considering the ease of reaching the place with the geophysical equipment and the absence of any natural and anthropic limits for power cables roll out. Moreover, the Venelle2 well characteristics constrain electrodes array length in the borehole (accessible down to 1.6 km, metallic casing down to 1 km).*

Following, taking into account the established surface and borehole electrodes positions, a modelling work phase was performed in order to individuate the best surface and borehole electrical dipoles arrangement and therefore optimize both the geophysical data acquisition time (respecting ENEL directives) and the geophysical result (confidential deliverable of IMAGE fp7 project).

In order to find the best electrodes configuration to replicate at site during the data acquisition phase, a possible scenario was taken into account considering the electrical resistivity distribution at the site, of the first 4 km, coming from previous MT inversion models integrated with geological information.

3. Data processing: While the processing of the acquired time-series is well discussed, the authors assume a 5% error for all data points during the inversion after apparent resistivities have been computed. This estimate seems rather optimistic (also reflected in the higher RMS errors after inversion) and I suspect that the situation will be different for surface and surface-borehole configurations. Were reciprocal measurements acquired? If not, have the authors considered an error estimate depending on the geometric factors?

Authors: *Thank you for this question. The reduction in geometric factors increases the probability for better SN levels in measured resistivities. Therefore, following the modeling phase we discharge all quadrupoles with a geometric factor > 1000.*

However, given the logistic limitations in survey time and electrical current flow through the long borehole cables, it was not possible to realize reciprocal measurements for this experiment.

Due to a general lack of reciprocal measurements in both survey setups (S-DERT and SH-DERT), data were filtered on the basis of the Fourier analysis results.

The choose of 5% data error was a compromise between data error, final RMS e smoothness of the final model. Probably, because of small resistivity contrasts and generally low resistivity values, 3D electrical resistivity tomography inversions using a greater error value (10%) leaded to very smooth results.

4. Comparison to MT Studies: Towards the end, the authors discuss the deep ERT technology in comparison to magnetotelluric studies, which are more common in geothermal exploration and monitoring. Has this comparison been attempted at a quantitative level, e.g. plotting resistivities of both methods at the same location as a function of depth? The ERT results range between 1 and 50 Ohm meters, while the upper colorbar limit of the MT results goes up to 6000 Ohm meters. How can this quantitative agreement be explained? I think this needs to be addressed within the paper.

Authors: *You pointed analysis needs some comments. The DERT and MT approach have very different investigation depths and resolutions. The MT results reached high resistive values, generally a depth greater than DERT investigated area. If we give a look on the 2D MT sections, we can observe at the first 2000m resistivity values < 100Ohm*m, that could be associated with the resistivity values indicated in our work (<90 Ohm*m). However, in order to emphasize the point raised by the reviewer, we add the location of the new 3D deep electrical resistivity model on Figure 13 (above the map and MT profiles) for a better comparison between MT and DERT results.*

5. Visualization: Many figures have missing, incomplete or overlapping labels and low resolution and should be improved.

Authors: *We tried to improve all the figures*

6. Linguistic shortcomings: The wording is sometimes a bit confusing (see line-specific comments below) and there are many typos, missing punctuation and several inconsistencies (e.g., British vs. American English). I strongly recommend to carefully proofread the revised manuscript and, if possible, consult native-speaking colleague proof reading service.

Authors: *Spelling and grammatical errors pointed out by the reviewer have been corrected. Moreover, we asked to native-speaking friend to improve our text.*

Line-specific comments

Authors: *We rewrote all the indicated highlights, and we thank you for the specific suggestions to help us to improve the manuscript. Therefore, all suggestions have been taken into consideration and all spelling and grammatical errors pointed out by the reviewer have been corrected.*

References

Authors: *The indicated works are added into the text and the references were updated.*

3D Deep Geoelectrical Exploration in the Larderello geothermal sites (Italy)

E. Rizzo[1,2,*], V. Giampaolo[2], L. Capozzoli[2], G. De Martino[2], G. Romano[3], A. Santilano[4], A. Manzella[4]

[1] University of Ferrara, Department of Physics and Earth Science, via Saragat,1 44122 Ferrara
[2] National Research Council, Institute of Methodologies for Environmental Analysis, Hydrogeosite Laboratory, c.da S. Loja Tito Scalo (PZ)
[4] University of Bari, Department of Earth Science and Environment
[4] National Research Council, Institute of Geosciences and Earth Resources, Via G. Moruzzi 1 56124 - Pisa

Corresponding author: enzo.rizzo@unife.it

Abstract

The paper describes a new experimental deep electrical resistivity acquisition (down to 1600 m) for exploring deep and shallow geothermal systems. The test site is located in the Larderello geothermal area, the oldest geothermal field in the world under exploitation for power production. In this area, many data have been acquired in the frame of previous exploration projects but nowadays several critical issues are still matter of debate: permeability distribution, depth and volume of the magmatic heat source, supercritical fluid condition at depth, and the occurrence of low resistivity anomalies in a dry-steam crystalline and carbonate reservoir. In order to develop new methods for contributing to the hydrothermal reservoir issues, an experimental high resolution 3D Surface-Hole Deep Electrical Resistivity Tomography (SH-DERT) was designed and the Venelle2 well in the Larderello geothermal site, hosted in the crystalline units, was used for the experiment. The design of the in-hole experiment and the results of the deep geoelectrical survey are hereby presented. SH-DERT was properly designed to face extreme conditions at depth characterizing the geothermal well. It provided a 3D resistivity distribution. Transmitting and receiving electrodes were distributed on a large surface (6 km^2) and in the Venelle2 well (down to 1600 m). The in-hole electrical cable was equipped to be able to operate in very high temperature conditions. The experiment represents a challenge and an opportunity for the applied geophysics in geothermal areas, where a lowest resistivity is highlighted in a zone above the reservoir and the resistivity of the reservoir is higher. Moreover, the relationship between temperature, clay alteration and resistivity can define a challenger to enable better prediction

of reservoir temperature distribution from resistivity measurements. It is a potential improvement of the reservoir knowledge and a useful success for exploration drilling.

Keywords: Deep Electrical Resistivity Tomography, electrical resistivity, surface-hole acquisition, geothermal site.

1. Introduction

In the Larderello geothermal system (Italy), the oldest field in the world under exploitation for power production, a vapor-dominated system with temperatures exceeding 350°C is exploited from two different reservoirs. The field is covered by a large quantity of data such as well stratigraphy, geological-structural studies, and geophysical data (e.g., magnetotelluric, active and passive seismic, thermal and gravity interpretative models). This huge amount of information allows to constrain the structure of Larderello geothermal system down to about 5 km of depth (Fiordelisi et al., 1998, Manzella, 2004; Orlando, 2005; Brogi et al., 2005; De Matteis et al., 2008; Romagnoli et al., 2010; Saccorotti et al., 2014; Gola et al., 2017; Liotta and Brogi, 2020). However, several critical issues on deep features of the field (> 5 km depth) are still matter of debate, e.g., permeability distribution in the hydrothermal reservoir, the presence of fluids at supercritical condition and the depth, and volume of the magmatic heat source. The main critical issue, that we aim to account for, is the occurrence of low resistivity anomalies in a dry-steam crystalline and carbonate reservoir (theoretically highly resistive). In detail, it must be established if the reduction in electrical resistivity in the Larderello geothermal system is linked with lithology, alteration mineralogy or occurrence of water in liquid phase (even reinjected) in pore and fractures.

Geophysical methods used for studying high-enthalpy geothermal systems (T > 250 °C) are selected according to the type and depth of the target and available budget (Kana et al., 2015). In general, active seismic and gravity are widely used (Majer, 2003; Guglielmetti et al. 2013; Altwegg et al., 2015; Schmelzbach et al., 2016; Witter et al., 2016; Kastner et al., 2020) however they are expensive and do not provide any information about the fluid distribution in the geothermal reservoir. The electrical resistivity (or conductivity) methods are the best prospecting tools for geothermal reservoirs. This is because of the high dependence of the electrical conductivity on physical parameters like temperature, porosity, pore fluid salinity, fluid saturation and the degree of interface conductivity (Flovenz et al., 2005 and 2012). Airborne and land-based electromagnetic (EM) methods, such as controlled-source electromagnetic (CSEM), magnetotelluric (MT), time domain electromagnetic (TDEM), are useful methods for geothermal resources (Demissie, Y., 2005; Santilano et al., 2015c; Spichak and Mazzella, 2009; Darnet et al., 2020a,b). Even if the EM methods are useful for deep target, they can be very challenging in noisy environment, such as urban and industrial area. Moreover, these methods suffer from the lack of spatial resolution mostly in the first 1-2 km of depth (Tietze et al., 2015, 2017; Irons et al., 2018). In the Larderello geothermal system, since the early '90s, several MT studies highlighted a strong heterogeneous distribution of the electrical resistivity values coupled with a large electromagnetic noise. Moreover, even if the MT method has been among the main geothermal exploration tools at the site, its resolution capacity was considered questionable. In fact, MT data quality could not exclude a bias or a noise effect, and sometimes, the misinterpretations of electrical resistivity models can lead to errors in the geothermal exploration phase (Muñoz, 2014). The electrical resistivity tomography (ERT) is largely applied in shallow investigations (< 200 m depth) to solve environmental, engineering, and geological problems (Kosinski and Kelly, 1981; Griffiths and Barker, 1993; Dahlin, 1996; Dam and Christensen, 2003; Darnet et al., 2003; Binley and Kemna, 2005). In recent years, there has been growing interest in developing cross-hole and surface-hole DC electrical surveying to image the 2D and 3D structure of the earth. Borehole geophysics uses boreholes or wells to make geophysical measurements and, compared to geophysical measurements made on the ground surface, they achieve a higher resolution at depth. For this reason, it is very commonly used in shallow environmental and hydrogeological application (< 100 m depth) as a monitoring tool (Daily et al., 1992; Slater et al., 1997; Daily and Ramirez, 2000; Binley et al., 2002; Slater and Binley, 2003; Goes and Meekes, 2004; LaBreque et al., 2004; Wilkinson et al., 2006; Chambers et al. 2007; Irving and Singha, 2010; Hermans et al., 2015; Thompson et al., 2017; Cheng et al., 2019; Palacios et al., 2020).

Moreover, improvements in field technology and data processing allow electrical resistivity method to be applied in deep investigations (down to 4 km depth) for studying geological structures (Storz et al., 2000; Suzuki et al., 2000; Rizzo et al., 2004; Giocoli et al., 2008; Balasco et al., 2011; Pucci et al., 2016; Rizzo and Giampaolo, 2019; Rizzo et al., 2019a; Rizzo et al., 2019b).

Even if the effect of geothermal fluid circulation on electrical resistivity is well known (Spichak and Manzella, 2009), deep electrical resistivity tomography (DERT) in geothermal application is much less abundant (Tamburriello et al., 2008; Santilano et al., 2015). Recently, Gresse et al. (2017) and Troiano et al. (2019) described results of 3D deep electrical resistivity surveys for characterizing the shallow hydrothermal system of the Solfatara volcano (down to 200 m of depth) and imaging the deep structure of Campi Flegrei central sector (down to 800 m of depth). These studies underline the capability of electrical resistivity to be an unrivalled indicator of the presence of deformation structures that conduit hot fluids and gases. Carrier et al. (2019) present a recent technology for geoelectrical investigation of medium-enthalpy geothermal resources until about 1 km depth in an industrial area. The adopted system is made of a distributed set of independent electric potential recorders, enabled to tackle logistics and noise data issues typical of urbanized areas.

This paper describes new electrical resistivity data, that were acquired in the Larderello area by a new electrical resistivity approach. The proposed approach permits to obtain high resolution down to 1600 m introducing an experimental setting merging deep surface and surface-down-hole DC resistivity measurements. The possibility to constrain the shallow resistivity distribution into the first 2 km with the contribution of a surface-to-borehole electrical tomography is new in the field of geothermal exploration. The experiment introduces high resolution 3D Surface-Hole Deep Electrical Resistivity Tomography (SH-DERT) carried out in a geothermal area, installing electrodes in a non-productive geothermal well (Venelle2) of the Larderello field characterized by extreme temperature conditions. At now, the only few examples of deep borehole DC electrical surveys concerns the monitoring of

CO_2 plume development in deep saline aquifers down to the maximum reached depth of 3200 m (Kiessling et al., 2010; Schmidt-Hattenberger et al., 2011; Carrigan et al., 2013; Bergmann et al., 2017). In these experiments, borehole electrodes were installed over electrically isolated well casings, covering only the target zone (along he the boreholes the maximum coverage of the electrodes was of 150 m with an electrodes vertical spacing of 10 m), while surface electrodes consist of few surface dipoles 150 m long, deployed on concentric circles approximately centered on the injection location (Bergmann et al., 2012).

Conversely, in this paper, 3D SH-DERT was carried out by lowering into Venelle2 geothermal well a 2000 m long multipolar cable, equipped with flexible, metallic electrodes. The cable was designed and built specifically for carrying out 3D surface to borehole geoelectrical measurements in the Larderello site. Moreover, 33 surface electrodes were installed around Venelle2 well, covering an area of about 15 km^2.

This experiment was aimed to characterize in detail the resistivity of rocks down to the depth reached in the well, in a much larger volume than the one sensed by standard resistivity logging data. This detailed resistivity imaging represents a valid support for verifying, interpreting, and constraining the resistivity distribution of MT data in this complex geological contest, resulting in an improved image of deep resistivity distribution down to 1600 m depth from the ground surface. For these reasons, the proposed experiment represented a challenge for the applied geophysics.

2. Overview of Larderello geothermal system

The Larderello geothermal system (Southern Tuscany, Italy) is the most ancient field in exploitation in the world, in production since 1913. It is located in the inner part of the Northern Apennine of Italy, a sector of the Apennine orogenic belt.

The present-day geologic setting is the result of a complex polyphase tectonics developed in the frame of the Apennine orogenesis as a consequence of the Cenozoic collision between the European and Adria plates (Carminati and Doglioni, 2004; Boccaletti et al., 2011).

The tectonic evolution of Southern Tuscany is still highly debated in literature. Several authors proposed a model that implies a first compression and a subsequent extensional tectonic affecting the area since at least the early Miocene (e.g., Carmignani et al., 1994; Brogi, 2006; Liotta and Brogi, 2020). Other studies suggest a more complex evolution with a prevalent contribution of compressive tectonics till the Pleistocene epoch (Bonini et al., 2001).

Southern Tuscany is characterized by shallow Moho discontinuity, crustal thinning with consequent upwelling of magma bodies and increased regional heat flow (Gianelli et al., 1997). The Larderello field is considered a convective young intrusive geothermal play (Santilano et al., 2015a). Neogene to Quaternary intrusive activity acts as heat sources of the very high temperature systems of Tuscany (as well as of other regions such as Latium and Campania), of which the most important is the Larderello field. The field produces superheated steam at a rate of 850 kg/s and its 200 wells provide fluid to 23 units with 594,5 MW of total installed capacity (Conti et al., 2016; Manzella et al., 2018). The Larderello area consists of different geothermal fields, even though the most significant is located in the Lago Basin, where the Venelle2 well is located (fig. 1a). This basin is a tectonic depression developed during Pliocene-Pleistocene from where the bulk of electricity production derives (Barbier, 2002). In this area, temperature higher than 500° C at depths of about 3-4 km (Bertani et al., 2018) and heat flow values higher than to 1000 mW/m^2 are reached.

The Lago Basin structural depression corresponds to that crustal sector where, the shear zone is more permeable, channeling deep geothermal fluids and resulting the preferential area for escaping of derived-mantle fluids (Liotta and Brogi, 2020). The heat source of the geothermal anomaly is unknown, although teleseismic data analyses (Foley et al., 1992), interpretation of deep reflection seismic lines (Brogi et al., 2005), MT studies (Manzella, 2004) and rheological models (Gola et al., 2017; Rochira et al., 2018) suggest the occurrence of a cooling magma at 3–6 km depth (fig. 1b).

In the studied area, the most recent outcrops correspond to the Quaternary marine and continental deposits, while the oldest ones are represented by the metamorphic rocks of the Paleozoic Basement

(Bertini et al., 2006). The stratigraphy (fig. 1c) is summarized as follows (Batini et al., 2003; Romagnoli et al., 2010):

- Neogene and Quaternary deposits or Neoautochthonous complex: late Miocene to Pliocene and Quaternary, continental to marine sediments (clays, with minor sands, conglomerates and detrital limestones, gypsum);

- The Ligurian Complex l.s. (Ligurian/sub-Ligurian):

(a) the Ligurian Units, composed of remnants of Jurassic-Eocene oceanic crust and of its pelagic sedimentary cover (clayey-marly units in flysch facies)

(b) the Subligurian Units made up of arenaceous and calcareous turbidites (Late Cretaceous-Oligocene age).

- Tuscan Nappe: Triassic-Lower Miocene sedimentary cover of the Adria continental palaeomargin (arenaceous and clayey-marly formations, calcareous-siliceous rocks, dolostone and anhydrites). The Tuscan Nappe was detached from its substratum along the Triassic evaporites level and was thrust over the outer palaeogeographical domains during the Late Oligocene-Early Miocene compression. Furthermore, it is often tectonically laminated and in places shows a reduced thickness or is completely missing (Bertini et al., 1994).

In the area of Larderello geothermal reservoir, a Tectonic Wedge Complex (TWC) is present between the Tuscan Nappe and the underlying crystalline basement. It is composed of Paleozoic metamorphic rocks, Triassic metasiliciclastics, carbonates and evaporates of the Tuscan Nappe (Gianelli et al., 1978; Pandeli et al., 1991).

The Metamorphic basement is composed by three main complexes: i) Phyllitic Complex made mainly by metagraywacke (Cambrian-Devonian), and locally by carbonate–siliciclastic metasediments (Silurian-Devonian); ii) Micaschist Complex (Precambrian? - Early Paleozoic?) and iii) Gneiss Complex (Precambrian? - Early Paleozoic?).

At different depths, deep boreholes encountered granitoids and felsic dykes of the Intrusive Complex (3.8–1.3 Ma, Villa and Puxeddu, 1994; Gianelli and Laurenzi, 2001; Dini et al., 2005) whose emplacement gave rise to contact aureoles in the metamorphic host rocks (Elter and Pandeli, 1990). Moreover, hydrothermal mineral associations (Gianelli, 1994), locally no older than 270,000 years and no younger than 10,000 years (Bertini et al., 1996), partially or totally fill the fractures affecting the Larderello metamorphic rocks.

Summing up, the Larderello exploited resource is a vapor-dominated geothermal system, characterized by two different reservoirs (fig. 1c):

i) the shallow reservoir consists mainly of Mesozoic limestone and anhydrite dolostone,

ii) the deep reservoir consists mainly of Paleozoic metamorphic rocks, Plio-Quaternary granites and thermo-metamorphic rocks.

Furthermore, there is the possibility of a deep-seated geothermal reservoir with fluids at supercritical conditions at relatively shallow depth (4-8 km) below the area in correspondence of the seismic marker called K-horizon (De Franco et al., 2019).

Structural and geological data from Liotta and Brogi (2020) indicate that Lago Basin can be interpreted as a pull-apart basin. This is in fact bounded by NE-striking faults with a left-lateral shear sense, SE- or NW-dipping of about 70-80° and with length up to 15 km, accompanied by shorter almost orthogonal faults with a dominant normal component. These NE-striking faults commonly dissect a NW-striking system: at the intersections between these two faults systems, geothermal manifestations occur at the surface. The age of faults activity is at least encompassed between Pliocene and Holocene.

Recently, a dominant vertical movement along the NW and NE-striking pre-existing brittle structures has been recorded. This is linked to the competition between crustal stretching and surface uplift induced by heat flow. This implies a continuous switch of the local intermediate stress axis promoting quick changes in the direction of the maximum permeability from vertical to horizontal, thus enhancing the longevity of the geothermal system. This switch in fact let the fluids to be channeled from depth to shallower levels and to be laterally stored in structural traps, commonly located within the Triassic evaporite and/or the overlying carbonate succession and/or in the damage zone of the main faults (Liotta and Brogi, 2020).

3. Materials and Methods

The aim of the proposed experiment was to better define the deep Larderello structure with a high-resolution 3D SH-DERT.

The basic principle of the electrical resistivity method is to inject an electric current into the earth using two current electrodes *A* and *B*, then measure the potential difference through two other electrodes *M* and *N*, giving us a way to measure the electrical resistivity of the subsoil:

$$\Delta V_{MN} = I_{AB} R \quad (1)$$

where, ΔV_{MN} (Volt) is the measured voltage between electrodes *M* and *N*, I_{AB} (A) is the injected current between electrodes *A* and *B*, and R (Ω) is the resistance of the material through which the current flows.

As ΔV_{MN}, I_{AB}, and the electrode configuration are known, the resistivity of the ground can be determined; this is referred to as the "apparent resistivity" (Ωm):

$$\rho_a = K \frac{V_{MN}}{I_{AB}}. \quad (2)$$

The electrolyte resistivity is directly related to viscosity which decreases with temperature. On the contrary, the temperature dependence of the resistivity of the solid phase (rock matrix) are given by the Arrhenius relation (Caldwell et al., 1986):

$$\rho = \rho_0 \, e^{\frac{\varepsilon}{RT}} \quad (3)$$

where ε is an activation energy for the conduction process (commonly about 0.2eV in water and for saturated rocks, varying with degree of alteration), *R* is Boltzman's constant (0.8617x10-4 eV/°K), *T* is temperature (°K) and ρ_0 is the resistivity at theoretically infinite temperature. The relationship is useful in understanding the expected effect of temperature and the alteration mechanism.

Inverse methods must be applied to apparent resistivity data in order to determine the real resistivity distribution. Moreover, *K* (m) is called geometric factor. It depends on electrodes arrangement (array) and can be calculated from the electrode spacing. There are, in fact, different electrode configurations and in general the choice is based upon the sensitivity of the device, the vertical and horizontal variations in resistivity, the depth of investigation, the cumulative sensitivity, and the length of the signal. The variety of electrode arrays located on the ground surface was summarized by Szalai and Szarka (2008). Furche and Weller (2002), Tsourlos et al. (2011), Leontarakis and Apostolopoulos (2012), and Binley (2015) described borehole electrode arrays, where electrodes can be arranged in single, two or more, vertical and horizontal boreholes.

Deep electrical resistivity tomography (DERT) technique is an unusual electrical resistivity approach, described for the first time by Hallof (1957), able to reach investigation depth > 200 m. The main concept of the deep approach consists of the use of physically separated tools between the injection system and the measured drop of potential tool. Usually, long stainless-steel current electrodes (*A* and *B*) are connected by long monopolar electric cable to a transmitting station constituted by a transmitter, a voltage regulator, and an external power system, which can inject into the ground a time-domain (50% duty cycle) square-waveforms current signal, with a maximum energizing current of 20 A. Unpolarizable potential electrodes (*M* and *N*) are connected to a multichannel receiver system composed by remote multichannel datalogger and a GPS antenna, radios connected to a personal computer, which can simultaneously record several generated voltage signals (mV) timing, and geographic position.

In general, the current and potential electrodes are arranged with Dipole–Dipole (DD) electrode configuration. The advantage of the DD with respect to the other electrode configurations lies in the fact that the distance between the measuring electrodes and the current ones is limited only in the sensitivity of the instruments and in the background noise. Therefore, it is more suitable for deep investigations (> 200 m) otherwise not to be tackled with other quadripolar configuration.

In detail, the main aim of this experiment was to acquire and analyze several electric potential (mV) recordings using sensors distributed at the ground surface and in-hole, following the injection of an electric current (A) at the ground surface, to constrain the resistivity distribution at depth of the studied area. Borehole experimental activities were carried out using the geothermal well Venelle2 (Lago Basin, Monterotondo Marittimo, Grosseto, Italy), which is one of the EGP deep well of Larderello field, drilled in the 2006 to exploit the geothermal resource but, in effect, non-productive for a low fracturing state of the rocks.

In short, the characteristics of the well were (at the moment of the geoelectrical experiment):

a) 2234 m deep, accessible down to about 1600 m;
b) temperature up to 350° C;
c) pressure up to 130 barA;
d) metallic casing down to 1020 m.

The well stratigraphic reconstruction is shown in table 1.

In 2016, Pechnig et al. (2018) recorded a suite of logging data in the open hole section of Venelle2 well down to 1600 m depth (for the basement rocks). The operation included standard physical tools such spectral gamma, induction resistivity and sonic as well as special tools such as an ultrasonic borehole wall imager and a geochemical tool (fig. 2a). Estimated porosity generated from sonic log is in general low with a mean of 2.2 %. Moreover, sonic curves and its derivates indicate two zones of increased fracturing (around 1050 m and 1400 m from the top of well), through which the high pressure and temperature vapor moves, and a greater content of water is present.

In 2017, after the here described experiment, Venelle2 well has been re-drilled and deepened up to 2900 m. Following the well deepening, temperature and pressure profiles of the well were measured reaching a bottom hole temperature higher than 400° C (fig. 2b from Bertani et al., 2018).

In order to determine high-resolution images of subsurface rock formations near the well and to delineate zones of higher permeability, 3D deep electrical resistivity imaging techniques were applied to the studied area. In particular, the experimental activities can be divided into four phases:

- phase 1: realization of an ad-hoc geoelectrical cable for deep electrical resistivity borehole measurements;
- phase 2: surface-borehole and surface-surface electrical resistivity data acquisition at the site using electrodes arranged both on the surface and in the borehole;
- phase 3: analysis and elaboration of all the acquired data (in the borehole and on surface) in order to define the 3D distribution of the apparent electrical resistivity values and, consequently, the inversion of them;
- phase 4: new deep geoelectrical data interpretation in light of available borehole log and geological data.

3.1 Resistivity field data acquisition

A special cable was built for the SH-DERT array, taking in account the maximum depth of the borehole and the minimum electrodes spacing necessary to obtain a good resolution at depth. The built multipolar geoelectrical cable is 2000 m long and resistant to temperatures up to 250° C. It was assembled in the laboratory with the materials described in table 2 (Fig.3). The first step was to interlace together 12 copper electric cables and the steel one by a tight tape for creating the multipolar geoelectrical cable core (Fig. 3a). Then, to increase its traction and rub resistance, the cable was completely coated by heat shrink tubing, leaving only 12 spaces each 50m, in correspondence of steel electrodes connection (Fig. 3d). Once assembled the cable, the steel electrodes were placed at the correct positions along the cable and connected mechanically to the corresponding copper cable (Fig. 3b). Furthermore, to ensure the electric contact between the cable and each electrode both during the descent into the borehole and the measurements phase, the cable-electrode connection has been reinforced using both a resistant to high temperatures tape and the heat shrink tubing (fig. 3b). The multipolar geoelectrical cable was coiled around a wooden reel equipped with a series of holes adaptable to the ENEL winch (fig. 3e). At the end, the cable was weighed with an iron cylinder connected to the end of the cable to facilitate the vertical descent along the borehole (fig. 3c).

One experimental work of this phase was to identify the best surface and borehole electrical dipoles arrangement, improving both the geophysical data acquisition time (respecting ENEL directives) and final results. This phase work consisted in a modelling work which taken into account the electrical resistivity distribution of the first 4 km coming from previous MT inversion models integrated with geological information. Finally, because of the reduction in geometric factors (K) increases the probability for better signal to noise levels in measured resistivities, all quadrupoles with a K > 1000 were discharged. Therefore, five areas of interest (colored boxes in fig. 4) surrounding the Venelle2 well (red dot in fig. 4) and 33 points (yellow and red points in fig. 4) represent the surface electrodes position for 3D surface-borehole and surface-surface electrical resistivity measurements. They were chosen considering the logistics and the absence of any natural and anthropic limits for power cables roll out.

The field activities were performed in two steps: SH-DERT lasted about four days of which the first day was necessary to drop the ad-hoc cable into the well and install the electrodes and the electric cable at the surface, while the Surface-Surface Deep Electrical Resistivity Tomography (S-DERT) lasted about 3 days.

In both measurement activities, current electrodes (*AB*) were connected to the Zonge transmitting station constituted by the GGT-10 transmitter and the ZMG-9 power system, while potential electrodes (*MN*) were connected to a multichannel receiver system made of 5 remotes multichannel dataloggers, radio-connected to a personal computer, simultaneously recording a total number of 32 generated voltage signals (mV). In our case, a maximum energizing current of 12 A was injected into the ground (3-12 A).

The SH-DERT measurements was to lower the ad-hoc cable in the well through a winch (fig. 5). Therefore, a long stuffing box (5 m) was installed above the pressure valve of the hole (fig. 5b), to permit the installation of the cable in the casing permitting to work safely. Successively, two pulleys were installed, one at about 3 m above the stuffing box and the second one close to the hole pressure valve (fig. 6a and 5c). The two pulleys helped the cable drop in the hole. Finally, the winch system dropped the cable in the well and, in 45 minutes, it reached the maximum pre-defined depth of about 1600 m (fig. 5d). When the winch system was switched off, the 12 electrodes were installed and located between 1050 m to 1600 m from the surface (fig. 5e). During all this experimental activity, the well was cooled by a continuous injection of 80 m^3/s condensed water (8.56 mS/cm or 1.17 Ωm) for three days in order to reach more favorable pressure and temperature condition and to allow a good electric contact between the rock and the borehole electrodes.

The second step consisted of installing on the topographic surface 33 steel current electrodes around the Venelle2 well. The investigated area was about 10 km^2 as established during the setting phase (fig. 4). The disposition of the surface electrodes and the borehole ones permitted to obtain several injection current dipoles. The transmitting system was placed in 5 different sites and the current electrodes were connected by long electric cables for a total length of about 18 km of cable used.

A DD array configuration was used. The *AB* distances ranged between 400 and 1600 m, and the *MN* distances ranged between 50 and 550 m (in the hole).

Therefore, for each current injection using a square wave of 32 seconds, 32 drops of potential recordings were simultaneously acquired. As a result, 2080 resistivity data, related to different current electrodes positions, were obtained.

In order to carry out the S-DERT measurements, 23 surface electrodes were fixed around the Venelle2 well, roughly in the same position and covering the same area of about 10 km^2 of the previous measurement phase (fig. 4). In this case, we used steel electrodes for current injection and unpolarized electrodes for potential measurement.

The studied area was divided in five main sub-sites (figure 4), where transmitter and receiver apparatus were installed. In detail, when the transmitter system was placed in one sub-site, 4 datalogger were installed in the other sub-sites. The transmitter system was connected with steel current electrodes, while each receiver (5 dataloggers) with unpolarized electrodes, both by long electrical cables. In this way, the complete system was able to obtain a multichannel collecting work.

A DD array configuration was used with *AB* and *MN* distances ranging between 400 and 1600 m. A square wave of 32 seconds was used for each dipole injection current (AB) and 28 electric potential signals (MN) were simultaneously acquired for 15-20 minutes. Consequently, 952 resistivity data were measured for each quadrupole (ABMN).

3.2 Data analysis and inversion

The considerable work in the field permitted to acquire several data during the two field trips. The large amount of acquired data prompted us to use an automated protocol for data analysis. Generally, in shallow investigations (multichannel system with an investigation depth < 300 m), a routine analysis of voltage signals is sufficient to reduce the errors associated to the estimate of the potential values. On the contrary, in deep geoelectrical explorations (> 300 m of depth) with a current system and drop of potential acquisition physically separated a crucial task is the extraction of the useful signal from the voltage recordings.

The amplitude of an electric potential signal depends, indeed, on the intensity of the current input, on the subsoil electrical characteristics and on the electrode distances. For large distances between the *AB* and *MN* electrodes, the measured electric potential is sometimes very low, which is due to disturbing currents present in the ground, such as industrial, telluric, and inductive currents (between cables), which may occur when the energizing circuit is activated.

The distribution of the electrical conductivity in the soil also affects the quality of the signal, in fact, in highly conductive areas, located between the transmitting and receiving dipoles, the electric potential is strongly masked to such an extent that the signal is completely erased from the background noise. Furthermore, deep geoelectrical data acquisition in anthropic areas is characterized by a greater noise level because of the disturbances due to environmental noise. For all these reasons, the voltage signal useful for calculating the apparent electrical resistivity values could be hidden (Rizzo et al., 2019).

Therefore, the rationale of field acquisition and processing is to record data for the time necessary for having enough current and electric potential cycles to extract the amplitude of the signals from the background noise.

The first elaboration step is the time correlation between the acquired current signals (A) and the electric potential data (mV), that is obtained by GPS system installed on each datalogger. The next stage was the data analysis, where the data analysis software was managed with OriginLab software (fig. 6). The first elaboration step was the spike removing, which consists of deleting the spikes on the active graph window (fig. 6c). The second step was the de-trending analysis, which consisted in a polynomial or linear fit of the voltage data and a subsequently de-trend approach. This elaboration step removes the natural trend that enveloped the data (fig. 6d, e). Successively, a FFT tool was applied to the de-trending voltage data (fig. 6f). The FFT analysis converts a signal from its original time domain to a representation in the frequency domain. Meanwhile, it can also provide the magnitude, amplitude, phase, power density and other computation results. In our case, the amplitude of the FFT results in the frequency of the acquired current signal defines the amount of the drop of potential.

After the analysis and elaboration steps, about 10% of electric potential data was rejected for a low signal/noise ratio and more than 2940 resistance values (V/I) were calculated taking in account the extrapolated potential data and the injected current.

Subsequently, the acquired data were inverted with ERTLab software (Geostudi Astier srl and Multi-Phase Technologies LLC) and the 3D electrical resistivity image of the studied area was depicted. It is an electrical resistivity inversion software that offers full three-dimensional modelling and inversion. Its numerical core uses the Finite Elements (FEM) approach to model the subsoil by adopting a mesh of hexahedrons to correctly incorporate complex terrain topography. Moreover, the software invert datasets collected using surface, borehole or surface-to-hole array configurations.

The inversion procedure is based on a smoothness constrained least-squared algorithm (LaBrecque et al., 1999) with Tikhonov model regularization, where the condition of the minimum roughness of the model is used as a stabilizing function. Throughout the inversion iterations, the effect of non-Gaussian noise is appropriately managed using a robust data weighting algorithm (Morelli and LaBrecque, 1996).

ERTlab allows to plot the apparent resistivity data in a 3D image starting from the resistance and the geometric factor. Figure 7 shows the surface-borehole (fig. 7a) and total (fig. 7b) 3D apparent resistivity data distribution with 2940 electrical resistivity value covering a volume of about 25 km^3. Then, the apparent resistivity data set was inverted by using a 100 m x 100 m x 50 m cell size for the core mesh (red box in figure 7), a mixed boundary condition (Dirichlet and Neumann), and a starting homogeneous apparent resistivity of 10 Ωm. An extra mesh, called the boundary mesh (green box), was generated around the core mesh to accommodate numerical boundary effects.

It is well known that conductive borehole fluids can affect ERT images, as they provide a strong electrical contrast close to the electrodes and can result in direct electrical connections between electrodes. In this case, the fluid may also represent an electrical connection to the metal casing. In general, potential mitigation techniques consist in incorporating the borehole and fluid characteristics in both the forward modeling and inversion codes.

According to Doetsch et al. (2010), current channeling phenomena can be favored when the well annulus is filled with highly conductive fluids (resistivity contrasts of 100:1) and borehole diameters of 10 and 20 cm yielded, for a dipole length of 5 m. In our case, the resistivity contrast between geological formations and the injected fluids (1.17 Ωm) is expected less than 100:1 while the borehole diameter is in the range between 30 – 60 cm for a dipole length of 50 m in the borehole and 400 m at surface. For these reasons, the borehole - fluid effects have been neglected.

Moreover, Wagner et al. (2015), discuss the effect of borehole filling, electrode shape/size and borehole deviation on ERT monitoring of a CO_2 storage reservoir. However, considering the small size of well and electrodes compared with the size of the mesh elements, it would be computationally prohibitive to use very fine grids to account well filling, electrode shape/size and borehole deviation into the 3D mesh used for this experiment. Moreover, according Rücker and Günther (2011), electrodes can be treated as ideal point sources if length/spacing < 0.2.

Finally, topographic correction was applied, and a 5% standard deviation estimate for noise was assumed to invert the data set with a robust inversion. The choice of 5% data error was a compromise between data error, final RMS e smoothness of the final model.

4. Results and discussion

In order to evaluate the capability of the deep electrical resistivity experiment, 3D apparent resistivity data were inverted considering at first, only surface measurements and then the full dataset (surface, surface to borehole, and in hole measurements). Moreover, inversion model errors were about 8% for S-DERT and 15% for the full dataset.

The figure 8 shows the 3D S-DERT, that was obtained considering only apparent resistivity values measured from surface electrodes. S-DERT has electrical resistivity values ranging from about 1 to 50 Ωm and a maximum investigation depth of about 1000 m from the ground surface. The best resolution was reached down to about 800 m from the ground surface underlining the presence of a highly conductive central zone with a "concave" shape up to 400-500 m deep, bounded laterally by areas with relatively higher resistivity (30 Ωm). Under it, a homogeneous resistivity distribution of about 10 Ωm is highlighted.

Figure 9 shows the results of the final 3D resistivity distribution obtained by the inversion of all the collected data (surface and borehole). In this case, the investigated depth reached is greater (about 1600 m), since the borehole electrodes within the Venelle2 well were arranged at depth of about 1000 to 1600 m. This electrical resistivity image combines the resistivity distribution characteristics of S-DERT and SH-DERT increasing the sensitivity both at surface and in borehole and better emphasizing, by sharper resistivity contrast, the geometric features of the investigated area.

The range of resistivity values is between 1 and 80 Ωm and shallow high conductive nucleus ($\rho < 10$ Ωm), bounded laterally by areas with relatively higher resistivity ($\rho > 30$ Ωm), are present down to -

300 m b.s.l. The deep geothermal reservoir hosted in crystalline rocks (from the depth of about 750 m b.s.l.) is in general characterized by average values lower than 25 Ωm, however, the resistivity distribution along Venelle2 well highlights a vertical variation with relatively higher resistive areas that could be associated to lithological/mineralogical heterogeneity or to a different fracturing rock state controlling the circulation of producing a different emission of high temperature dry vapors (> 200 °C) in the area.

Obviously, 3D imaging visualization allows to appreciate the trend of resistivity values of the study area in its entirety, while 2D imaging visualization allows to focus on specific elements of the investigated area, already identified in the 3D resistivity inversion models, and understand the best electrodes configurations to use in future applications in the geothermal field. Therefore, in order to interpret the 3D electrical resistivity distribution and facilitate the understanding of the complex geothermal system of the area around Venelle2 well, 3D electrical resistivity models were dissected along two selected profiles where lithostratigraphic and temperature information of some geothermal wells are available (Trumpy and Manzella, 2017) and summarized in figures 10. Figures 11 shows the resistivity sections of the previous 3D electrical models extracted along A-A' (SE-NW) and B-B' (NE-SW) profiles. The two sections of the 3D S-DERT model have an investigation depth of about 800 m (Figure 11a,b), while the figure 11c,d shows the two sections coming from the full 3D model with an investigation depth of about 1600 m. The 2D geoelectrical profiles show a range of electrical resistivity ranging from 1 Ωm to about 50 Ωm, even if the resistivity models are similar, sharper resistivity contrasts are well delineated in the deeper ones.

The figure 12 shows the 2D deep profiles compared with the borehole data, the temperature and the porosity of the Venelle2. In general, measured resistivity values are very low therefore they are only partly associated to the geological units. More probably, they are linked to the presence of tectonic structures that influence the circulation of hot fluids derived mainly from meteoric water heated by rock conduction (due to the high geothermal gradient) and, in limited cases, from direct inflows of shallow vapor, enriched near the surface, following partial condensation of deep-sourced vapor

(Duchi et al., 1986). Moreover, in high-temperature geothermal systems, the shallow geology is characterized by an unaltered zone, and the electrical conduction is mainly pore-fluid conduction. The deep electrical conduction is dominated by mineral or surface conduction due to temperature increment and high content of mineral alteration. On the contrary, at high temperature (above 230°C), the resistivity increases due to formation of high-temperature secondary alteration minerals and the conduction is dominated by surface and pore fluid conduction (Flóvenz et al., 2012).

In detail, the shallower conductive body (ρ < 15 Ωm) are associated to Neogenic deposits and to the clayey-marly units in flysch facies of the Ligurian l.s. Complex. Furthermore, higher resistivity values (ρ > 20 Ωm) characterizes the deep part of the DERTs close the Venelle2 well, at a depth where well stratigraphy refers to the Tectonic wedge complex (TWC). In the study area, the depth and thickness of pre-neogenic units varies indicating, in addition, the asymmetry of the tectonic depression. Sharp resistivity contrasts are associated to tectonic structure that bound the more conductive area. These geological structures bring into contact different lithologies and/or the same lithologies but with different chemical-physical characteristics of the subsoil. Finally, the resistivity distribution along Venelle2 well (Figure 12) allowed to analyze the behavior of deep geothermal reservoir hosted in crystalline rocks. In general, the Phyllitic-Quartzitic unit is characterized by low resistivity value (average value lower than 25 Ωm). Moreover, the comparison between the geophysical results, the porosity and temperature data (Figure 12) underlines some correlations. In detail, relatively low electrical resistivity values (< 10 Ωm) were recorded in correspondence of higher porosity zone (-800 and -1100 m a.s.l.), where a larger amount of liquid phase in two large fractures was recorded. A third conductive layer was recorded at depth (1300 m b.s.l.) in correspondence of higher percentage of phyllosilicate. On the contrary, the crystalline basement is characterized by ρ > 30 Ωm. Moreover, the temperature distribution controls the electrical conduction and some surface (<400m) extensive low resistivity zones are characterized with low temperature (<100°C). The low resistivity in this zone could be associated with the hot saline fluids of the geothermal system, but low resistivities can be correlated with clay hydrothermal alteration that occurs in that temperature regime. On the contrary, a deep high temperature zone is observed and the resistivity increment should be rightly correlated with some vapor dominated reservoir and a secondary alteration mineral with surface and pore fluid conduction. These phenomena are well highlighted on the relationship between the resistivity values extracted from the 3D resistivity inverted model at each depth where temperature data were collected in previous work (Fig. 13a). Close the Venelle2 well in the deep part (> 1000m) relative conductive and resistive alternances are detected, this behavior should be associated to the presence of high porosity, due to large fractures where the condensed water in the well flows, and high clay hydrothermal alteration. Therefore, the trend line toward increasing resistivity with depth, where an increase in temperature is observed, leads us to consider the equation 3, that can be presented in this form:

$$\ln \rho = \ln \rho_0 + \varepsilon/R(1/T) \tag{4}$$

This linear correlation (figure 13b) shows a coefficient of determination is 0.7564 indicated a good fit of the measured values to the Arrhenius law, in according to the previous consideration on the relationship between temperature data and the resistivity values (without the previous outliers). The correlation coefficient defines an activation energy of about -0.05 eV. This value suggests a complex conduction behavior of the electrical charge transport mechanism in this geothermal area, where a mixing of dry condition and high concentration of alteration minerals characterize the investigated area. However, a comparative study of the variation of the electrical conductivity with temperature in the presence of high temperature alteration minerals, such as chlorites, that is encountered in this hydrothermal system, by sample analysis could improve quantitatively these results.

As mentioned previously, MT results in the Lago Boracifero area form Santilano, 2017 (fig. 13), confirmed low resistivity values in the Lago basin allowing to recognize four main sub-horizontal electro layers: a) a low resistivity shallow layer (down to about 300 m from the ground surface), with values in the range of 3-30 Ωm, corresponds to the Neoautochthonous and Ligurian Complexes; b) the second layer, characterized by resistivity values in the range of 40-100 Ωm, located at a structural level coincident with the Tuscan Complex, Tectonic Wedge Complex and most of the Phyllitic

Complex (down to 2 km b.s.l.); c) the third layer, characterized by resistivity values in the range of 1000-5000 Ωm, corresponds mainly to the Micaschist, Gneiss and Intrusive complexes (2-7 km depth); d) at depth higher than 7 km, a general decrease of resistivity is observed with values locally lower than 400 Ωm.

Finally, MT profiles in the Lago Boracifero sector show a very important sub-vertical structure (elongated N30E) crosscutting the main sub-horizontal layers previously described and characterized by low resistivity, with average values of about 150 Ωm. The decrease of resistivity in the Micaschist, Gneiss and Intrusive complexes would suggest a strong influence of the hydrothermal circulation. This interpretation can imply two main processes: i) the occurrence of a contribution of liquid phase in the vapor dominated reservoir (hypothesis not confirmed by well tests) and/or ii) the effect of more or less pervasive hydrothermal alteration, possibly a remnant of the effect of an old, liquid phase fluid circulation. The MT results led the authors to interpret this structure as a fault that controlled the magmatic activity in this specific sector and possibly controls the hydrothermal circulation, along a very wide (some kilometers) shear zone oriented N30E. Rosenkjær et al. (2017) particularly refer to the Cornia Fault that is imaged as a wide sub-vertical low resistivity structure located along the homonymous river.

5. Conclusions

In this paper we described the main results of a geophysical experiment carried out in the frame of the FP7 IMAGE project. The Larderello Geothermal fields (Italy), since the first investigations conducted more than a century ago, have been the object of a myriad of studies. Due to the complexity of the system and the abundance of data, the field represents the ideal site to test the effectiveness of an experimental geoelectrical survey.

We propose an innovative Surface-Hole Deep Electrical Resistivity Tomography (SH-DERT) technique in extreme subsurface temperature condition, by using an ad-hoc geoelectrical cable in the deep well, 2000 m long, resistant up to 250° C and equipped with flexible steel electrodes. This ad-hoc cable was lowered in the Venelle2 well, a non-productive deep well, down to 1600 m from ground surface. Furthermore, 46 electrodes were arranged radially with respect to the Venelle2 well in an area of about 4 km^2 for a total investigated volume of about 10 km^3. The various combinations used between electric and potential electrodes allowed to measure a huge amount of data (2552 apparent resistivity data obtained) in a relatively short time (6 workdays). The dataset was firstly appropriately processed and then inverted to obtain the 3D electrical resistivity distribution of the area down to a depth of 1600 m.

Important hints for interpretation can be derived: first, a very low resistivity was recognized in the Tuscan Nappe and in the Tectonic Wedge Complex. This result agrees with MT studies, which results could have been biased by the passive nature of the method in a noisy area. It is assumed that the low resistivity values are due to the effect of more or less pervasive hydrothermal alteration, possibly a remnant of the effect of an old, liquid phase fluid circulation. Second, strong lateral variation of resistivity has been recognized along tectonic structures that could represent an actual (or fossil) pathway for hydrothermal fluids.

In conclusion, the innovative nature of this work can be summarized in three elements: the experiment represents the first one that applies deep 3D surface to borehole electrical resistivity measurements in geothermal applications; the geoelectrical investigation reaches very deep areas by the use of an ad-hoc geoelectrical cable; a large number of data was acquired in a deep context.

Finally, 3D deep surface to borehole electrical resistivity measurements can be applied also to more conventional geothermal systems both for characterization and monitoring.

Monitoring resistivity changes associated to temperature changes and/or fluid movement in geothermal reservoirs from the surface generally involves measuring small variations and therefore higher modeling errors. On the contrary, surface to hole and cross-hole geoelectrical methods showed a high benefit-to-cost ratio and a high sensitivity (around 1.2° C for temperature changes) to the temperature distribution in operating shallow geothermal systems or during heat tracing resistivity

(Hermans et al., 2015; Lesparre et al., 2019). Therefore, as regarding the use of geoelectrical methods in deeper geothermal systems, the combined use of data acquired in boreholes and surface can significantly increase the spatial resolution in depth.

The only needs consist in the presence of available not metallic wells. To overcome this last issue, an appropriately insulated array of electrodes permanently installed on the well casing and electrically coupled with the geological formations could enable the system to perform quasi-continuous geoelectrical surveys (Bottazzi et al., 2020). However, electrode and cable decay should be carefully evaluated. Finally, advanced data analysis (Machine Learning algorithm) can bring relevant and quantitative information aimed at optimizing geothermal reservoir management.

Acknowledgements

We thank the colleagues that supported the field work during the DC surveys. This study is part of the EU FP7-funded Integrated Methods for Advanced Geothermal Exploration (IMAGE) Project under grant agreement n° 608553. We thank the master thesis student Dr. Geol. Michele Tricarico and the archaeologist Dr. Felice Perciante that supported the fieldwork during the DC surveys. We thank Enel Green Power for the precious technical and logistical support on carrying out the borehole experiment. The access and in-well activities were possible thanks to the support of the operator (EGP).

Credit author statement

E. Rizzo: Conceptualization, Methodology, Investigation, Software Writing-Original Draft, Supervision; V. Giampaolo and L. Capozzoli: Software, Writing-Original Draft, Visualization, Investigation; G. De Martino, G. Romano: Investigation; A. Santilano: Writing-Original Draft, Visualization; A. Manzella: Funding acquisition.

Data Availability

The Data are available from the corresponding author

References

Altwegg, P., Schill, E., Abdelfettah, Y., Radogna, P.-V. & Mauri, G., 2015. Toward fracture porosity assessment by gravity forward modeling for geothermal exploration (Sankt Gallen, Switzerland), Geothermics, 57, 26–38.

Balasco M., P. Galli, A. Giocoli, E. Gueguen, V. Lapenna, A. Perrone, S. Piscitelli, E. Rizzo, G. Romano, A. Siniscalchi and M. Votta, 2011. Deep geophysical electromagnetic section across the middle Aterno Valley (central Italy): preliminary results after the April 6, 2009 L'Aquila earthquake. Boll. Geofis. Teor. Appl. doi:10.4430/bgta0028.

Batini F., Brogi A., Lazzarotto A., Liotta D., Pandeli E., 2003. Geological features of Larderello–Travale and Mt Amiata geothermal areas (southern Tuscany Italy). Episodes 26:239–244 .

Bergmann P., Schmidt-Hattenberger C., Kiessling D., Rücker C., Labitzke T., Henninges J., Baumann G., Schütt H., 2012. Surface-downhole electrical resistivity tomography applied to monitoring of CO2 storage at Ketzin, Germany, Geophysics, 77, B253-B267.

Bergmann, P., Schmidt-Hattenberger, C., Labitzke, T., Wagner, F. M., Just, A., Flechsig, C., Rippe, D., 2017. Fluid injection monitoring using electrical resistivity tomography - five years of CO2 injection at Ketzin, Germany. Geophysical Prospecting, 65, 859-875.

Bertani R., Bertini G., Cappetti G., Fiordelisi A., Marocco B.M., 2005. An update of the Larderello-Travale/Radicondoli deep geothermal system. Proceedings World Geothermal Congress 2005, Antalya, Turkey.

Bertani, R., Büsing, H., Buske, S., Dini, A, Hjelstuen, M., Luchini, M., Manzella, A., Nybo, R., Rabbel, W., Serniotti, L., the DESCRAMBLE Science and Technology Team, 2018. The First Results of the DESCRAMBLE Project. Proceedings of the 43rd Workshop on Geothermal Reservoir Engineering, Stanford University, Stanford, California, February 12-14, 2018

Bertini G., Cameli G.M., Costantini A., Decandia F.A., Dini I., Elter F.M., Lazzarotto A., Liotta D., Pandeli E., Sandrelli F., 1994. Structural features of southern Tuscany along the Monti di Campiglia–Rapolano Terme cross-section. Memorie della Società Geologica Italiana, 48, 51–59.

Bertini G., Casini M., Gianelli G., and Pandeli E., 2006. Geological structure of a long-living geothermal system, Larderello, Italy, Terra Nova, 18, 163-169.

Bertini G., Gianelli G., Battaglia, A., 1996. Risultati ed interpretazione delle datazioni radiometriche (metodo 230Th/234U) dei campioni di minerali idrotermali presenti nelle rocce attraversate dai sondaggi geotermici (Larderello e Monteverdi) e negli affioramenti di rocce mineralizzate (Sassa e Canneto-Malentrata). ENEL-CNR-CISE joint report, Pisa. 12 pp.

Binley A., 2015. 11.08 Tools and Techniques: Electrical Methods. In Treatise on Geophysics, Second Edition, Ed. Gerald Schubert, Elsevier, 2015, Pages 233-259.

Binley A., Cassiani G., Middleton R., Winship P., 2002. Vadose zone flow model parameterisation using cross-borehole radar and resistivity imaging. Journal of Hydrology 267, 147–159.

Binley A. and Kemna, A., 2005. DC resistivity and induced polarization methods. In: R.a. Hubbard (Editor), Hydrogeophysics. Springer, pp. 129-156.

Boccaletti, M., Corti, G., Martelli, L. (2011). Recent and active tectonics of the external zone of the Northern Apennines (Italy). Int. J. Earth. Sci., 100, 1331-1348.

Bonini, M., Boccaletti, M., Moratti, G. and Sani, F. (2001). Neogene crustal shortening and basin evolution in Tuscany (Northern Apennines). Ofioliti, 26, 275–286.

Bottazzi, F., Dell’Aversana, P., Molaschi, C., Gallino, G., Carniani, C., Cappuccio, P., Servodio, R., 2020. A New Downhole System for Real Time Reservoir Fluid Distribution Mapping: E-

REMM, the Eni-Reservoir Electro-Magnetic Mapping System. International Petroleum Technology Conference, Dhahran, Kingdom of Saudi Arabia, IPTC-19807-MS, 1-9.

Brogi, A. (2006). Neogene extension in the Northern Apennines (Italy): insights from the southern part of the Mt. Amiata geothermal area. Geodin. Acta, 19/1, 1-9, doi:10.3166/ga.19.33-50

Brogi A., Lazzarotto A. Liotta, D., Ranalli, G., CROP18 Working Group, 2005. Crustal structures in the geothermal areas of southern Tuscany (Italy): Insights from the CROP 18 deep seismic reflection lines. Journal of Volcanology and Geothermal Research, 148, 60– 80.

Bruno, P.P.G., Ricciardi, G.P., Petrillo, Z., Di Fiore, V., Troiano, A., Chiodini, G., 2007. Geophysical and hydrogeological experiments from a shallow hydrothermal system at solfatara volcano, Campi Flegrei, Italy: response to caldera unrest, J. Geophys. Res.: Solid Earth, 112(B6).

Byrdina, S., Vandemeulebrouck, J., Cardellini, C., Legaz, A., Camerlynck, C., Chiodini, G., Lebourg, T., Gresse, M., Bascou, P., Motos, G., Carrier, A., Caliro, S., 2014. Relations between electrical resistivity, carbon dioxide flux, and self-potential in the shallow hydrothermal system of Solfatara (Phlegrean Fields, Italy), Journal of Volcanology and Geothermal Research, 283, 172-182.

Caldwell, G., Pearson, C., Zayadi, H. (1986). Resistivity of rocks in geothermal systems: a laboratory study. In Proceedings 8th NZ Geothermal Workshop, 227-231.

Cameli G.M., Dini I., Liotta D., 1998. Brittle/Ductile boundary from seismic reflection lines of southern Tuscany (Northern Apennines, Italy). Memorie Società Geologica Italiana, 52, 152-162.

Carmignani, L., Decandia, F.A., Fantozzi, P.L., Lazzarotto, A., Liotta, D., Meccheri, M. (1994). Tertiary extensional tectonics in Tuscany (Northern Apennines, Italy). Tectonophysics, 238, 295-315.

Carminati E., and Doglioni C., 2004. Mediterranean geodynamics, in Encyclopaedia of Geology, pp. 135–146, Elsevier Acad., Amsterdam.

Carrier A., F. Fischanger, J. Gance, G. Cocchiararo, G. Morelli, M. Lupi, 2019. Deep electrical resistivity tomography for the prospection of low- to medium-enthalpy geothermal resources. Volume 219, Issue 3, 2056–2072.

Carrigan C.R., Yang X., LaBrecque D.J., Larsen D., Freeman D., Ramirez A.L., Daily W., Aines R., Newmark R., Friedmann S.J., Hovorka S., 2013. Electrical resistance tomographic monitoring of CO2 movement in deep geologic reservoirs Int. J. Greenh. Gas Control, 18, 401–408.

Chambers J. E., Wilkinson P. B., Weller A. L., Meldrum P. I., Gilvy R. D., Caunt S., 2007. Mineshaft imaging using surface and crosshole 3D electrical resistivity tomography: A case history from the East Pennine Coalfield, UK, Journal of Applied Geophysics, 62, 324-337.

Cheng Q., Chen X., Tao M., Binley A., 2019. Characterization of karst structures using quasi‐ 3D electrical resistivity tomography. Environmental Earth Sciences (2019) 78:285.

Conti P., M. Cei, F. Razzano, 2016. Geothermal energy use, country update for Italy (2010–2015) European Geothermal Congress 2016, Strasbourg, France, 19–24 September 2016.

Dahlin T., 1996. 2D resistivity surveying for environmental and engineering applications. First Break, 14, 275-284.

Daily W. and Ramirez A., 2000. Electrical imaging of engineered hydraulic barriers, Geophysics, 65, 83-94.

Daily W., Ramirez A., Labrecque D., Nitao J., 1992. Electrical-resistivity tomography of vadose water-movement. Water Resources Research, 28, 1429–1442.

Dam D. and Christensen S., 2003. Including geophysical data in ground water model inverse calibration, Ground Water, 41, 178–189.

Darnet M., Marquis G., Sailhac P., 2003. Estimating aquifer hydraulic properties from the inversion of surface Streaming Potential (SP) anomalies. Geophys. Res. Lett., 30, 13.

Darnet, M., Wawrzyniak, P., Baltassat, J., Bretaudeau, F., Coppo, N., Vedrine, S., Reninger, P., Vittecoq, B., 2020a. Airborne and land-based electromagnetic (CSEM and MT) surveying for geothermal exploration in the Martinique island. Proceedings World Geothermal Congress 2020 Reykjavik, Iceland, April 26 – May 2, 2020.

Darnet, M., Wawrzyniak, P., Coppo, N., Nielsson, S., Schill, E., Fridleifsson, G.Ó., 2020b. Monitoring geothermal reservoir developments with the Controlled-Source Electro-Magnetic method - A calibration study on the Reykjanes geothermal field. Journal of Volcanology and Geothermal Research, 391, 106437.

De Franco R., L. Petracchini, D. Scrocca, G. Caielli, G. Montegrossi, A. Santilano, A. Manzella, 2019. Synthetic Seismic Reflection Modelling in a Supercritical Geothermal System: An Image of the K-Horizon in the Larderello Field (Italy), Geofluids, vol. 2019, 21 pages.

De Matteis R., Vanorio T., Zollo A., Ciuffi S., Fiordelisi A., Spinelli E., 2008. Three dimensional tomography and rock properties of the Larderello-Travale geothermal area, Italy. Physics of the Earth and Planetary Interiors, 168, 37-48.

Del Moro A., Puxeddu M., Radicati di Brozolo F., Villa I., 1982. Rb-Sr and K-Ar ages of minerals at temperatures of 300°-400°C from deep wells in the Larderello geothermal field (Italy). Contrib. Mineral. Petrol., 81, 340-349.

Dini, A., Gianelli, G., Puxeddu, M., Ruggieri, G. (2005). Origin and evolution of Pliocene–Pleistocene granites from the Larderello geothermal field (Tuscan Magmatic Province, Italy), Lithos, 81, 1-31.

Doetsch, J. A., Coscia, I., Greenhalgh, S., Linde, N., Green, A., & Günther, T. (2010): The borehole-fluid effect in electrical resistivity imaging. Geophysics, F107-F114.

Elter M. and Pandeli E., 1990. Alpine and Hercynian orogenic phases in the basement rocks of the Northern Apennines (Larderello geothermal field, Southern Tuscany, Italy). Eclogae Geologicae Helveticae, 83, 241-264.

Fiordelisi A., Mackie R., Manzella A., Zaja A., 1998. Electrical features of deep structures in Southern Tuscany (Italy), Annals of Geophysics, 41(3), 333-341.

Flóvenz, Ó.G., Spangenberg, E., Kulenkampff, J., Árnason, K., Karlsdóttir, R., and Huenges, E., 2005. The role of electrical conduction in geothermal exploration. Proceedings World Geothermal Congress 2005, Antalya, Turkey, CD, 9 pp.

Flóvenz, Ó.G., Hersir, G.P., Saemundsson, K., Ármannsson, H and Fridriksson, Th., 2012: Geothermal energy exploration techniques. In: Syigh, A., (ed.) Comprehensive renewable energy, Vol. 7. Elsevier, Oxford, 51-95.

Foley, lE, Toksoz, M.N., Batini, F., 1992. Inversion of teleseismic traveltime residuals for velocity structure in the Larderello geothermal field. Italy. Geophys. Res. Lett. 19, 5–8.

Furche M., Weller A., 2002. Sensitivity distributions of different borehole electrode configurations considering a model with a cylindrical coaxial boundary. Geophysical Journal International, 149, 2, 338–348.

Gianelli G., Puxeddu M., Squarci P. (1978). Structural setting of the Larderello-Travale geothermal region. Mem.Soc. Geol. It., 19, 469-476

Gianelli G.,1994. Condizioni di pressione e temperatura del termometamorfismo nel sistema geotermico di Larderello. Atti Soc. tosc. Sci. nat., Mem., Serie A, 105, 17-35.

Gianelli, G., and M. A. Laurenzi, Age and cooling rate of the geothermal system of Larderello, Trans. Geotherm. Res. Counc., 25, 731 – 735, 2001.

Gianelli, G., Manzella, A. & Puxeddu, M. 1997. Crustal models of the geothermal areas of southern Tuscany (Italy). Tectonophysics, 281, 221 – 239.

Giocoli, A, Magrì, C., Vannoli, P., Piscitelli, S., Rizzo, E., Siniscalchi, A., Burrato, P., Basso, C., Di Nocera, C., 2008, Electrical resistivity tomography investigations in the Ufita Valley (southern Italy): Annals of Geophysics, 51(1), 213-223.

Gresse M., Vandemeulebrouck J., Byrdina S., Chiodini G., Revil A., Johnson T.C., Ricci T., Vilardo G., Mangiacapra A., Lebourg T., Grangeon J., Bascou P., Metral L., 2017. Three-Dimensional Electrical Resistivity Tomography of the Solfatara Crater (Italy): Implication for the

Multiphase Flow Structure of the Shallow Hydrothermal System. Journal of Geophysical Research: Solid Earth, 122, 8749–8768.

Griffiths, D.H., Barker, R.D., 1993. Two-dimensional resistivity imaging and modelling in areas of complex geology. Journal of Applied Geophysics, 29, 211–226.

Goes, B.J.M., Meekes, J.A.C., 2004. An effective electrode configuration for the detection of DNAPLs with electrical resistivity tomography. Journal of Environmental and Engineering Geophysics 9, 127–141.

Gola G., Bertini G., Bonini M., Botteghi S., Brogi A., De Franco R., Dini A., Donato A., Gianelli G., Liotta D., Manzella A., Montanari D., Montegrossi G., Petracchini L., Ruggieri G., Santilano A., Scrocca D., Trumpy E., 2017. Data integration and conceptual modelling of the Larderello geothermal area, Italy. Energy Procedia, 125, 300-309.

Guglielmetti, L., Comina, C., Abdelfettah, Y., Schill, E. & Mandrone, G., 2013. Integration of 3d geological modeling and gravity surveys for geothermal prospection in an alpine region, Tectonophysics, 608, 1025–1036.

Hermans, T.; Wildemeersch, S.; Jamin, P.; Orban, P.; Brouyère, S.; Dassargues, A.; Nguyen, F. Quantitative temperature monitoring of a heat tracing experiment using cross-borehole ERT. Geothermics 2015, 53, 14–26.

Irons, T.P., McPhserson, B.J.O.L., Moodie, N., Krahenbuhl, R., Li, Y., 2018. Integrating geophysical monitoring data into multiphase fluid flow reservoir simulation. AEGC 2018: Sydney, Australia.

Irving, J., and K. Singha (2010), Stochastic inversion of tracer test and electrical geophysical data to estimate hydraulic conductivities, Water Resour. Res., 46(11), W11514, doi:10.1029/2009WR008340.

ISPRA, 2002. Geological map of Italy at scale 1:50.000. http://www.isprambiente.gov.it/Media/carg/306_MASSA_MARITTIMA/Foglio.html.

Kana, J.D., Djongyang,N., Raïdandi, D., Nouck, P.N., Dadjé, A., 2015. A review of geophysical methods for geothermal exploration. Renewable and Sustainable Energy Reviews, 44 (2015), 87–95.

Kästner, F., Giese, R., Planke, S., Millett, J.M., Flóvenz, O.G., 2020. Seismic imaging in the Krafla high-temperature geothermal field, NE Iceland, using zero- and far-offset vertical seismic profiling (VSP) data. Journal of Volcanology and Geothermal Research, 391, 106315.

Kiessling, D., Schmidt-Hattenberger, C., Schuett, H., Schilling, F., Krueger, K., Schoebel, B., Danckwardt, E., Kummerow, J. and the CO2SINK group, 2010: Geoelectrical methods for monitoring geological CO2 storage, First results from crosshole and surface-downhole measurements from the CO2SINK test site at Ketzin (Germany). – International Journal of Greenhouse Gas Control, 4, 816-826.

Kosinski, W. K., Kelly, W. E. 1981. Geoelectric soundings for predicting aquifer properties. Ground Water 19, 163-171.

LaBrecque, D. J., G. Heath, R. Sharpe, and R. Versteeg, 2004, Autonomous monitoring of fluid movement using 3D electrical resistivity tomography: Journal of Environmental and Engineering Geophysics, 9, no. 3, 167–176.

LaBrecque, D., G. Morelli, W. Daily, A. Ramirez, and P. Lundegard (1999), Occam's inversion of 3D electrical resistivity tomography, in ThreeDimensional Eelectromagnetics, edited by M. Oristaglio, B. Spies, and M. R. Cooper, pp. 575 – 590, Soc. of Explor. Geophys., Tulsa, Okla.

Leontarakis K., Apostolopoulos G. V., 2012. Laboratory study of the cross-hole resistivity tomography: The Model Stacking (MOST) Technique, Journal of Applied Geophysics, 80, 67-82.

Lesparre, N., Robert, T., Nguyen, F., Boyle, A., Hermans, T., 2019. 4D electrical resistivity tomography (ERT) for aquifer thermal energy storage monitoring. Geothermics, 77, 368-382.

Liotta D and Brogi A.: 2020. Pliocene-Quaternary fault kinematics in the Larderello geothermal area (Italy): Insights for the interpretation of the present stress field. Geothermics, 83, 101714.

Manzella A.: 2004 Resistivity and heterogeneity of Earth crust in an active tectonic region, southern Tuscany, Italy. Annals of Geophysics, 47, 107-118.

Manzella A., Bonciani R., Allansdottir A., Botteghi S., Donato A., Giamberini S., Lenzi A., Paci b M., Pellizzone A., Scrocca D., 2018. Environmental and social aspects of geothermal energy in Italy. Geothermics, 72, March 2018, Pages 232-248.

Majer, E. (2003). 3-D Seismic Methods for Geothermal Reservoir Exploration and Assessment--Summary. Lawrence Berkeley National Laboratory, 1-33.

Morelli, G. and LaBrecque, D.J. 1996. Advances in ERT inverse modeling. European Journal of EEGS 1, 171–186

Muñoz, G.: Exploring for Geothermal Resources with Electromagnetic Methods. Surveys in Geophysics 35.1 (2014), 101-122.

Musumeci G., Bocini L., Corsi R., 2002. Alpine tectonothermal evolution of the Tuscan Metamorphic Complex in the Larderello geothermal field (northern Apennines, Italy). Journal of the Geological Society, London, Vol. 159, 443–456.

Orlando L. 2005. Interpretation of Tuscan gravity data. Bull. Soc. Geol. It., Special Issue n. 3., 179-186.

Palacios A., Ledo J.J., Linde N., Luquot L., Bellmunt F., Folch A., Marcuello A., Queralt P., Pezard P.A., Martínez L., del Val L., Bosch D., Carrera J., 2020. Time-lapse cross-hole electrical resistivity tomography (CHERT) for monitoring seawater intrusion dynamics in a Mediterranean aquifer. Hydrol. Earth Syst. Sci., 24, 2121–2139.

Pandeli, E., Bertini G., Castellucci, P. (1991). The tectonic wedge complex of the Larderello area (Southern Tuscany, Italy). Boll. Soc. Geol. It., 110, 621-629

Pandeli, E., Gianelli, G., Puxeddu, M. and Elter, F.M. (1994). The Paleozoic Basement of the Northern Apennines: stratigraphy, tectono-metamorphic evolution and alpine hydrothermal processes. Memorie Società geologica italiana, Vol. 48, pp. 627-654.

Pechnig R., Niederau J., Rabbel W., 2018. Petrophysical Characteristics of Basement Rocks –Results of Log and Core Data Interpretation. In Manzella A., Botteghi S., Trumpy E., D6.3 Proceedings of the DESCRAMBLE project Final Conference, 25-28.Pucci S., R. Civico, F. Villani, T. Ricci, E. Delcher, A. Finizola, V. Sapia, P. M. De Martini, D. Pantosti, S. Barde-Cabusson, E. Brothelande, R. Gusset, C. Mezon, S. Orefice, A. Peltier, M. Poret, L. Torres, B. Suski. Deep electrical resistivity tomography along the tectonically active Middle Aterno Valley (2009 L'Aquila earthquake area, central Italy). Geophys J Int (2016) 207 (2): 967-982.

Pucci S., R. Civico, F. Villani, T. Ricci, E. Delcher, A. Finizola, V. Sapia, P. M. De Martini, D. Pantosti, S. Barde- Cabusson, E. Brothelande, R. Gusset, C. Mezon, S. Orefice, A. Peltier, M. Poret, L. Torres, B. Suski. Deep electrical resistivity tomography along the tectonically active Middle Aterno Valley (2009 L'Aquila earthquake area, central Italy). Geophys J Int, 207 (2), 967-982.

Rizzo, E., Colella, A., Lapenna, V. and Piscitelli, S. 2004. High-resolution images of the fault controlled High Agri Valley basin (Southern Italy) with deep and shallow Electrical Resistivity Tomographies. Physics and Chemistry of the Earth, 29, 321-327.

Rizzo E. and Giampaolo V., 2019. New Deep Electrical Resistivity Tomography in the High Agri Valley basin (Basilicata, Southern Italy). Geomatics Natural Hazards and Risk, doi: 10.1080/19475705.2018.1520150, in press.

Rizzo E., Giampaolo V., Capozzoli L., Grimaldi S., 2019a. Deep Electrical Resistivity Tomography for the Hydrogeological Setting of Muro Lucano Mounts Aquifer (Basilicata, Southern Italy). Geofluids, Volume 2019, Article ID 6594983, 11 pages.

Rizzo E., S. Piscitelli, J. Bellanova, L. Capozzoli, G. De Martino, M. Guerriero, G. Morelli, F. Fischanger, R. Caputo e V. Lapenna (2019b). Tomografie Geoelettriche Profonde (DERT) per lo studio geologico-idrogeologico di Ferrara. Bollettino di Geofisica Teorica e Applicata, 60, n.Suppl. 2, s100-s105.

Rochira, F., Caggianelli, A., de Lorenzo, S., 2018. Regional thermo-rheological field related to granite emplacement in the upper crust: implications for the Larderello area (Tuscany, Italy). Geodin. Acta 30, 225–240.

Romagnoli, P., Arias, A., Barelli, A., Cei, M. and Casini, M., 2010. An updated numerical model of the Larderello–Travale geothermal system, Italy. Geothermics, 39, 292-313.

Rosenkjær K., Karlsdóttir R., Botteghi S., Calvi E., Donato A., Gola G., Manzella A., Montegrossi G., Santilano A., Trumpy E., Trifirò S., Capozzoli L., De Martino G., Giampaolo V., Perciante F., Rizzo E., Romano G., Godio A., 2017. MT-Inversion techniques with external constraints. IMAGE-D5.6, 65 pages.

Rücher C. and Günther T., 2011. The simulation of finite ERT electrodes using the complete electrode model. Geophysics, 76 (4), F227-F238.

Saccorotti, G., Piccinini, D. Zupo, M., Mazzarini, F., Chiarabba, C., Piana Agostinetti, N. Licciardi, A. and Bagaglia, M. 2014. The deep structure of the Larderello-Travale geothermal field (Italy) from integrated, passive seismic investigations. Energy Procedia 59 (2014) 227 – 234.

Santilano, A., 2017. Deep geothermal exploration by means of electromagnetic methods: new insights from the Larderello geothermal field (Italy). Doctoral dissertation, Politecnico di Torino

Santilano, A., Manzella, A., Gianelli, G., Donato, A., Gola, G., Nardini, I., Trumpy E., Botteghi, S. 2015a. Convective, intrusive geothermal plays: What about tectonics?. Geothermal Energy Science, 3, 51–59.

Santilano A., Godio A., Manzella A., Menghini A., Rizzo E, Romano G., 2015b. Electromagnetic and DC methods for geothermal exploration in Italy, state-of-the-art, case studies and future developments. First Break, 33 (8), 81-86.

Santilano A., Godio A., Manzella A., Dini I., 2015. Electrical resistivity structures and their relation to geological features at the Larderello geothermal field (Italy). Near Surface Geoscience, Turin, Italy, 6-10 September 2015.

Schmelzbach, C., Greenhalgh, S., Reiser, F., Girard, J., Bretaudeau, F., Capar, L., Bitri, A., 2016. Advanced seismic processing/imaging techniques and their potential for geothermal exploration. Interpretation, 4:4, SR1-SR18.

Schmidt-Hattenberger, C., P. Bergmann, D. Kiessling, K. Krüger, C. Rücker, and H. Schütt, CO2SINK Group, 2011, Application of a vertical electrical resistivity array (VERA) for monitoring CO2 migration at the Ketzin site: First performance evaluation: Energy Procedia, 4, 3363–3370.

Slater, L., Binley, A., 2003. Evaluation of permeable reactive barrier (PRB) integrity using electrical imaging methods. Geophysics 68, 911–921.

Slater, L., M. D. Zaidman, A. M. Binley and L. J. West, Electrical imaging of saline tracer migration for the investigation of unsaturated zone transport mechanisms, Hydrology and Earth System Sciences, 1(2): 291-302, 1997.

Spichak V., Manzella A.: *Electromagnetic sounding of geothermal zones*. Journal of Applied Geophysics, 68, 459–478, 2009.

Spichak, V.V., Zakharova, O.K., 2015. Electromagnetic Geothermometry. Elsevier, 1-183.

Storz, H., W. Storz and F. Jacobs (2000): Electrical resistivity tomography to investigate geological structures of the earth's upper crust, Geophysical Prospecting, 48, 455-471.

Suzuki, K., Toda, S., Kusunoki, K., Fujimitsu, Y., Mogi, T., Jomori, A., 2000. Case studies of electrical and electromagnetic methods applied to mapping active faults beneath the thick quaternary, Engineering Geology, 56, 29-45.

Tamburriello G., Balasco M., Rizzo E., Harabaglia P., Lapenna V., Siniscalchi A., 2008. Deep electrical resistivity tomography and geothermal analysis of Bradano foredeep deposits in Venosa area (Southern Italy): preliminary results, Annals of Geophysics, Vol 51, N. 1.

Thompson S., B. Kulessa, D. I. Benn, J. R. Mertes, 2017. Anatomy of terminal moraine segments and implied lake stability on Ngozumpa Glacier, Nepal, from electrical resistivity tomography (ERT). Scientific Reports, 7:46766.

Tietze, K., Ritter, O., Veeken, P., 2015. Controlled-source electromagnetic monitoring of reservoir oil saturation using a novel borehole-to-surface configuration. Geophysical Prospecting, , 63, 1468–1490.

Tietze, K., Ritter, O. Veeken, P., 2017. Erratum/Corrigendum: Controlled-source electromagnetic monitoring of reservoir oil-saturation using a novel borehole-to-surface configuration. Geophysical Prospecting, 65: 317-321.

Troiano A., R. Isaia, M. G. Di Giuseppe, F. D. A. Tramparulo, S. Vitale, 2019. Deep Electrical Resistivity Tomography for a 3D picture of the most active sector of Campi Flegrei caldera. Scientific Reports, 9:15124.

Truesdell, A.H., Haizlip, J.R., Armannsson, H., D'Amore, F., 1989. Origin and transport of chloride in superheated geothermal steam. Geothermics, 18, 295-304.

Trumpy, E. and Manzella, A., 2017 Geothopica and the interactive analysis and visualization of the updated Italian National Geothermal Database. International Journal of Applied Earth Observation and Geoinformation, 54,28-37.

Tsourlos P., Ogilvy R., Papazachos C., Meldrum P., 2011. Measurement and inversion schemes for single borehole-to-surface electrical resistivity tomography surveys. Journal of Geophysics and Engineering, 8, 4, 487–497.

Tuscan Region web site, 2015. Continuum Geologico at scale 1:10000. http://www502.regione.toscana.it/geoscopio/geologia.html

Villa M. and Puxeddu M., 1994. Geochronology of the Larderello geothermal field: new data and the «closure temperature» issue. Contrib. Mineral. Petrol., 315, 4 15-426.

Wagner, F. M., Bergmann, P., Rücker, C., Wiese, B., Labitzke, T., Schmidt-Hattenberger, C., Maurer, H., 2015. Impact and mitigation of borehole related effects in permanent crosshole resistivity imaging: An example from the Ketzin CO2 storage site. Journal of Applied Geophysics, 123, 102-111.

Wilkinson, P.B., Chambers, J.E., Meldrum, P.I., Ogilvy, R.D., Caunt, S., 2006. Optimization of array configurations and panel combinations for the detection and imaging of abandoned mineshafts using 3D cross-hole electrical resistivity tomography. Journal of Environmental and Engineering Geophysics 11, 213–221.

Witter, J.B., Siler, D.L., Faulds, J.E., Hinz, N.H., 2016. 3D geophysical inversion modeling of gravity data to test the 3D geologic model of the bradys geothermal area, Nevada, USA. Geother. Ener., 4(1), 14.

Table 1 – Venelle2 well stratigraphy.

m (from ground level)	**Stratigraphy**
0 ÷ 260	Neogenic and Quaternary deposits
260 ÷ 640	Clayey-marly units in flysch facies of the Ligurian l.s. Complex
640 ÷ 1020	Tectonic Wedge Complex
1020 ÷ 2234	Phyllitic–Quartzitic Group

Table 2 – Material used for the assemblage of the ad-hoc multipolar geoelectrical in-hole cable.

N.	Type	Length	Diameter	Function and characteristics
1	Steel cable	2000 m	4 mm	To increase the traction resistance of the entire cable.
12	Sheathed monopolar copper electric cables	1500 ÷ 2000 m	2 mm	To connect the electrodes to the surface acquisition system. They are resistant to temperatures up to 250° C.
12	Cylindrical steel electrodes	1.5 m	20 mm	To inject current (A) and measures electric potential values (V) in the borehole. They are flexible, to allow a better descent in the borehole, and resistant to high temperatures. They were mechanically connected to copper cables and coupled to the entire cable by hardening foam.
3	Heat shrinks tubing	1500 ÷ 2000 m	16, 19, and 33 mm	To increase the traction and rub resistance of the entire cable.
1	Tape	-	-	It is resistant to medium temperatures.

Figures

Figure 1 – (a) Geological map and geological cross sections of the study area (modified form Liotta and Brogi, 2020). The red dot is Venelle2 well, the red square represents the 3D DERT survey area. (b) Schematic crustal section below Larderello-Travale Geothermal Area and magma emplacement conceptual model, (c) structural stratigraphic framework and the modelled geological surfaces, (d) Temperature evidence from the mineral assemblage of the Plio-Quaternary HT-LP metamorphism (Bt: Biotite, Crd: Cordierite, Chl: Chlorite, Mus: Muscovite, Cor: Corindum), modified from Gola et al. (2017).

Figure 2 – a) Lithology results of multi mineral and standard approach. (Pechnig et al., 2018); b) Temperature data collected in the Venelle-2 well during DESCRAMBLE project (Bertani et al., 2018).

Figure 3 – Realization of ad-hoc multiconductor geoelectrical cable for down-hole electrical resistivity measurements: a) electrical cables assembling, b) steel electrodes placements, c) cylindrical weight; d) heat shrink tubing; e) final packaged cable.

Figure 4 – Position of surface electrodes in an area of about 4 x 5 km surrounding the Venelle2 well.

Figure 5 – Disposition of the multi-conductor in the Venelle2 well: a) installation of the pulley on the top of the hole; b) installation of the stuffing box; c) installation of the pulley close the hole; d) winch system; e) final distribution of the 12 steel electrodes in the hole.

Figure 6 – Data analysis: a) an example of the injected current square waves (A); b) the amplitude of the current signal after FFT; c) an example of the original potential difference (mV) data set with spikes; d) the potential difference (mV) data after the spike removing with polynomial fit (red line);

e) the potential difference (mV) data after the de-trending approach; f) the amplitude of the potential difference signal after FFT.

Figure 7 – (a) 3D distribution of the surface-borehole apparent electrical resistivity data acquired; (b) 3D distribution of all apparent electrical resistivity data acquired.

Figure 8 – a) 3D S-DERT and b) resistivity isosurfaces obtained using only surface electrodes.

Figure 9 – a) 3D Full data DERT and b) resistivity isosurfaces obtained using both surface and borehole electrodes.

Figure 10 – Available geological and lithostratigraphic information of the investigated area near Venelle2 well along A-A' (c) and B-B' (d) profiles. Temperature logs of geothermal wells along A-A' and B-B' profiles (b). In brackets, the year in which temperature log were acquired

Figure 11 - 2D deep electrical resistivity tomography along profiles SE-NW direction (a, c) and NE-SW direction (b, d) delineated in A-A' and B-B' lines in figure 10. They are extracted from 3D S-DERT (a, b) and 3D full data DERT (c, d). The resistivity is in Ωm and the red dots are surface and borehole electrodes.

Figure 12 - 2D sections extracted from the full 3D DERT image along profiles A-A' and B-B' compared with the lithostratigraphic information (a, c) and the porosity and temperature dataset (b, d).

Figure 13. Resistivity data extracted from the 3D resistivity inverted model plotted vs temperature data (a) and the fit correlation (b) taking in account the equation 4 (without the previous outliers).

Figure 14 – 2D MT profiles in the Lago basin area (modified from Santilano, 2017). 1) Quaternary deposits; 2) Neoautochthonous terrigenous deposits (Miocene-Pliocene); 3) Ligurian and sub-Ligurian Flysch complex (Jurassic-Eocene); 4) Tuscan Nappe formations (Upper Trias-Miocene); 5) Calcare Cavernoso and anhydrites; 6) Metamorphic Units (Paleozoic); 7) area investigated by MT surveys; 8) area investigated by the new 3D deep electrical resistivity survey. The red squares on the MT profiles (P1 and P3) are the coverage area by DERT survey.

Figure 1

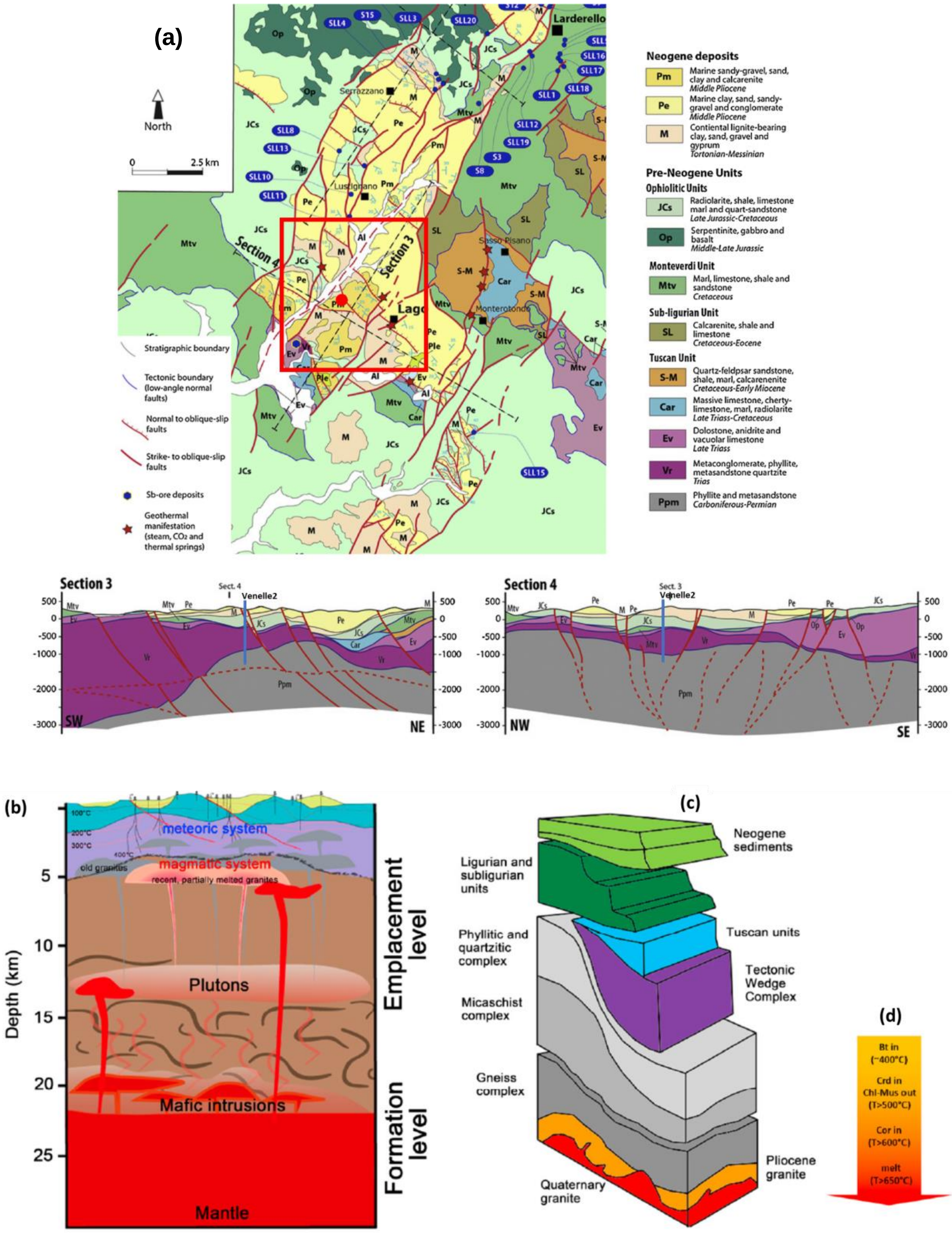
(a)
North
0
2.5 km
Larderello
Serrazzano
Lustignano
Sasso Pisano
Monterotondo
Lago
Section 4
Section 3
Stratigraphic boundary
Tectonic boundary (low-angle normal faults)
Normal to oblique-slip faults
Strike- to oblique-slip faults
Sb-ore deposits
Geothermal manifestation (steam, CO2 and thermal springs)
Neogene deposits
Pm Marine sandy-gravel, sand, clay and calcarenite Middle Pliocene
Pe Marine clay, sand, sandy-gravel and conglomerate Middle Pliocene
M Continental lignite-bearing clay, sand, gravel and gyprum Tortonian-Messinian
Pre-Neogene Units
Ophiolitic Units
JCs Radiolarite, shale, limestone marl and quart-sandstone Late Jurassic-Cretaceous
Op Serpentinite, gabbro and basalt Middle-Late Jurassic
Monteverdi Unit
Mtv Marl, limestone, shale and sandstone Cretaceous
Sub-ligurian Unit
SL Calcarenite, shale and limestone Cretaceous-Eocene
Tuscan Unit
S-M Quartz-feldspar sandstone, shale, marl, calcarenenite Cretaceous-Early Miocene
Car Massive limestone, cherty-limestone, marl, radiolarite Late Triass-Cretaceous
Ev Dolostone, anidrite and vacuolar limestone Late Triass
Vr Metaconglomerate, phyllite, metasandstone quartzite Trias
Ppm Phyllite and metasandstone Carboniferous-Permian
Section 3
Sect. 4
Venelle2
SW
NE
Section 4
Sect. 3
Venelle2
NW
SE
(b)
Depth (km)
meteoric system
magmatic system
old granites
recent, partially melted granites
Plutons
Mafic intrusions
Mantle
Emplacement level
Formation level
(c)
Neogene sediments
Ligurian and subligurian units
Tuscan units
Phyllitic and quartzitic complex
Tectonic Wedge Complex
Micaschist complex
Gneiss complex
Pliocene granite
Quaternary granite
(d)
Bt in (~400°C)
Crd in Chl-Mus out (T>500°C)
Cor in (T>600°C)
melt (T>650°C)

Figure 2

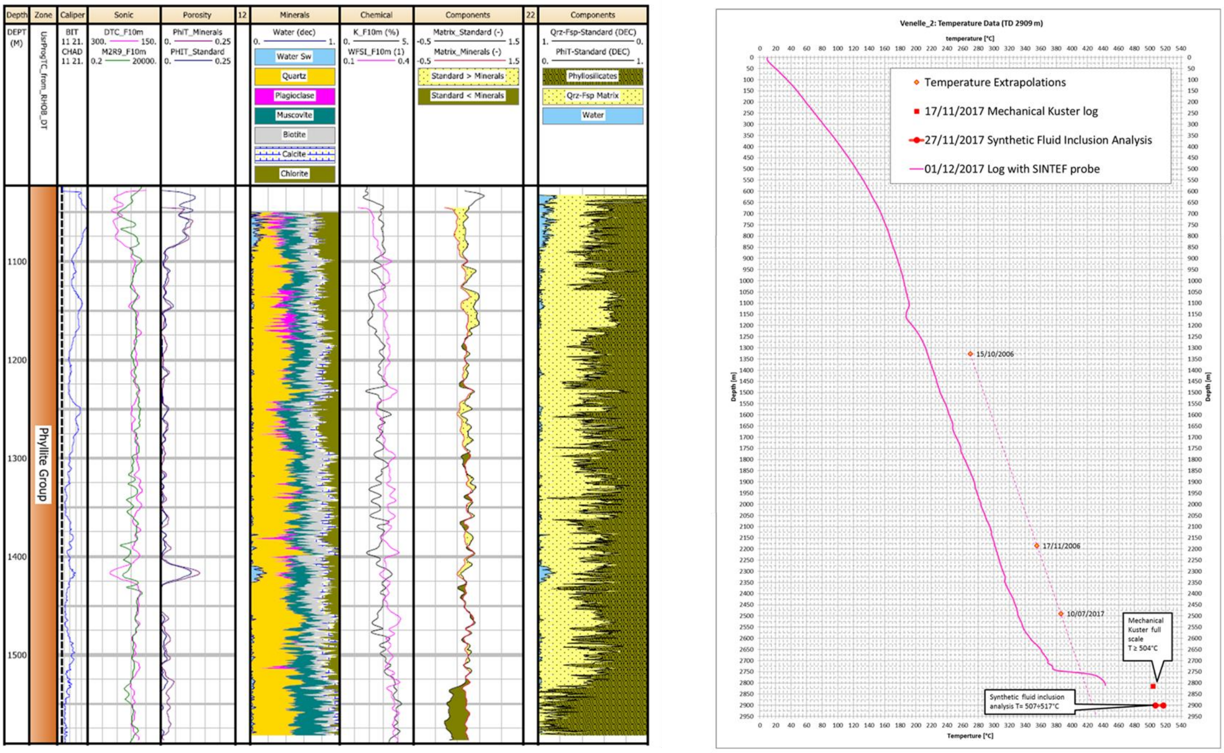

Depth
Zone
Caliper
Sonic
Porosity
Minerals
Chemical
Components
Water Sw
Quartz
Plagioclase
Muscovite
Biotite
Calcite
Chlorite
Standard > Minerals
Standard < Minerals
Phyllosilicates
Qrz-Fsp Matrix
Water
Phyllite Group
Venelle_2: Temperature Data (TD 2909 m)
Temperature Extrapolations
17/11/2017 Mechanical Kuster log
27/11/2017 Synthetic Fluid Inclusion Analysis
01/12/2017 Log with SINTEF probe
15/10/2006
17/11/2006
10/07/2017

a b

Figure 3

Figure 4

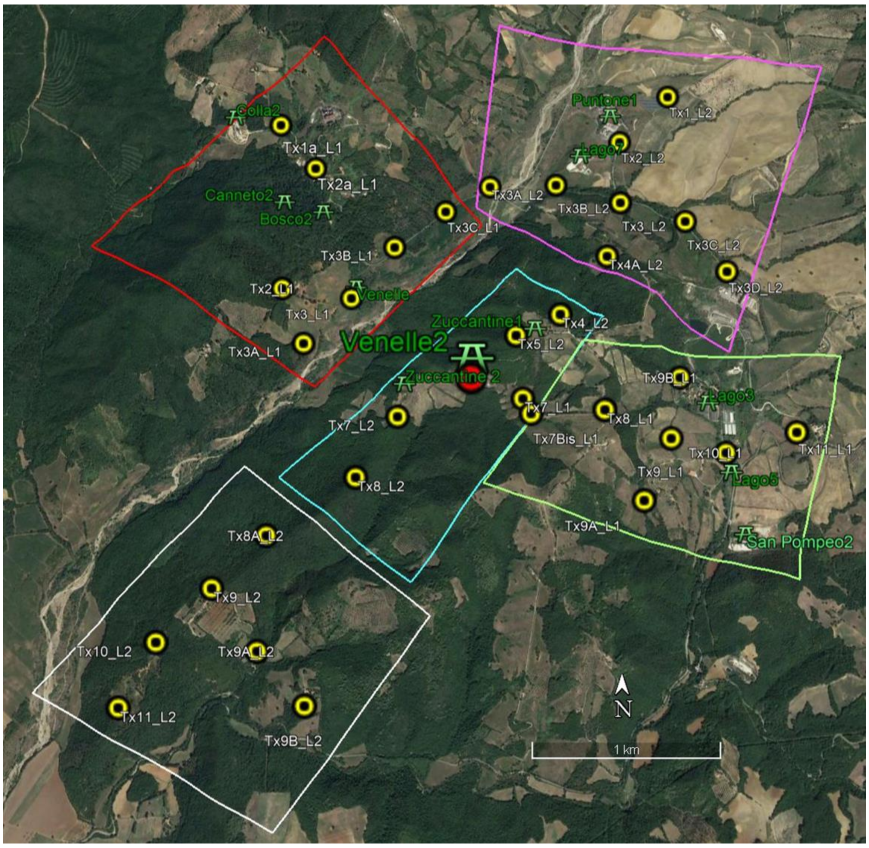
Colla2
Tx1a_L1
Tx2a_L1
Canneto2
Bosco2
Tx3B_L1
Tx3C_L1
Tx2_L1
Venelle
Tx3_L1
Tx3A_L1
Venelle2
Zuccantine1
Zuccantine 2
Puntone1
Tx1_L2
Lago7
Tx2_L2
Tx3A_L2
Tx3B_L2
Tx3_L2
Tx3C_L2
Tx4A_L2
Tx3D_L2
Tx4_L2
Tx5_L2
Tx7_L2
Tx8_L2
Tx7_L1
Tx7Bis_L1
Tx8_L1
Tx9B_L1
Lago3
Tx10_L1
Tx11_L1
Tx9_L1
Lago5
Tx9A_L1
San Pompeo2
Tx8A_L2
Tx9_L2
Tx10_L2
Tx9A_L2
Tx11_L2
Tx9B_L2
N
1 km

Figure 5

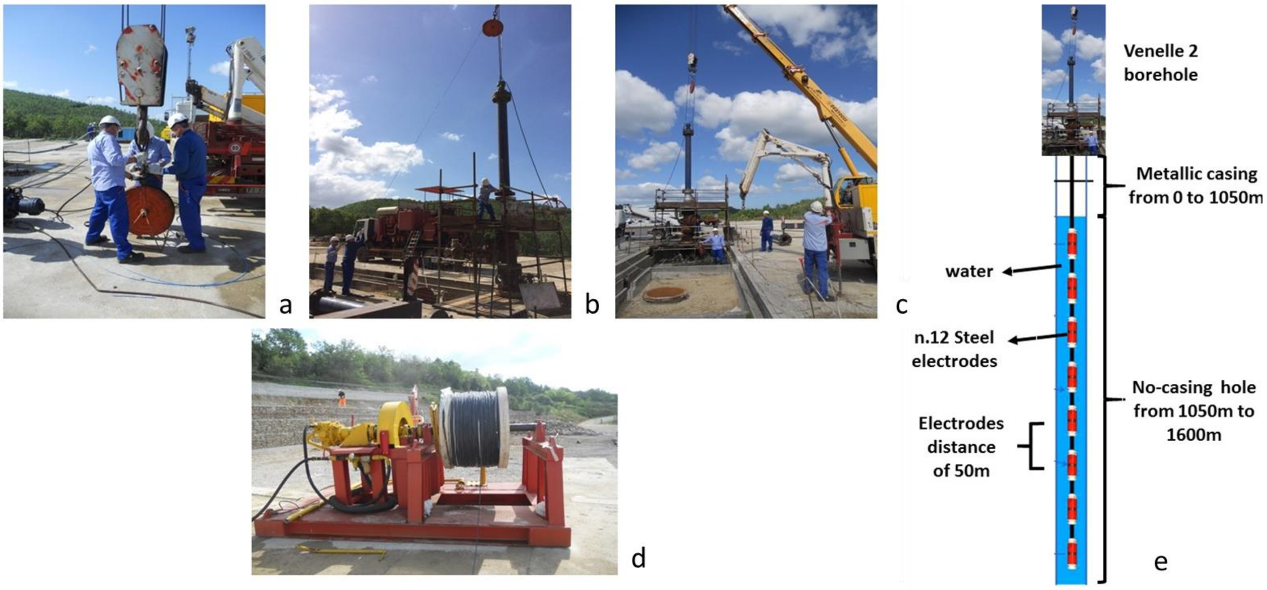

a
b
c
d
Venelle 2 borehole
Metallic casing from 0 to 1050m
water
n.12 Steel electrodes
No-casing hole from 1050m to 1600m
Electrodes distance of 50m
e

Figure 6

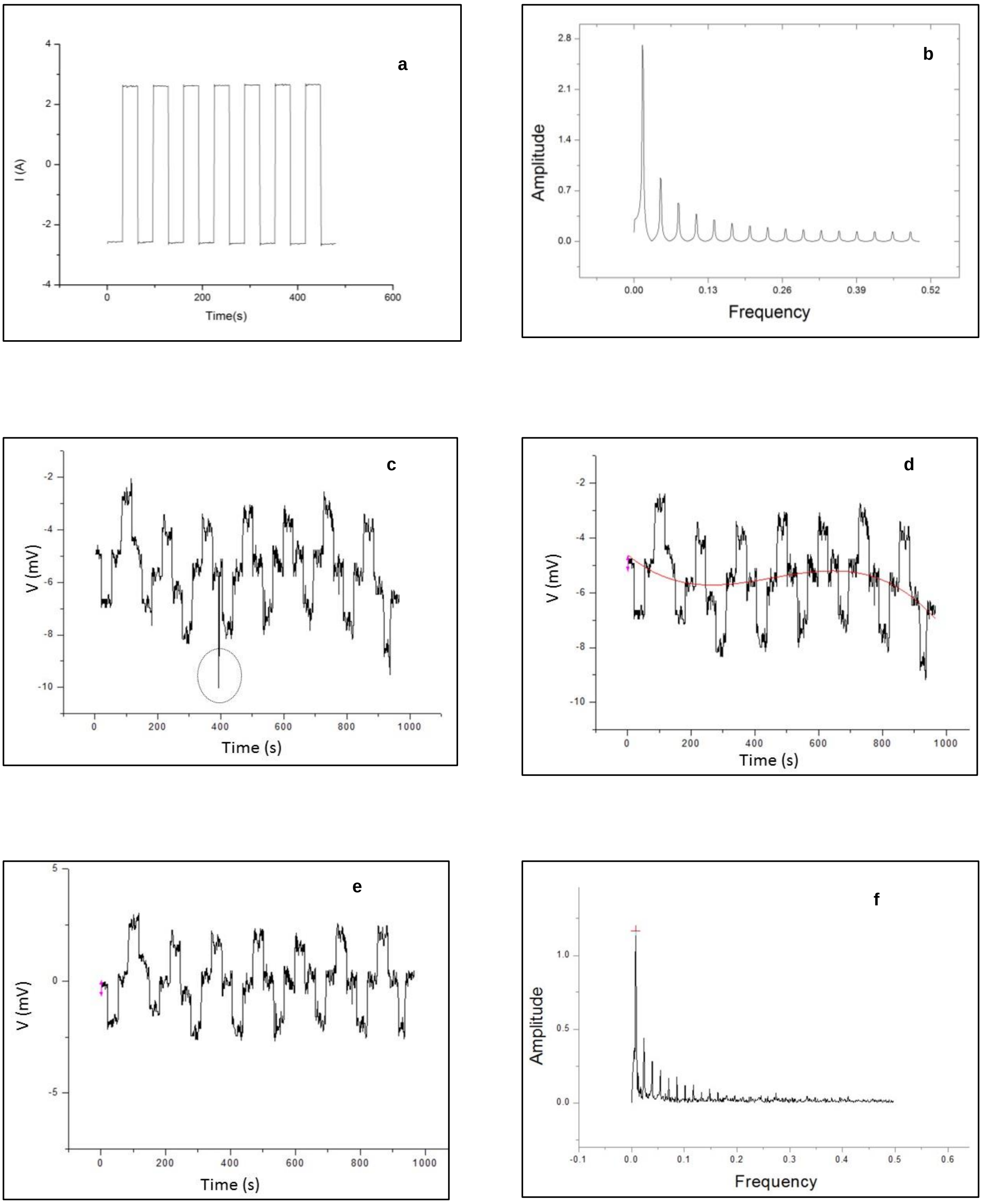
a
I (A)
4
2
0
-2
-4
0
200
400
600
Time(s)
b
Amplitude
2.8
2.1
1.4
0.7
0.0
0.00
0.13
0.26
0.39
0.52
Frequency
c
V (mV)
-2
-4
-6
-8
-10
0
200
400
600
800
1000
Time (s)
d
V (mV)
-2
-4
-6
-8
-10
0
200
400
600
800
1000
Time (s)
e
V (mV)
5
0
-5
0
200
400
600
800
1000
Time (s)
f
Amplitude
1.0
0.5
0.0
-0.1
0.0
0.1
0.2
0.3
0.4
0.5
0.6
Frequency

Figure 7

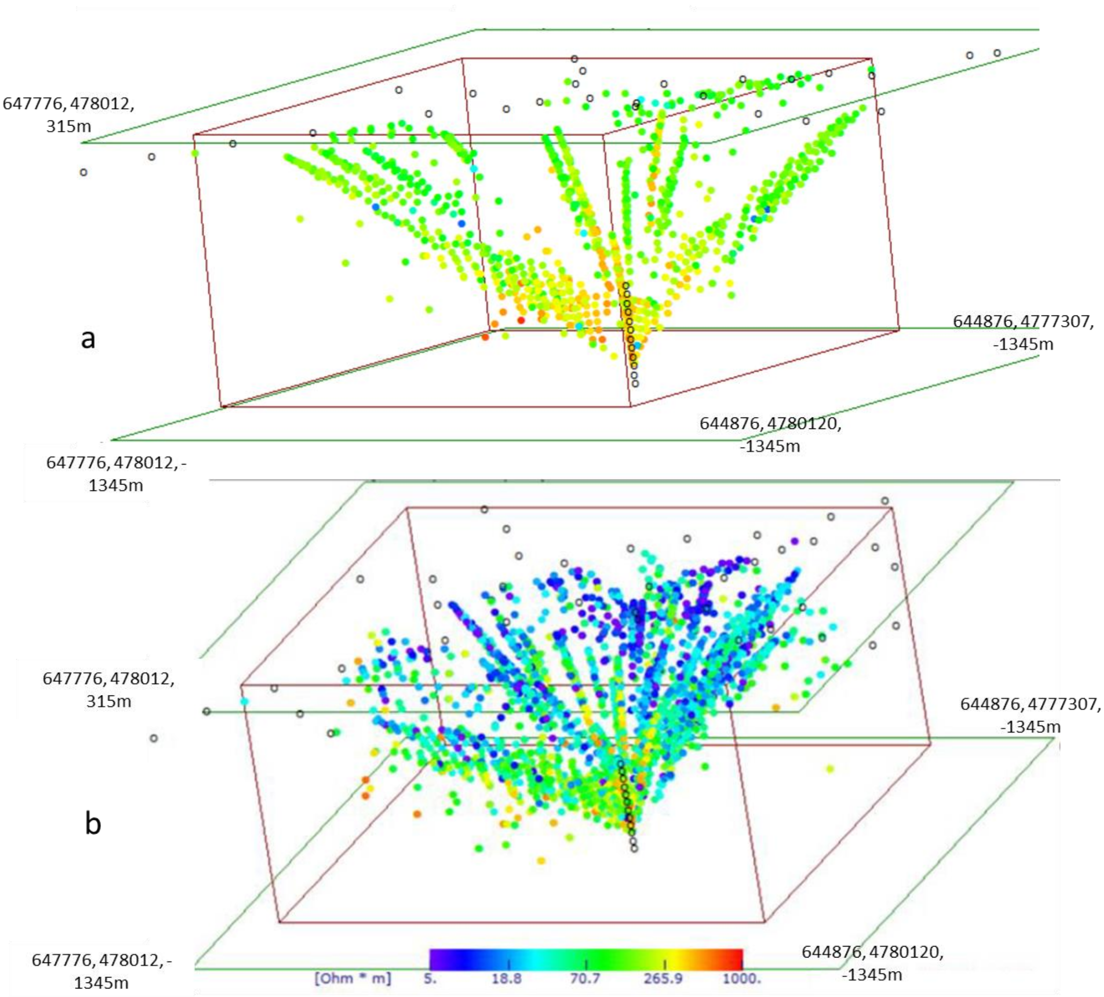

647776, 478012, 315m
a
644876, 4777307, -1345m
644876, 4780120, -1345m
647776, 478012, -1345m
647776, 478012, 315m
644876, 4777307, -1345m
b
647776, 478012, -1345m
[Ohm * m]
5.
18.8
70.7
265.9
1000.
644876, 4780120, -1345m

Figure 8

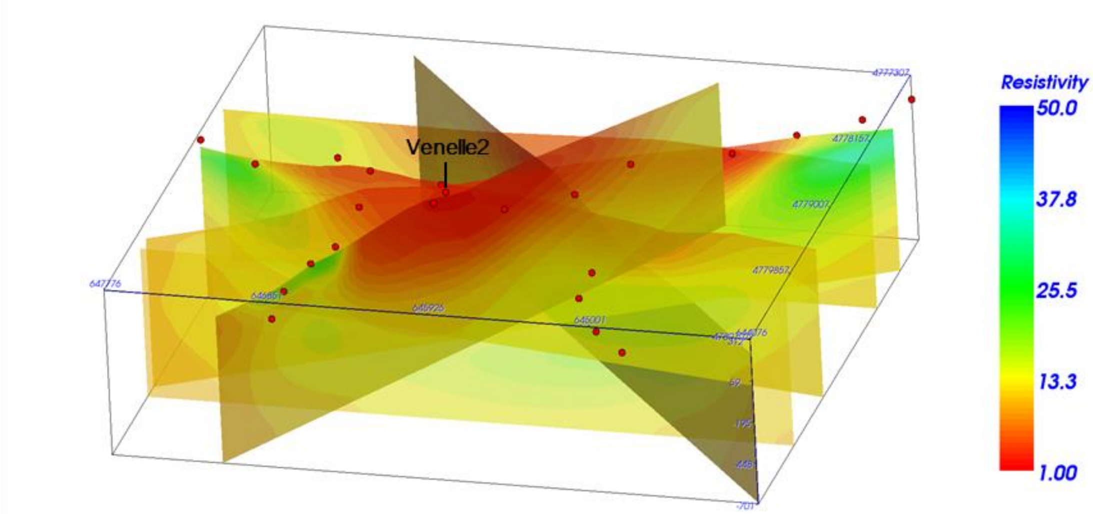
Venelle2
Resistivity
50.0
37.8
25.5
13.3
1.00

(a)

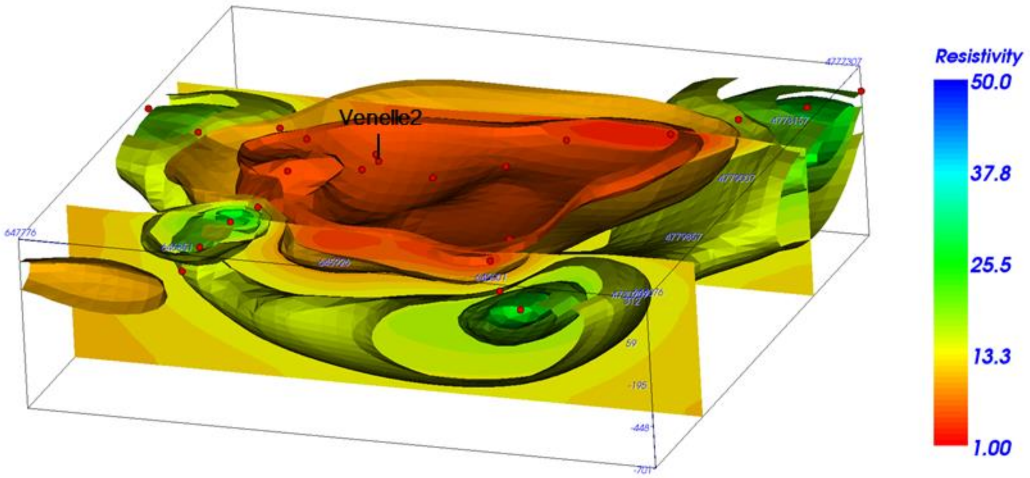
Venelle2
Resistivity
50.0
37.8
25.5
13.3
1.00

(b)

Figure 9

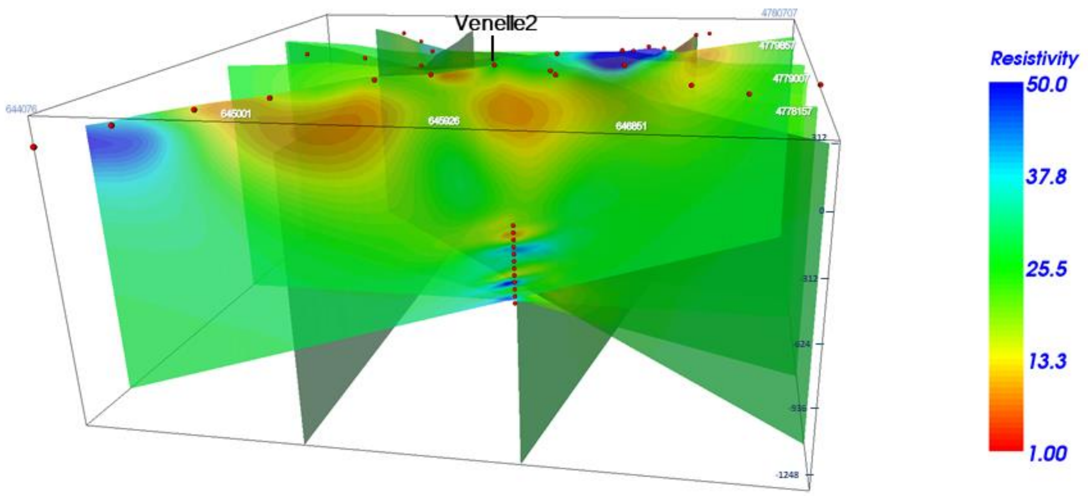
Venelle2
645001
645926
646851
4779857
4779007
4778157
Resistivity
50.0
37.8
25.5
13.3
1.00

(a)

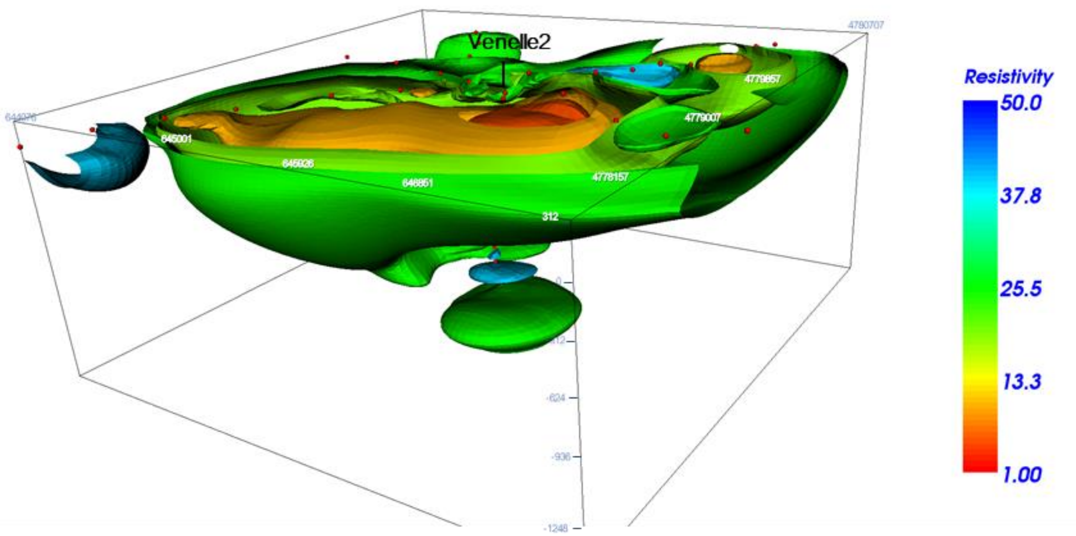
Venelle2
645001
645926
646851
4779857
4779007
4778157
312
Resistivity
50.0
37.8
25.5
13.3
1.00

(b)

Figure 10

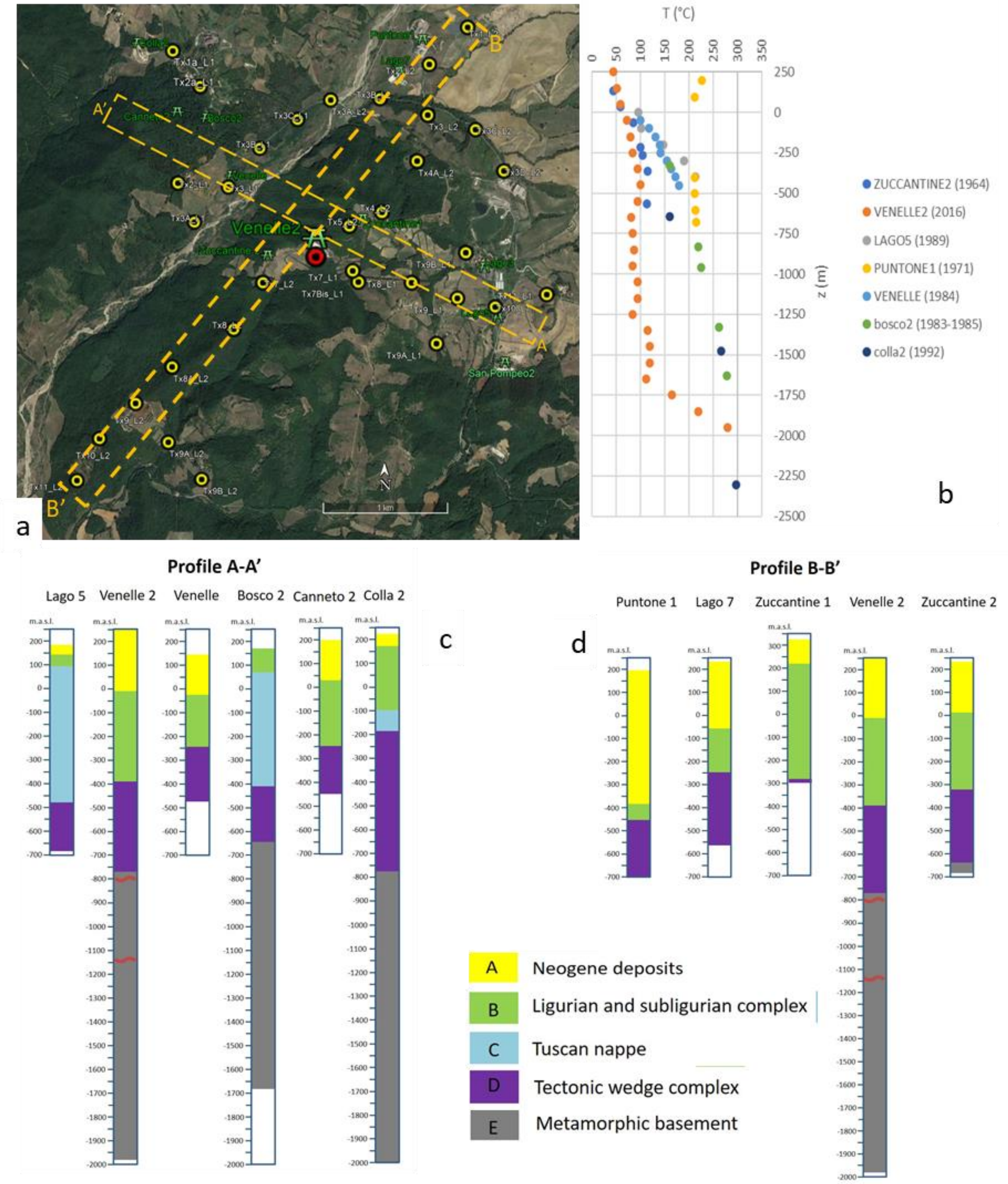

a
b
c
d
T (°C)
z (m)
ZUCCANTINE2 (1964)
VENELLE2 (2016)
LAGO5 (1989)
PUNTONE1 (1971)
VENELLE (1984)
bosco2 (1983-1985)
colla2 (1992)
Profile A-A'
Lago 5
Venelle 2
Venelle
Bosco 2
Canneto 2
Colla 2
Profile B-B'
Puntone 1
Lago 7
Zuccantine 1
Venelle 2
Zuccantine 2
m.a.s.l.
A Neogene deposits
B Ligurian and subligurian complex
C Tuscan nappe
D Tectonic wedge complex
E Metamorphic basement

Figure 11

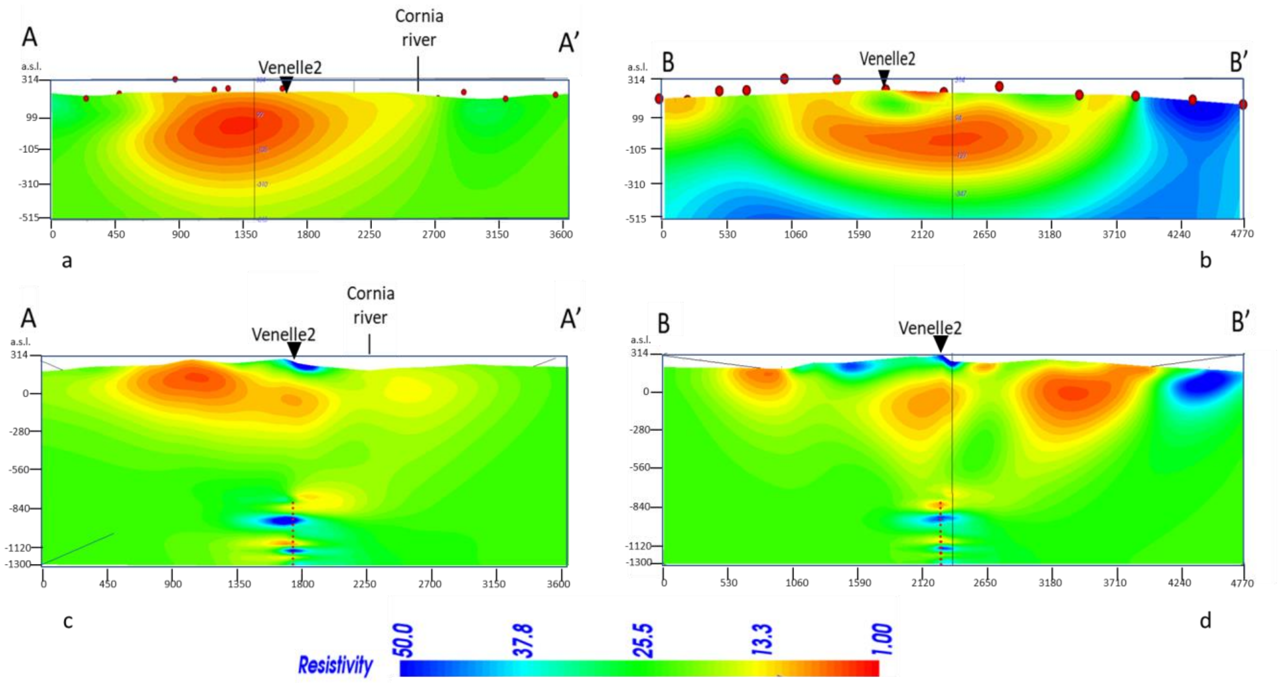

A
Cornia river
A’
a.s.l.
314
99
-105
-310
-515
Venelle2
0
450
900
1350
1800
2250
2700
3150
3600
a
B
B’
Venelle2
530
1060
1590
2120
2650
3180
3710
4240
4770
b
A
Cornia river
A’
Venelle2
-280
-560
-840
-1120
-1300
c
B
Venelle2
B’
d
Resistivity
50.0
37.8
25.5
13.3
1.00

Figure 12

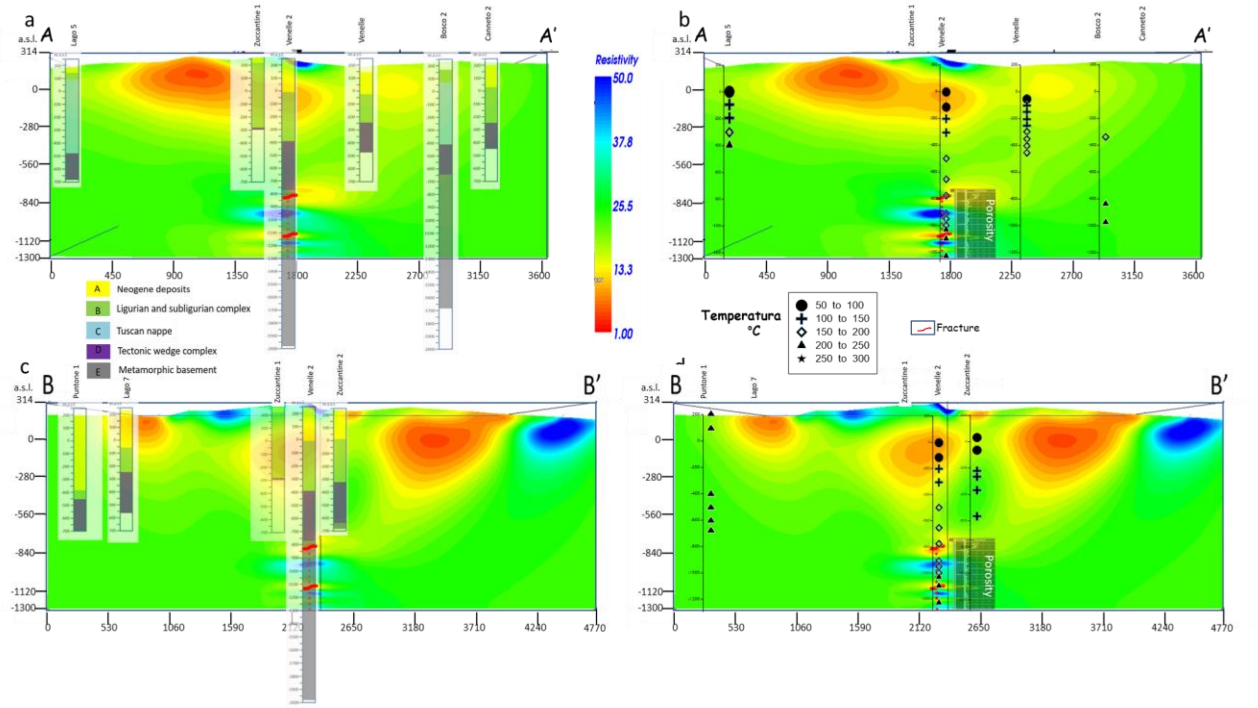

a
b
c
A
A'
B
B'
a.s.l.
Resistivity
50.0
37.8
25.5
13.3
1.00
A Neogene deposits
B Ligurian and subligurian complex
C Tuscan nappe
D Tectonic wedge complex
E Metamorphic basement
Temperatura °C
50 to 100
100 to 150
150 to 200
200 to 250
250 to 300
Fracture
Porosity

Figure 13

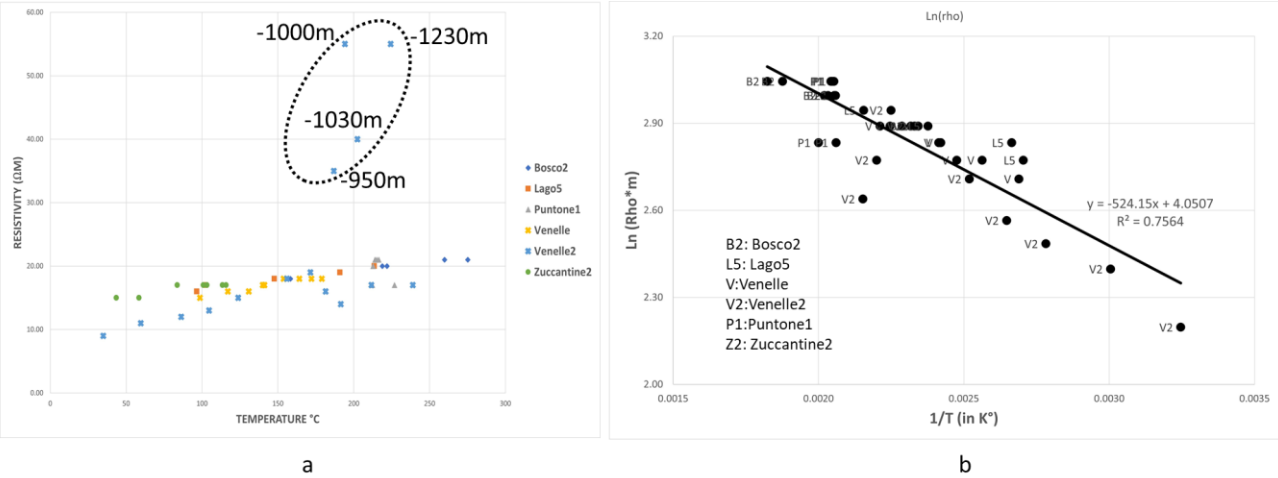

-1000m
-1230m
-1030m
-950m
RESISTIVITY (ΩM)
TEMPERATURE °C
Bosco2
Lago5
Puntone1
Venelle
Venelle2
Zuccantine2
a
Ln(rho)
Ln (Rho*m)
1/T (in K°)
y = -524.15x + 4.0507
R² = 0.7564
B2: Bosco2
L5: Lago5
V:Venelle
V2:Venelle2
P1:Puntone1
Z2: Zuccantine2
b

Figure 14

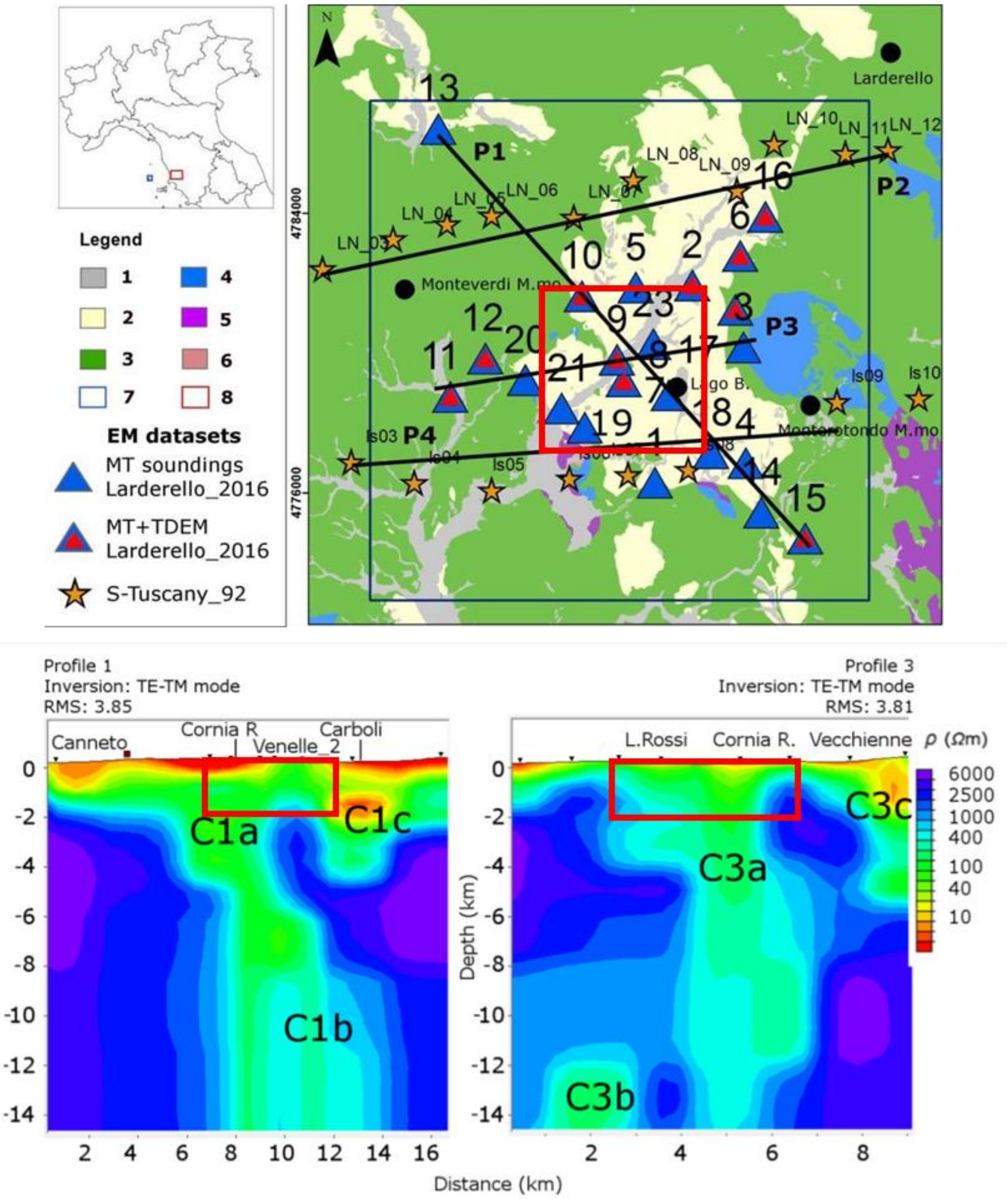
N
Larderello
Monteverdi M.mo
Lago B.
Monterotondo M.mo
P1
P2
P3
P4
LN_03
LN_04
LN_05
LN_06
LN_07
LN_08
LN_09
LN_10
LN_11
LN_12
ls03
ls04
ls05
ls09
ls10
4784000
4776000
Legend
1
2
3
4
5
6
7
8
EM datasets
MT soundings Larderello_2016
MT+TDEM Larderello_2016
S-Tuscany_92
Profile 1
Inversion: TE-TM mode
RMS: 3.85
Canneto
Cornia R
Venelle_2
Carboli
C1a
C1b
C1c
Profile 3
Inversion: TE-TM mode
RMS: 3.81
L.Rossi
Cornia R.
Vecchienne
C3a
C3b
C3c
ρ (Ωm)
6000
2500
1000
400
100
40
10
Depth (km)
Distance (km)

Highlights

- The electrical resistivity is the most useful geophysical parameter for the study of geothermal systems
- Combining surface and boreholes electrode can significantly improve the effectiveness of geoelectrical method while increasing spatial resolution at depth
- A complex geological subsurface structure is well defined using 3D data acquisition and modeling
- High temperature condition needs special sensors and cables

Graphical Abstract

Click here to access/download;Graphical Abstract;Graphic Abstract.jpg

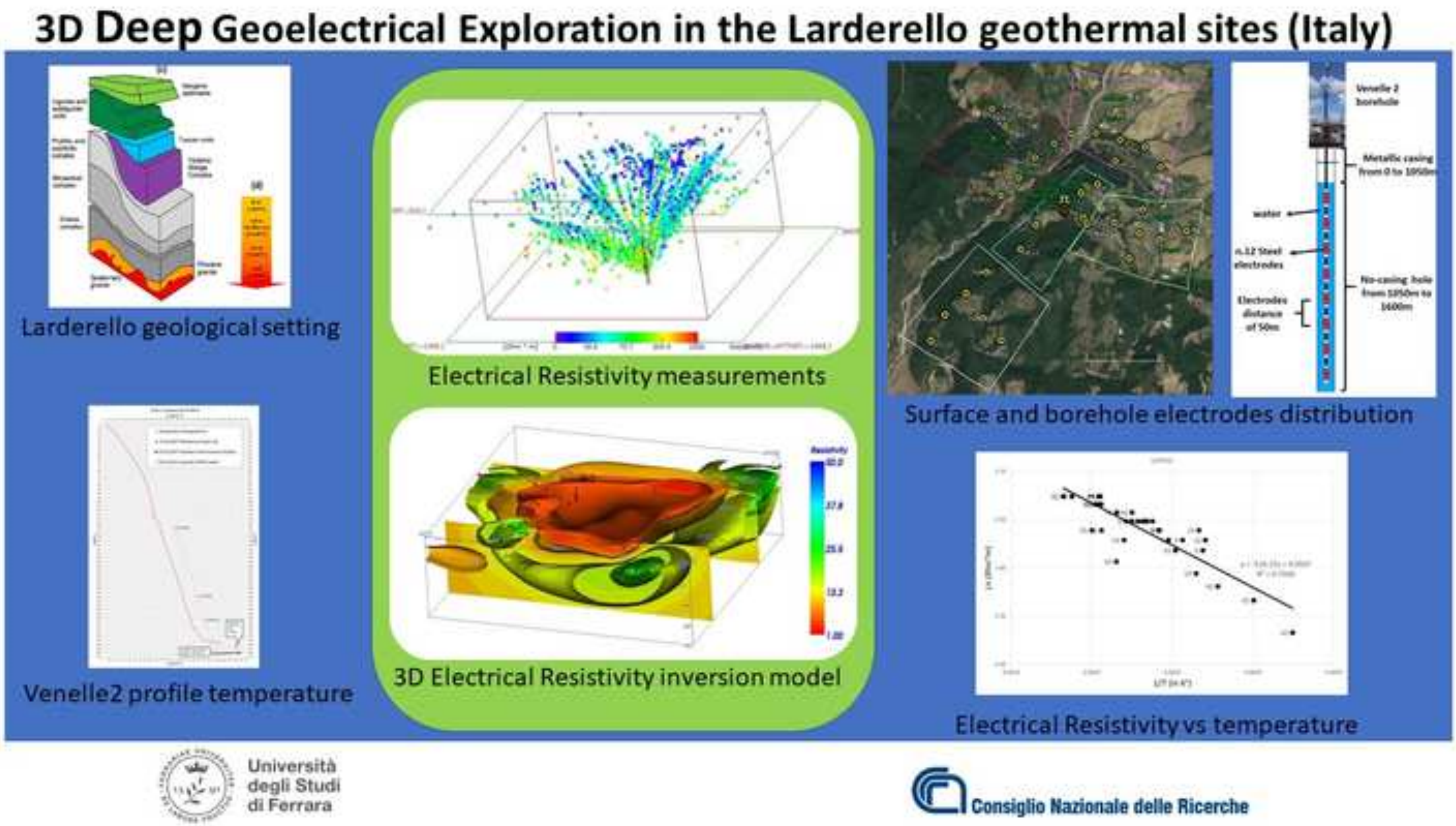

3D Deep Geoelectrical Exploration in the Larderello geothermal sites (Italy)

E. Rizzo[1,2,*], V. Giampaolo[2], L. Capozzoli[2], G. De Martino[2], G. Romano[3], A. Santilano[4], A. Manzella[4]

[1] University of Ferrara, Department of Physics and Earth Science, via Saragat,1 44122 Ferrara
[2] National Research Council, Institute of Methodologies for Environmental Analysis, Hydrogeosite Laboratory, c.da S. Loja Tito Scalo (PZ)
[4] University of Bari, Department of Earth Science and Environment
[4] National Research Council, Institute of Geosciences and Earth Resources, Via G. Moruzzi 1 56124 - Pisa

Corresponding author: enzo.rizzo@unife.it

Abstract

The paper describes a new experimental deep electrical resistivity acquisition (down to 1600 m) for exploring deep and shallow geothermal systems. The test site is located in the Larderello geothermal area, the oldest geothermal field in the world under exploitation for power production. In this area, many data have been acquired in the frame of previous exploration projects but nowadays several critical issues are still matter of debate: permeability distribution, depth and volume of the magmatic heat source, supercritical fluid condition at depth, and the occurrence of low resistivity anomalies in a dry-steam crystalline and carbonate reservoir. In order to develop new methods for contributing to the hydrothermal reservoir issues, an experimental high resolution 3D Surface-Hole Deep Electrical Resistivity Tomography (SH-DERT) was designed and the Venelle2 well in the Larderello geothermal site, hosted in the crystalline units, was used for the experiment. The design of the in-hole experiment and the results of the deep geoelectrical survey are hereby presented. SH-DERT was properly designed to face extreme conditions at depth characterizing the geothermal well. It provided a 3D resistivity distribution. Transmitting and receiving electrodes were distributed on a large surface (6 km^2) and in the Venelle2 well (down to 1600 m). The in-hole electrical cable was equipped to be able to operate in very high temperature conditions. The experiment represents a challenge and an opportunity for the applied geophysics in geothermal areas, where a lowest resistivity is highlighted in a zone above the reservoir and the resistivity of the reservoir is higher. Moreover, the relationship between temperature, clay alteration and resistivity can define a challenger to enable better prediction

of reservoir temperature distribution from resistivity measurements. It is a potential improvement of the reservoir knowledge and a useful success for exploration drilling.

Keywords: Deep Electrical Resistivity Tomography, electrical resistivity, surface-hole acquisition, geothermal site.

1. Introduction

In the Larderello geothermal system (Italy), the oldest field in the world under exploitation for power production, a vapor-dominated system with temperatures exceeding 350°C is exploited from two different reservoirs. The field is covered by a large quantity of data such as well stratigraphy, geological-structural studies, and geophysical data (e.g., magnetotelluric, active and passive seismic, thermal and gravity interpretative models). This huge amount of information allows to constrain the structure of Larderello geothermal system down to about 5 km of depth (Fiordelisi et al., 1998, Manzella, 2004; Orlando, 2005; Brogi et al., 2005; De Matteis et al., 2008; Romagnoli et al., 2010; Saccorotti et al., 2014; Gola et al., 2017; Liotta and Brogi, 2020). However, several critical issues on deep features of the field (> 5 km depth) are still matter of debate, e.g., permeability distribution in the hydrothermal reservoir, the presence of fluids at supercritical condition and the depth, and volume of the magmatic heat source. The main critical issue, that we aim to account for, is the occurrence of low resistivity anomalies in a dry-steam crystalline and carbonate reservoir (theoretically highly resistive). In detail, it must be established if the reduction in electrical resistivity in the Larderello geothermal system is linked with lithology, alteration mineralogy or occurrence of water in liquid phase (even reinjected) in pore and fractures.

Geophysical methods used for studying high-enthalpy geothermal systems (T > 250 °C) are selected according to the type and depth of the target and available budget (Kana et al., 2015). In general, active seismic and gravity are widely used (Majer, 2003; Guglielmetti et al. 2013; Altwegg et al., 2015; Schmelzbach et al., 2016; Witter et al., 2016; Kastner et al., 2020) however they are expensive and do not provide any information about the fluid distribution in the geothermal reservoir. The electrical resistivity (or conductivity) methods are the best prospecting tools for geothermal reservoirs. This is because of the high dependence of the electrical conductivity on physical parameters like temperature, porosity, pore fluid salinity, fluid saturation and the degree of interface conductivity (Flovenz et al., 2005 and 2012). Airborne and land-based electromagnetic (EM) methods, such as controlled-source electromagnetic (CSEM), magnetotelluric (MT), time domain electromagnetic (TDEM), are useful methods for geothermal resources (Demissie, Y., 2005; Santilano et al., 2015c; Spichak and Mazzella, 2009; Darnet et al., 2020a,b). Even if the EM methods are useful for deep target, they can be very challenging in noisy environment, such as urban and industrial area. Moreover, these methods suffer from the lack of spatial resolution mostly in the first 1-2 km of depth (Tietze et al., 2015, 2017; Irons et al., 2018). In the Larderello geothermal system, since the early ‘90s, several MT studies highlighted a strong heterogeneous distribution of the electrical resistivity values coupled with a large electromagnetic noise. Moreover, even if the MT method has been among the main geothermal exploration tools at the site, its resolution capacity was considered questionable. In fact, MT data quality could not exclude a bias or a noise effect, and sometimes, the misinterpretations of electrical resistivity models can lead to errors in the geothermal exploration phase (Muñoz, 2014). The electrical resistivity tomography (ERT) is largely applied in shallow investigations (< 200 m depth) to solve environmental, engineering, and geological problems (Kosinski and Kelly, 1981; Griffiths and Barker, 1993; Dahlin, 1996; Dam and Christensen, 2003; Darnet et al., 2003; Binley and Kemna, 2005). In recent years, there has been growing interest in developing cross-hole and surface-hole DC electrical surveying to image the 2D and 3D structure of the earth. Borehole geophysics uses boreholes or wells to make geophysical measurements and, compared to geophysical measurements made on the ground surface, they achieve a higher resolution at depth. For this reason, it is very commonly used in shallow environmental and hydrogeological application (< 100 m depth) as a monitoring tool (Daily et al., 1992; Slater et al., 1997; Daily and Ramirez, 2000; Binley et al., 2002; Slater and Binley, 2003; Goes and Meekes, 2004; LaBreque et al., 2004; Wilkinson et al., 2006; Chambers et al. 2007; Irving and Singha, 2010; Hermans et al., 2015; Thompson et al., 2017; Cheng et al., 2019; Palacios et al., 2020).

Moreover, improvements in field technology and data processing allow electrical resistivity method to be applied in deep investigations (down to 4 km depth) for studying geological structures (Storz et al., 2000; Suzuki et al., 2000; Rizzo et al., 2004; Giocoli et al., 2008; Balasco et al., 2011; Pucci et al., 2016; Rizzo and Giampaolo, 2019; Rizzo et al., 2019a; Rizzo et al., 2019b).

Even if the effect of geothermal fluid circulation on electrical resistivity is well known (Spichak and Manzella, 2009), deep electrical resistivity tomography (DERT) in geothermal application is much less abundant (Tamburriello et al., 2008; Santilano et al., 2015). Recently, Gresse et al. (2017) and Troiano et al. (2019) described results of 3D deep electrical resistivity surveys for characterizing the shallow hydrothermal system of the Solfatara volcano (down to 200 m of depth) and imaging the deep structure of Campi Flegrei central sector (down to 800 m of depth). These studies underline the capability of electrical resistivity to be an unrivalled indicator of the presence of deformation structures that conduit hot fluids and gases. Carrier et al. (2019) present a recent technology for geoelectrical investigation of medium-enthalpy geothermal resources until about 1 km depth in an industrial area. The adopted system is made of a distributed set of independent electric potential recorders, enabled to tackle logistics and noise data issues typical of urbanized areas.

This paper describes new electrical resistivity data, that were acquired in the Larderello area by a new electrical resistivity approach. The proposed approach permits to obtain high resolution down to 1600 m introducing an experimental setting merging deep surface and surface-down-hole DC resistivity measurements. The possibility to constrain the shallow resistivity distribution into the first 2 km with the contribution of a surface-to-borehole electrical tomography is new in the field of geothermal exploration. The experiment introduces high resolution 3D Surface-Hole Deep Electrical Resistivity Tomography (SH-DERT) carried out in a geothermal area, installing electrodes in a non-productive geothermal well (Venelle2) of the Larderello field characterized by extreme temperature conditions. At now, the only few examples of deep borehole DC electrical surveys concerns the monitoring of

CO_2 plume development in deep saline aquifers down to the maximum reached depth of 3200 m (Kiessling et al., 2010; Schmidt-Hattenberger et al., 2011; Carrigan et al., 2013; Bergmann et al., 2017). In these experiments, borehole electrodes were installed over electrically isolated well casings, covering only the target zone (along he the boreholes the maximum coverage of the electrodes was of 150 m with an electrodes vertical spacing of 10 m), while surface electrodes consist of few surface dipoles 150 m long, deployed on concentric circles approximately centered on the injection location (Bergmann et al., 2012).

Conversely, in this paper, 3D SH-DERT was carried out by lowering into Venelle2 geothermal well a 2000 m long multipolar cable, equipped with flexible, metallic electrodes. The cable was designed and built specifically for carrying out 3D surface to borehole geoelectrical measurements in the Larderello site. Moreover, 33 surface electrodes were installed around Venelle2 well, covering an area of about 15 km^2.

This experiment was aimed to characterize in detail the resistivity of rocks down to the depth reached in the well, in a much larger volume than the one sensed by standard resistivity logging data. This detailed resistivity imaging represents a valid support for verifying, interpreting, and constraining the resistivity distribution of MT data in this complex geological contest, resulting in an improved image of deep resistivity distribution down to 1600 m depth from the ground surface. For these reasons, the proposed experiment represented a challenge for the applied geophysics.

2. Overview of Larderello geothermal system

The Larderello geothermal system (Southern Tuscany, Italy) is the most ancient field in exploitation in the world, in production since 1913. It is located in the inner part of the Northern Apennine of Italy, a sector of the Apennine orogenic belt.

The present-day geologic setting is the result of a complex polyphase tectonics developed in the frame of the Apennine orogenesis as a consequence of the Cenozoic collision between the European and Adria plates (Carminati and Doglioni, 2004; Boccaletti et al., 2011).

The tectonic evolution of Southern Tuscany is still highly debated in literature. Several authors proposed a model that implies a first compression and a subsequent extensional tectonic affecting the area since at least the early Miocene (e.g., Carmignani et al., 1994; Brogi, 2006; Liotta and Brogi, 2020). Other studies suggest a more complex evolution with a prevalent contribution of compressive tectonics till the Pleistocene epoch (Bonini et al., 2001).

Southern Tuscany is characterized by shallow Moho discontinuity, crustal thinning with consequent upwelling of magma bodies and increased regional heat flow (Gianelli et al., 1997). The Larderello field is considered a convective young intrusive geothermal play (Santilano et al., 2015a). Neogene to Quaternary intrusive activity acts as heat sources of the very high temperature systems of Tuscany (as well as of other regions such as Latium and Campania), of which the most important is the Larderello field. The field produces superheated steam at a rate of 850 kg/s and its 200 wells provide fluid to 23 units with 594,5 MW of total installed capacity (Conti et al., 2016; Manzella et al., 2018).

The Larderello area consists of different geothermal fields, even though the most significant is located in the Lago Basin, where the Venelle2 well is located (fig. 1a). This basin is a tectonic depression developed during Pliocene-Pleistocene from where the bulk of electricity production derives (Barbier, 2002). In this area, temperature higher than 500° C at depths of about 3-4 km (Bertani et al., 2018) and heat flow values higher than to 1000 mW/m^2 are reached.

The Lago Basin structural depression corresponds to that crustal sector where, the shear zone is more permeable, channeling deep geothermal fluids and resulting the preferential area for escaping of derived-mantle fluids (Liotta and Brogi, 2020). The heat source of the geothermal anomaly is unknown, although teleseismic data analyses (Foley et al., 1992), interpretation of deep reflection seismic lines (Brogi et al., 2005), MT studies (Manzella, 2004) and rheological models (Gola et al., 2017; Rochira et al., 2018) suggest the occurrence of a cooling magma at 3–6 km depth (fig. 1b).

In the studied area, the most recent outcrops correspond to the Quaternary marine and continental deposits, while the oldest ones are represented by the metamorphic rocks of the Paleozoic Basement

(Bertini et al., 2006). The stratigraphy (fig. 1c) is summarized as follows (Batini et al., 2003; Romagnoli et al., 2010):

- Neogene and Quaternary deposits or Neoautochthonous complex: late Miocene to Pliocene and Quaternary, continental to marine sediments (clays, with minor sands, conglomerates and detrital limestones, gypsum);

- The Ligurian Complex l.s. (Ligurian/sub-Ligurian):

(a) the Ligurian Units, composed of remnants of Jurassic-Eocene oceanic crust and of its pelagic sedimentary cover (clayey-marly units in flysch facies)

(b) the Subligurian Units made up of arenaceous and calcareous turbidites (Late Cretaceous-Oligocene age).

- Tuscan Nappe: Triassic-Lower Miocene sedimentary cover of the Adria continental palaeomargin (arenaceous and clayey-marly formations, calcareous-siliceous rocks, dolostone and anhydrites). The Tuscan Nappe was detached from its substratum along the Triassic evaporites level and was thrust over the outer palaeogeographical domains during the Late Oligocene-Early Miocene compression. Furthermore, it is often tectonically laminated and in places shows a reduced thickness or is completely missing (Bertini et al., 1994).

In the area of Larderello geothermal reservoir, a Tectonic Wedge Complex (TWC) is present between the Tuscan Nappe and the underlying crystalline basement. It is composed of Paleozoic metamorphic rocks, Triassic metasiliciclastics, carbonates and evaporates of the Tuscan Nappe (Gianelli et al., 1978; Pandeli et al., 1991).

The Metamorphic basement is composed by three main complexes: i) Phyllitic Complex made mainly by metagraywacke (Cambrian-Devonian), and locally by carbonate–siliciclastic metasediments (Silurian-Devonian); ii) Micaschist Complex (Precambrian? - Early Paleozoic?) and iii) Gneiss Complex (Precambrian? - Early Paleozoic?).

At different depths, deep boreholes encountered granitoids and felsic dykes of the Intrusive Complex (3.8–1.3 Ma, Villa and Puxeddu, 1994; Gianelli and Laurenzi, 2001; Dini et al., 2005) whose emplacement gave rise to contact aureoles in the metamorphic host rocks (Elter and Pandeli, 1990). Moreover, hydrothermal mineral associations (Gianelli, 1994), locally no older than 270,000 years and no younger than 10,000 years (Bertini et al., 1996), partially or totally fill the fractures affecting the Larderello metamorphic rocks.

Summing up, the Larderello exploited resource is a vapor-dominated geothermal system, characterized by two different reservoirs (fig. 1c):

i) the shallow reservoir consists mainly of Mesozoic limestone and anhydrite dolostone,

ii) the deep reservoir consists mainly of Paleozoic metamorphic rocks, Plio-Quaternary granites and thermo-metamorphic rocks.

Furthermore, there is the possibility of a deep-seated geothermal reservoir with fluids at supercritical conditions at relatively shallow depth (4-8 km) below the area in correspondence of the seismic marker called K-horizon (De Franco et al., 2019).

Structural and geological data from Liotta and Brogi (2020) indicate that Lago Basin can be interpreted as a pull-apart basin. This is in fact bounded by NE-striking faults with a left-lateral shear sense, SE- or NW-dipping of about 70-80° and with length up to 15 km, accompanied by shorter almost orthogonal faults with a dominant normal component. These NE-striking faults commonly dissect a NW-striking system: at the intersections between these two faults systems, geothermal manifestations occur at the surface. The age of faults activity is at least encompassed between Pliocene and Holocene.

Recently, a dominant vertical movement along the NW and NE-striking pre-existing brittle structures has been recorded. This is linked to the competition between crustal stretching and surface uplift induced by heat flow. This implies a continuous switch of the local intermediate stress axis promoting quick changes in the direction of the maximum permeability from vertical to horizontal, thus enhancing the longevity of the geothermal system. This switch in fact let the fluids to be channeled from depth to shallower levels and to be laterally stored in structural traps, commonly located within the Triassic evaporite and/or the overlying carbonate succession and/or in the damage zone of the main faults (Liotta and Brogi, 2020).

3. Materials and Methods

The aim of the proposed experiment was to better define the deep Larderello structure with a high-resolution 3D SH-DERT.

The basic principle of the electrical resistivity method is to inject an electric current into the earth using two current electrodes *A* and *B*, then measure the potential difference through two other electrodes *M* and *N*, giving us a way to measure the electrical resistivity of the subsoil:

$$\Delta V_{MN} = I_{AB} R \tag{1}$$

where, ΔV_{MN} (Volt) is the measured voltage between electrodes *M* and *N*, I_{AB} (A) is the injected current between electrodes *A* and *B*, and R (Ω) is the resistance of the material through which the current flows.

As ΔV_{MN}, I_{AB}, and the electrode configuration are known, the resistivity of the ground can be determined; this is referred to as the “apparent resistivity” (Ωm):

$$\rho_a = K \frac{V_{MN}}{I_{AB}}. \tag{2}$$

The electrolyte resistivity is directly related to viscosity which decreases with temperature. On the contrary, the temperature dependence of the resistivity of the solid phase (rock matrix) are given by the Arrhenius relation (Caldwell et al., 1986):

$$\rho = \rho_0 \, e^{\frac{\varepsilon}{RT}} \tag{3}$$

where ε is an activation energy for the conduction process (commonly about 0.2eV in water and for saturated rocks, varying with degree of alteration), *R* is Boltzman’s constant (0.8617x10-4 eV/°K), *T* is temperature (°K) and ρ_0 is the resistivity at theoretically infinite temperature. The relationship is useful in understanding the expected effect of temperature and the alteration mechanism.

Inverse methods must be applied to apparent resistivity data in order to determine the real resistivity distribution. Moreover, *K* (m) is called geometric factor. It depends on electrodes arrangement (array) and can be calculated from the electrode spacing. There are, in fact, different electrode configurations and in general the choice is based upon the sensitivity of the device, the vertical and horizontal variations in resistivity, the depth of investigation, the cumulative sensitivity, and the length of the signal. The variety of electrode arrays located on the ground surface was summarized by Szalai and Szarka (2008). Furche and Weller (2002), Tsourlos et al. (2011), Leontarakis and Apostolopoulos (2012), and Binley (2015) described borehole electrode arrays, where electrodes can be arranged in single, two or more, vertical and horizontal boreholes.

Deep electrical resistivity tomography (DERT) technique is an unusual electrical resistivity approach, described for the first time by Hallof (1957), able to reach investigation depth > 200 m. The main concept of the deep approach consists of the use of physically separated tools between the injection system and the measured drop of potential tool. Usually, long stainless-steel current electrodes (*A* and *B*) are connected by long monopolar electric cable to a transmitting station constituted by a transmitter, a voltage regulator, and an external power system, which can inject into the ground a time-domain (50% duty cycle) square-waveforms current signal, with a maximum energizing current of 20 A. Unpolarizable potential electrodes (*M* and *N*) are connected to a multichannel receiver system composed by remote multichannel datalogger and a GPS antenna, radios connected to a personal computer, which can simultaneously record several generated voltage signals (mV) timing, and geographic position.

In general, the current and potential electrodes are arranged with Dipole–Dipole (DD) electrode configuration. The advantage of the DD with respect to the other electrode configurations lies in the fact that the distance between the measuring electrodes and the current ones is limited only in the sensitivity of the instruments and in the background noise. Therefore, it is more suitable for deep investigations (> 200 m) otherwise not to be tackled with other quadripolar configuration.

In detail, the main aim of this experiment was to acquire and analyze several electric potential (mV) recordings using sensors distributed at the ground surface and in-hole, following the injection of an electric current (A) at the ground surface, to constrain the resistivity distribution at depth of the studied area. Borehole experimental activities were carried out using the geothermal well Venelle2 (Lago Basin, Monterotondo Marittimo, Grosseto, Italy), which is one of the EGP deep well of Larderello field, drilled in the 2006 to exploit the geothermal resource but, in effect, non-productive for a low fracturing state of the rocks.

In short, the characteristics of the well were (at the moment of the geoelectrical experiment):

a) 2234 m deep, accessible down to about 1600 m;
b) temperature up to 350° C;
c) pressure up to 130 barA;
d) metallic casing down to 1020 m.

The well stratigraphic reconstruction is shown in table 1.

In 2016, Pechnig et al. (2018) recorded a suite of logging data in the open hole section of Venelle2 well down to 1600 m depth (for the basement rocks). The operation included standard physical tools such spectral gamma, induction resistivity and sonic as well as special tools such as an ultrasonic borehole wall imager and a geochemical tool (fig. 2a). Estimated porosity generated from sonic log is in general low with a mean of 2.2 %. Moreover, sonic curves and its derivates indicate two zones of increased fracturing (around 1050 m and 1400 m from the top of well), through which the high pressure and temperature vapor moves, and a greater content of water is present.

In 2017, after the here described experiment, Venelle2 well has been re-drilled and deepened up to 2900 m. Following the well deepening, temperature and pressure profiles of the well were measured reaching a bottom hole temperature higher than 400° C (fig. 2b from Bertani et al., 2018).

In order to determine high-resolution images of subsurface rock formations near the well and to delineate zones of higher permeability, 3D deep electrical resistivity imaging techniques were applied to the studied area. In particular, the experimental activities can be divided into four phases:

- phase 1: realization of an ad-hoc geoelectrical cable for deep electrical resistivity borehole measurements;
- phase 2: surface-borehole and surface-surface electrical resistivity data acquisition at the site using electrodes arranged both on the surface and in the borehole;
- phase 3: analysis and elaboration of all the acquired data (in the borehole and on surface) in order to define the 3D distribution of the apparent electrical resistivity values and, consequently, the inversion of them;
- phase 4: new deep geoelectrical data interpretation in light of available borehole log and geological data.

3.1 Resistivity field data acquisition

A special cable was built for the SH-DERT array, taking in account the maximum depth of the borehole and the minimum electrodes spacing necessary to obtain a good resolution at depth. The built multipolar geoelectrical cable is 2000 m long and resistant to temperatures up to 250° C. It was assembled in the laboratory with the materials described in table 2 (Fig.3). The first step was to interlace together 12 copper electric cables and the steel one by a tight tape for creating the multipolar geoelectrical cable core (Fig. 3a). Then, to increase its traction and rub resistance, the cable was completely coated by heat shrink tubing, leaving only 12 spaces each 50m, in correspondence of steel electrodes connection (Fig. 3d). Once assembled the cable, the steel electrodes were placed at the correct positions along the cable and connected mechanically to the corresponding copper cable (Fig. 3b). Furthermore, to ensure the electric contact between the cable and each electrode both during the descent into the borehole and the measurements phase, the cable-electrode connection has been reinforced using both a resistant to high temperatures tape and the heat shrink tubing (fig. 3b). The multipolar geoelectrical cable was coiled around a wooden reel equipped with a series of holes adaptable to the ENEL winch (fig. 3e). At the end, the cable was weighed with an iron cylinder connected to the end of the cable to facilitate the vertical descent along the borehole (fig. 3c).

One experimental work of this phase was to identify the best surface and borehole electrical dipoles arrangement, improving both the geophysical data acquisition time (respecting ENEL directives) and final results. This phase work consisted in a modelling work which taken into account the electrical resistivity distribution of the first 4 km coming from previous MT inversion models integrated with geological information. Finally, because of the reduction in geometric factors (K) increases the probability for better signal to noise levels in measured resistivities, all quadrupoles with a K > 1000 were discharged. Therefore, five areas of interest (colored boxes in fig. 4) surrounding the Venelle2 well (red dot in fig. 4) and 33 points (yellow and red points in fig. 4) represent the surface electrodes position for 3D surface-borehole and surface-surface electrical resistivity measurements. They were chosen considering the logistics and the absence of any natural and anthropic limits for power cables roll out.

The field activities were performed in two steps: SH-DERT lasted about four days of which the first day was necessary to drop the ad-hoc cable into the well and install the electrodes and the electric cable at the surface, while the Surface-Surface Deep Electrical Resistivity Tomography (S-DERT) lasted about 3 days.

In both measurement activities, current electrodes (*AB*) were connected to the Zonge transmitting station constituted by the GGT-10 transmitter and the ZMG-9 power system, while potential electrodes (*MN*) were connected to a multichannel receiver system made of 5 remotes multichannel dataloggers, radio-connected to a personal computer, simultaneously recording a total number of 32 generated voltage signals (mV). In our case, a maximum energizing current of 12 A was injected into the ground (3-12 A).

The SH-DERT measurements was to lower the ad-hoc cable in the well through a winch (fig. 5). Therefore, a long stuffing box (5 m) was installed above the pressure valve of the hole (fig. 5b), to permit the installation of the cable in the casing permitting to work safely. Successively, two pulleys were installed, one at about 3 m above the stuffing box and the second one close to the hole pressure valve (fig. 6a and 5c). The two pulleys helped the cable drop in the hole. Finally, the winch system dropped the cable in the well and, in 45 minutes, it reached the maximum pre-defined depth of about 1600 m (fig. 5d). When the winch system was switched off, the 12 electrodes were installed and located between 1050 m to 1600 m from the surface (fig. 5e). During all this experimental activity, the well was cooled by a continuous injection of 80 m^3/s condensed water (8.56 mS/cm or 1.17 Ωm) for three days in order to reach more favorable pressure and temperature condition and to allow a good electric contact between the rock and the borehole electrodes.

The second step consisted of installing on the topographic surface 33 steel current electrodes around the Venelle2 well. The investigated area was about 10 km^2 as established during the setting phase (fig. 4). The disposition of the surface electrodes and the borehole ones permitted to obtain several injection current dipoles. The transmitting system was placed in 5 different sites and the current electrodes were connected by long electric cables for a total length of about 18 km of cable used.

A DD array configuration was used. The *AB* distances ranged between 400 and 1600 m, and the *MN* distances ranged between 50 and 550 m (in the hole).

Therefore, for each current injection using a square wave of 32 seconds, 32 drops of potential recordings were simultaneously acquired. As a result, 2080 resistivity data, related to different current electrodes positions, were obtained.

In order to carry out the S-DERT measurements, 23 surface electrodes were fixed around the Venelle2 well, roughly in the same position and covering the same area of about 10 km^2 of the previous measurement phase (fig. 4). In this case, we used steel electrodes for current injection and unpolarized electrodes for potential measurement.

The studied area was divided in five main sub-sites (figure 4), where transmitter and receiver apparatus were installed. In detail, when the transmitter system was placed in one sub-site, 4 datalogger were installed in the other sub-sites. The transmitter system was connected with steel current electrodes, while each receiver (5 dataloggers) with unpolarized electrodes, both by long electrical cables. In this way, the complete system was able to obtain a multichannel collecting work.

A DD array configuration was used with *AB* and *MN* distances ranging between 400 and 1600 m. A square wave of 32 seconds was used for each dipole injection current (AB) and 28 electric potential signals (MN) were simultaneously acquired for 15-20 minutes. Consequently, 952 resistivity data were measured for each quadrupole (ABMN).

3.2 Data analysis and inversion

The considerable work in the field permitted to acquire several data during the two field trips. The large amount of acquired data prompted us to use an automated protocol for data analysis. Generally, in shallow investigations (multichannel system with an investigation depth < 300 m), a routine analysis of voltage signals is sufficient to reduce the errors associated to the estimate of the potential values. On the contrary, in deep geoelectrical explorations (> 300 m of depth) with a current system and drop of potential acquisition physically separated a crucial task is the extraction of the useful signal from the voltage recordings.

The amplitude of an electric potential signal depends, indeed, on the intensity of the current input, on the subsoil electrical characteristics and on the electrode distances. For large distances between the *AB* and *MN* electrodes, the measured electric potential is sometimes very low, which is due to disturbing currents present in the ground, such as industrial, telluric, and inductive currents (between cables), which may occur when the energizing circuit is activated.

The distribution of the electrical conductivity in the soil also affects the quality of the signal, in fact, in highly conductive areas, located between the transmitting and receiving dipoles, the electric potential is strongly masked to such an extent that the signal is completely erased from the background noise. Furthermore, deep geoelectrical data acquisition in anthropic areas is characterized by a greater noise level because of the disturbances due to environmental noise. For all these reasons, the voltage signal useful for calculating the apparent electrical resistivity values could be hidden (Rizzo et al., 2019).

Therefore, the rationale of field acquisition and processing is to record data for the time necessary for having enough current and electric potential cycles to extract the amplitude of the signals from the background noise.

The first elaboration step is the time correlation between the acquired current signals (A) and the electric potential data (mV), that is obtained by GPS system installed on each datalogger. The next stage was the data analysis, where the data analysis software was managed with OriginLab software (fig. 6). The first elaboration step was the spike removing, which consists of deleting the spikes on the active graph window (fig. 6c). The second step was the de-trending analysis, which consisted in a polynomial or linear fit of the voltage data and a subsequently de-trend approach. This elaboration step removes the natural trend that enveloped the data (fig. 6d, e). Successively, a FFT tool was applied to the de-trending voltage data (fig. 6f). The FFT analysis converts a signal from its original time domain to a representation in the frequency domain. Meanwhile, it can also provide the magnitude, amplitude, phase, power density and other computation results. In our case, the amplitude of the FFT results in the frequency of the acquired current signal defines the amount of the drop of potential.

After the analysis and elaboration steps, about 10% of electric potential data was rejected for a low signal/noise ratio and more than 2940 resistance values (V/I) were calculated taking in account the extrapolated potential data and the injected current.

Subsequently, the acquired data were inverted with ERTLab software (Geostudi Astier srl and Multi-Phase Technologies LLC) and the 3D electrical resistivity image of the studied area was depicted. It is an electrical resistivity inversion software that offers full three-dimensional modelling and inversion. Its numerical core uses the Finite Elements (FEM) approach to model the subsoil by adopting a mesh of hexahedrons to correctly incorporate complex terrain topography. Moreover, the software invert datasets collected using surface, borehole or surface-to-hole array configurations.

The inversion procedure is based on a smoothness constrained least-squared algorithm (LaBrecque et al., 1999) with Tikhonov model regularization, where the condition of the minimum roughness of the model is used as a stabilizing function. Throughout the inversion iterations, the effect of non-Gaussian noise is appropriately managed using a robust data weighting algorithm (Morelli and LaBrecque, 1996).

ERTlab allows to plot the apparent resistivity data in a 3D image starting from the resistance and the geometric factor. Figure 7 shows the surface-borehole (fig. 7a) and total (fig. 7b) 3D apparent resistivity data distribution with 2940 electrical resistivity value covering a volume of about 25 km^3. Then, the apparent resistivity data set was inverted by using a 100 m x 100 m x 50 m cell size for the core mesh (red box in figure 7), a mixed boundary condition (Dirichlet and Neumann), and a starting homogeneous apparent resistivity of 10 Ωm. An extra mesh, called the boundary mesh (green box), was generated around the core mesh to accommodate numerical boundary effects.

It is well known that conductive borehole fluids can affect ERT images, as they provide a strong electrical contrast close to the electrodes and can result in direct electrical connections between electrodes. In this case, the fluid may also represent an electrical connection to the metal casing. In general, potential mitigation techniques consist in incorporating the borehole and fluid characteristics in both the forward modeling and inversion codes.

According to Doetsch et al. (2010), current channeling phenomena can be favored when the well annulus is filled with highly conductive fluids (resistivity contrasts of 100:1) and borehole diameters of 10 and 20 cm yielded, for a dipole length of 5 m. In our case, the resistivity contrast between geological formations and the injected fluids (1.17 Ωm) is expected less than 100:1 while the borehole diameter is in the range between 30 – 60 cm for a dipole length of 50 m in the borehole and 400 m at surface. For these reasons, the borehole - fluid effects have been neglected.

Moreover, Wagner et al. (2015), discuss the effect of borehole filling, electrode shape/size and borehole deviation on ERT monitoring of a CO_2 storage reservoir. However, considering the small size of well and electrodes compared with the size of the mesh elements, it would be computationally prohibitive to use very fine grids to account well filling, electrode shape/size and borehole deviation into the 3D mesh used for this experiment. Moreover, according Rücker and Günther (2011), electrodes can be treated as ideal point sources if length/spacing < 0.2.

Finally, topographic correction was applied, and a 5% standard deviation estimate for noise was assumed to invert the data set with a robust inversion. The choice of 5% data error was a compromise between data error, final RMS e smoothness of the final model.

4. Results and discussion

In order to evaluate the capability of the deep electrical resistivity experiment, 3D apparent resistivity data were inverted considering at first, only surface measurements and then the full dataset (surface, surface to borehole, and in hole measurements). Moreover, inversion model errors were about 8% for S-DERT and 15% for the full dataset.

The figure 8 shows the 3D S-DERT, that was obtained considering only apparent resistivity values measured from surface electrodes. S-DERT has electrical resistivity values ranging from about 1 to 50 Ωm and a maximum investigation depth of about 1000 m from the ground surface. The best resolution was reached down to about 800 m from the ground surface underlining the presence of a highly conductive central zone with a "concave" shape up to 400-500 m deep, bounded laterally by areas with relatively higher resistivity (30 Ωm). Under it, a homogeneous resistivity distribution of about 10 Ωm is highlighted.

Figure 9 shows the results of the final 3D resistivity distribution obtained by the inversion of all the collected data (surface and borehole). In this case, the investigated depth reached is greater (about 1600 m), since the borehole electrodes within the Venelle2 well were arranged at depth of about 1000 to 1600 m. This electrical resistivity image combines the resistivity distribution characteristics of S-DERT and SH-DERT increasing the sensitivity both at surface and in borehole and better emphasizing, by sharper resistivity contrast, the geometric features of the investigated area.

The range of resistivity values is between 1 and 80 Ωm and shallow high conductive nucleus ($\rho < 10$ Ωm), bounded laterally by areas with relatively higher resistivity ($\rho > 30$ Ωm), are present down to -

300 m b.s.l. The deep geothermal reservoir hosted in crystalline rocks (from the depth of about 750 m b.s.l.) is in general characterized by average values lower than 25 Ωm, however, the resistivity distribution along Venelle2 well highlights a vertical variation with relatively higher resistive areas that could be associated to lithological/mineralogical heterogeneity or to a different fracturing rock state controlling the circulation of producing a different emission of high temperature dry vapors (> 200 °C) in the area.

Obviously, 3D imaging visualization allows to appreciate the trend of resistivity values of the study area in its entirety, while 2D imaging visualization allows to focus on specific elements of the investigated area, already identified in the 3D resistivity inversion models, and understand the best electrodes configurations to use in future applications in the geothermal field. Therefore, in order to interpret the 3D electrical resistivity distribution and facilitate the understanding of the complex geothermal system of the area around Venelle2 well, 3D electrical resistivity models were dissected along two selected profiles where lithostratigraphic and temperature information of some geothermal wells are available (Trumpy and Manzella, 2017) and summarized in figures 10. Figures 11 shows the resistivity sections of the previous 3D electrical models extracted along A-A' (SE-NW) and B-B' (NE-SW) profiles. The two sections of the 3D S-DERT model have an investigation depth of about 800 m (Figure 11a,b), while the figure 11c,d shows the two sections coming from the full 3D model with an investigation depth of about 1600 m. The 2D geoelectrical profiles show a range of electrical resistivity ranging from 1 Ωm to about 50 Ωm, even if the resistivity models are similar, sharper resistivity contrasts are well delineated in the deeper ones.

The figure 12 shows the 2D deep profiles compared with the borehole data, the temperature and the porosity of the Venelle2. In general, measured resistivity values are very low therefore they are only partly associated to the geological units. More probably, they are linked to the presence of tectonic structures that influence the circulation of hot fluids derived mainly from meteoric water heated by rock conduction (due to the high geothermal gradient) and, in limited cases, from direct inflows of shallow vapor, enriched near the surface, following partial condensation of deep-sourced vapor

(Duchi et al., 1986). Moreover, in high-temperature geothermal systems, the shallow geology is characterized by an unaltered zone, and the electrical conduction is mainly pore-fluid conduction. The deep electrical conduction is dominated by mineral or surface conduction due to temperature increment and high content of mineral alteration. On the contrary, at high temperature (above 230°C), the resistivity increases due to formation of high-temperature secondary alteration minerals and the conduction is dominated by surface and pore fluid conduction (Flóvenz et al., 2012).

In detail, the shallower conductive body (ρ < 15 Ωm) are associated to Neogenic deposits and to the clayey-marly units in flysch facies of the Ligurian l.s. Complex. Furthermore, higher resistivity values (ρ > 20 Ωm) characterizes the deep part of the DERTs close the Venelle2 well, at a depth where well stratigraphy refers to the Tectonic wedge complex (TWC). In the study area, the depth and thickness of pre-neogenic units varies indicating, in addition, the asymmetry of the tectonic depression. Sharp resistivity contrasts are associated to tectonic structure that bound the more conductive area. These geological structures bring into contact different lithologies and/or the same lithologies but with different chemical-physical characteristics of the subsoil. Finally, the resistivity distribution along Venelle2 well (Figure 12) allowed to analyze the behavior of deep geothermal reservoir hosted in crystalline rocks. In general, the Phyllitic-Quartzitic unit is characterized by low resistivity value (average value lower than 25 Ωm). Moreover, the comparison between the geophysical results, the porosity and temperature data (Figure 12) underlines some correlations. In detail, relatively low electrical resistivity values (< 10 Ωm) were recorded in correspondence of higher porosity zone (-800 and -1100 m a.s.l.), where a larger amount of liquid phase in two large fractures was recorded. A third conductive layer was recorded at depth (1300 m b.s.l.) in correspondence of higher percentage of phyllosilicate. On the contrary, the crystalline basement is characterized by ρ > 30 Ωm. Moreover, the temperature distribution controls the electrical conduction and some surface (<400m) extensive low resistivity zones are characterized with low temperature (<100°C). The low resistivity in this zone could be associated with the hot saline fluids of the geothermal system, but low resistivities can be correlated with clay hydrothermal alteration that occurs in that temperature regime. On the contrary, a deep high temperature zone is observed and the resistivity increment should be rightly correlated with some vapor dominated reservoir and a secondary alteration mineral with surface and pore fluid conduction. These phenomena are well highlighted on the relationship between the resistivity values extracted from the 3D resistivity inverted model at each depth where temperature data were collected in previous work (Fig. 13a). Close the Venelle2 well in the deep part (> 1000m) relative conductive and resistive alternances are detected, this behavior should be associated to the presence of high porosity, due to large fractures where the condensed water in the well flows, and high clay hydrothermal alteration. Therefore, the trend line toward increasing resistivity with depth, where an increase in temperature is observed, leads us to consider the equation 3, that can be presented in this form:

$$\ln \rho = \ln \rho_0 + \varepsilon/R(1/T) \tag{4}$$

This linear correlation (figure 13b) shows a coefficient of determination is 0.7564 indicated a good fit of the measured values to the Arrhenius law, in according to the previous consideration on the relationship between temperature data and the resistivity values (without the previous outliers). The correlation coefficient defines an activation energy of about -0.05 eV. This value suggests a complex conduction behavior of the electrical charge transport mechanism in this geothermal area, where a mixing of dry condition and high concentration of alteration minerals characterize the investigated area. However, a comparative study of the variation of the electrical conductivity with temperature in the presence of high temperature alteration minerals, such as chlorites, that is encountered in this hydrothermal system, by sample analysis could improve quantitatively these results.

As mentioned previously, MT results in the Lago Boracifero area form Santilano, 2017 (fig. 13), confirmed low resistivity values in the Lago basin allowing to recognize four main sub-horizontal electro layers: a) a low resistivity shallow layer (down to about 300 m from the ground surface), with values in the range of 3-30 Ωm, corresponds to the Neoautochthonous and Ligurian Complexes; b) the second layer, characterized by resistivity values in the range of 40-100 Ωm, located at a structural level coincident with the Tuscan Complex, Tectonic Wedge Complex and most of the Phyllitic

Complex (down to 2 km b.s.l.); c) the third layer, characterized by resistivity values in the range of 1000-5000 Ωm, corresponds mainly to the Micaschist, Gneiss and Intrusive complexes (2-7 km depth); d) at depth higher than 7 km, a general decrease of resistivity is observed with values locally lower than 400 Ωm.

Finally, MT profiles in the Lago Boracifero sector show a very important sub-vertical structure (elongated N30E) crosscutting the main sub-horizontal layers previously described and characterized by low resistivity, with average values of about 150 Ωm. The decrease of resistivity in the Micaschist, Gneiss and Intrusive complexes would suggest a strong influence of the hydrothermal circulation. This interpretation can imply two main processes: i) the occurrence of a contribution of liquid phase in the vapor dominated reservoir (hypothesis not confirmed by well tests) and/or ii) the effect of more or less pervasive hydrothermal alteration, possibly a remnant of the effect of an old, liquid phase fluid circulation. The MT results led the authors to interpret this structure as a fault that controlled the magmatic activity in this specific sector and possibly controls the hydrothermal circulation, along a very wide (some kilometers) shear zone oriented N30E. Rosenkjær et al. (2017) particularly refer to the Cornia Fault that is imaged as a wide sub-vertical low resistivity structure located along the homonymous river.

5. Conclusions

In this paper we described the main results of a geophysical experiment carried out in the frame of the FP7 IMAGE project. The Larderello Geothermal fields (Italy), since the first investigations conducted more than a century ago, have been the object of a myriad of studies. Due to the complexity of the system and the abundance of data, the field represents the ideal site to test the effectiveness of an experimental geoelectrical survey.

We propose an innovative Surface-Hole Deep Electrical Resistivity Tomography (SH-DERT) technique in extreme subsurface temperature condition, by using an ad-hoc geoelectrical cable in the deep well, 2000 m long, resistant up to 250° C and equipped with flexible steel electrodes. This ad-hoc cable was lowered in the Venelle2 well, a non-productive deep well, down to 1600 m from ground surface. Furthermore, 46 electrodes were arranged radially with respect to the Venelle2 well in an area of about 4 km^2 for a total investigated volume of about 10 km^3. The various combinations used between electric and potential electrodes allowed to measure a huge amount of data (2552 apparent resistivity data obtained) in a relatively short time (6 workdays). The dataset was firstly appropriately processed and then inverted to obtain the 3D electrical resistivity distribution of the area down to a depth of 1600 m.

Important hints for interpretation can be derived: first, a very low resistivity was recognized in the Tuscan Nappe and in the Tectonic Wedge Complex. This result agrees with MT studies, which results could have been biased by the passive nature of the method in a noisy area. It is assumed that the low resistivity values are due to the effect of more or less pervasive hydrothermal alteration, possibly a remnant of the effect of an old, liquid phase fluid circulation. Second, strong lateral variation of resistivity has been recognized along tectonic structures that could represent an actual (or fossil) pathway for hydrothermal fluids.

In conclusion, the innovative nature of this work can be summarized in three elements: the experiment represents the first one that applies deep 3D surface to borehole electrical resistivity measurements in geothermal applications; the geoelectrical investigation reaches very deep areas by the use of an ad-hoc geoelectrical cable; a large number of data was acquired in a deep context.

Finally, 3D deep surface to borehole electrical resistivity measurements can be applied also to more conventional geothermal systems both for characterization and monitoring.

Monitoring resistivity changes associated to temperature changes and/or fluid movement in geothermal reservoirs from the surface generally involves measuring small variations and therefore higher modeling errors. On the contrary, surface to hole and cross-hole geoelectrical methods showed a high benefit-to-cost ratio and a high sensitivity (around 1.2° C for temperature changes) to the temperature distribution in operating shallow geothermal systems or during heat tracing resistivity

(Hermans et al., 2015; Lesparre et al., 2019). Therefore, as regarding the use of geoelectrical methods in deeper geothermal systems, the combined use of data acquired in boreholes and surface can significantly increase the spatial resolution in depth.

The only needs consist in the presence of available not metallic wells. To overcome this last issue, an appropriately insulated array of electrodes permanently installed on the well casing and electrically coupled with the geological formations could enable the system to perform quasi-continuous geoelectrical surveys (Bottazzi et al., 2020). However, electrode and cable decay should be carefully evaluated. Finally, advanced data analysis (Machine Learning algorithm) can bring relevant and quantitative information aimed at optimizing geothermal reservoir management.

Acknowledgements

We thank the colleagues that supported the field work during the DC surveys. This study is part of the EU FP7-funded Integrated Methods for Advanced Geothermal Exploration (IMAGE) Project under grant agreement n° 608553. We thank the master thesis student Dr. Geol. Michele Tricarico and the archaeologist Dr. Felice Perciante that supported the fieldwork during the DC surveys. We thank Enel Green Power for the precious technical and logistical support on carrying out the borehole experiment. The access and in-well activities were possible thanks to the support of the operator (EGP).

Credit author statement

E. Rizzo: Conceptualization, Methodology, Investigation, Software Writing-Original Draft, Supervision; V. Giampaolo and L. Capozzoli: Software, Writing-Original Draft, Visualization, Investigation; G. De Martino, G. Romano: Investigation; A. Santilano: Writing-Original Draft, Visualization; A. Manzella: Funding acquisition.

Data Availability

The Data are available from the corresponding author

References

Altwegg, P., Schill, E., Abdelfettah, Y., Radogna, P.-V. & Mauri, G., 2015. Toward fracture porosity assessment by gravity forward modeling for geothermal exploration (Sankt Gallen, Switzerland), Geothermics, 57, 26–38.

Balasco M., P. Galli, A. Giocoli, E. Gueguen, V. Lapenna, A. Perrone, S. Piscitelli, E. Rizzo, G. Romano, A. Siniscalchi and M. Votta, 2011. Deep geophysical electromagnetic section across the middle Aterno Valley (central Italy): preliminary results after the April 6, 2009 L'Aquila earthquake. Boll. Geofis. Teor. Appl. doi:10.4430/bgta0028.

Batini F., Brogi A., Lazzarotto A., Liotta D., Pandeli E., 2003. Geological features of Larderello–Travale and Mt Amiata geothermal areas (southern Tuscany Italy). Episodes 26:239–244 .

Bergmann P., Schmidt-Hattenberger C., Kiessling D., Rücker C., Labitzke T., Henninges J., Baumann G., Schütt H., 2012. Surface-downhole electrical resistivity tomography applied to monitoring of CO2 storage at Ketzin, Germany, Geophysics, 77, B253-B267.

Bergmann, P., Schmidt-Hattenberger, C., Labitzke, T., Wagner, F. M., Just, A., Flechsig, C., Rippe, D., 2017. Fluid injection monitoring using electrical resistivity tomography - five years of CO2 injection at Ketzin, Germany. Geophysical Prospecting, 65, 859-875.

Bertani R., Bertini G., Cappetti G., Fiordelisi A., Marocco B.M., 2005. An update of the Larderello-Travale/Radicondoli deep geothermal system. Proceedings World Geothermal Congress 2005, Antalya, Turkey.

Bertani, R., Büsing, H., Buske, S., Dini, A, Hjelstuen, M., Luchini, M., Manzella, A., Nybo, R., Rabbel, W., Serniotti, L., the DESCRAMBLE Science and Technology Team, 2018. The First Results of the DESCRAMBLE Project. Proceedings of the 43rd Workshop on Geothermal Reservoir Engineering, Stanford University, Stanford, California, February 12-14, 2018

Bertini G., Cameli G.M., Costantini A., Decandia F.A., Dini I., Elter F.M., Lazzarotto A., Liotta D., Pandeli E., Sandrelli F., 1994. Structural features of southern Tuscany along the Monti di Campiglia–Rapolano Terme cross-section. Memorie della Società Geologica Italiana, 48, 51–59.

Bertini G., Casini M., Gianelli G., and Pandeli E., 2006. Geological structure of a long-living geothermal system, Larderello, Italy, Terra Nova, 18, 163-169.

Bertini G., Gianelli G., Battaglia, A., 1996. Risultati ed interpretazione delle datazioni radiometriche (metodo 230Th/234U) dei campioni di minerali idrotermali presenti nelle rocce attraversate dai sondaggi geotermici (Larderello e Monteverdi) e negli affioramenti di rocce mineralizzate (Sassa e Canneto-Malentrata). ENEL-CNR-CISE joint report, Pisa. 12 pp.

Binley A., 2015. 11.08 Tools and Techniques: Electrical Methods. In Treatise on Geophysics, Second Edition, Ed. Gerald Schubert, Elsevier, 2015, Pages 233-259.

Binley A., Cassiani G., Middleton R., Winship P., 2002. Vadose zone flow model parameterisation using cross-borehole radar and resistivity imaging. Journal of Hydrology 267, 147–159.

Binley A. and Kemna, A., 2005. DC resistivity and induced polarization methods. In: R.a. Hubbard (Editor), Hydrogeophysics. Springer, pp. 129-156.

Boccaletti, M., Corti, G., Martelli, L. (2011). Recent and active tectonics of the external zone of the Northern Apennines (Italy). Int. J. Earth. Sci., 100, 1331-1348.

Bonini, M., Boccaletti, M., Moratti, G. and Sani, F. (2001). Neogene crustal shortening and basin evolution in Tuscany (Northern Apennines). Ofioliti, 26, 275–286.

Bottazzi, F., Dell'Aversana, P., Molaschi, C., Gallino, G., Carniani, C., Cappuccio, P., Servodio, R., 2020. A New Downhole System for Real Time Reservoir Fluid Distribution Mapping: E-

REMM, the Eni-Reservoir Electro-Magnetic Mapping System. International Petroleum Technology Conference, Dhahran, Kingdom of Saudi Arabia, IPTC-19807-MS, 1-9.

Brogi, A. (2006). Neogene extension in the Northern Apennines (Italy): insights from the southern part of the Mt. Amiata geothermal area. Geodin. Acta, 19/1, 1-9, doi:10.3166/ga.19.33-50

Brogi A., Lazzarotto A. Liotta, D., Ranalli, G., CROP18 Working Group, 2005. Crustal structures in the geothermal areas of southern Tuscany (Italy): Insights from the CROP 18 deep seismic reflection lines. Journal of Volcanology and Geothermal Research, 148, 60– 80.

Bruno, P.P.G., Ricciardi, G.P., Petrillo, Z., Di Fiore, V., Troiano, A., Chiodini, G., 2007. Geophysical and hydrogeological experiments from a shallow hydrothermal system at solfatara volcano, Campi Flegrei, Italy: response to caldera unrest, J. Geophys. Res.: Solid Earth, 112(B6).

Byrdina, S., Vandemeulebrouck, J., Cardellini, C., Legaz, A., Camerlynck, C., Chiodini, G., Lebourg, T., Gresse, M., Bascou, P., Motos, G., Carrier, A., Caliro, S., 2014. Relations between electrical resistivity, carbon dioxide flux, and self-potential in the shallow hydrothermal system of Solfatara (Phlegrean Fields, Italy), Journal of Volcanology and Geothermal Research, 283, 172-182.

Caldwell, G., Pearson, C., Zayadi, H. (1986). Resistivity of rocks in geothermal systems: a laboratory study. In Proceedings 8th NZ Geothermal Workshop, 227-231.

Cameli G.M., Dini I., Liotta D., 1998. Brittle/Ductile boundary from seismic reflection lines of southern Tuscany (Northern Apennines, Italy). Memorie Società Geologica Italiana, 52, 152-162.

Carmignani, L., Decandia, F.A., Fantozzi, P.L., Lazzarotto, A., Liotta, D., Meccheri, M. (1994). Tertiary extensional tectonics in Tuscany (Northern Apennines, Italy). Tectonophysics, 238, 295-315.

Carminati E., and Doglioni C., 2004. Mediterranean geodynamics, in Encyclopaedia of Geology, pp. 135–146, Elsevier Acad., Amsterdam.

Carrier A., F. Fischanger, J. Gance, G. Cocchiararo, G. Morelli, M. Lupi, 2019. Deep electrical resistivity tomography for the prospection of low- to medium-enthalpy geothermal resources. Volume 219, Issue 3, 2056–2072.

Carrigan C.R., Yang X., LaBrecque D.J., Larsen D., Freeman D., Ramirez A.L., Daily W., Aines R., Newmark R., Friedmann S.J., Hovorka S., 2013. Electrical resistance tomographic monitoring of CO2 movement in deep geologic reservoirs Int. J. Greenh. Gas Control, 18, 401–408.

Chambers J. E., Wilkinson P. B., Weller A. L., Meldrum P. I., Gilvy R. D., Caunt S., 2007. Mineshaft imaging using surface and crosshole 3D electrical resistivity tomography: A case history from the East Pennine Coalfield, UK, Journal of Applied Geophysics, 62, 324-337.

Cheng Q., Chen X., Tao M., Binley A., 2019. Characterization of karst structures using quasi‑ 3D electrical resistivity tomography. Environmental Earth Sciences (2019) 78:285.

Conti P., M. Cei, F. Razzano, 2016. Geothermal energy use, country update for Italy (2010–2015) European Geothermal Congress 2016, Strasbourg, France, 19–24 September 2016.

Dahlin T., 1996. 2D resistivity surveying for environmental and engineering applications. First Break, 14, 275-284.

Daily W. and Ramirez A., 2000. Electrical imaging of engineered hydraulic barriers, Geophysics, 65, 83-94.

Daily W., Ramirez A., Labrecque D., Nitao J., 1992. Electrical-resistivity tomography of vadose water-movement. Water Resources Research, 28, 1429–1442.

Dam D. and Christensen S., 2003. Including geophysical data in ground water model inverse calibration, Ground Water, 41, 178–189.

Darnet M., Marquis G., Sailhac P., 2003. Estimating aquifer hydraulic properties from the inversion of surface Streaming Potential (SP) anomalies. Geophys. Res. Lett., 30, 13.

Darnet, M., Wawrzyniak, P., Baltassat, J., Bretaudeau, F., Coppo, N., Vedrine, S., Reninger, P., Vittecoq, B., 2020a. Airborne and land-based electromagnetic (CSEM and MT) surveying for geothermal exploration in the Martinique island. Proceedings World Geothermal Congress 2020 Reykjavik, Iceland, April 26 – May 2, 2020.

Darnet, M., Wawrzyniak, P., Coppo, N., Nielsson, S., Schill, E., Fridleifsson, G.Ó., 2020b. Monitoring geothermal reservoir developments with the Controlled-Source Electro-Magnetic method - A calibration study on the Reykjanes geothermal field. Journal of Volcanology and Geothermal Research, 391, 106437.

De Franco R., L. Petracchini, D. Scrocca, G. Caielli, G. Montegrossi, A. Santilano, A. Manzella, 2019. Synthetic Seismic Reflection Modelling in a Supercritical Geothermal System: An Image of the K-Horizon in the Larderello Field (Italy), Geofluids, vol. 2019, 21 pages.

De Matteis R., Vanorio T., Zollo A., Ciuffi S., Fiordelisi A., Spinelli E., 2008. Three dimensional tomography and rock properties of the Larderello-Travale geothermal area, Italy. Physics of the Earth and Planetary Interiors, 168, 37-48.

Del Moro A., Puxeddu M., Radicati di Brozolo F., Villa I., 1982. Rb-Sr and K-Ar ages of minerals at temperatures of 300°-400°C from deep wells in the Larderello geothermal field (Italy). Contrib. Mineral. Petrol., 81, 340-349.

Dini, A., Gianelli, G., Puxeddu, M., Ruggieri, G. (2005). Origin and evolution of Pliocene–Pleistocene granites from the Larderello geothermal field (Tuscan Magmatic Province, Italy), Lithos, 81, 1-31.

Doetsch, J. A., Coscia, I., Greenhalgh, S., Linde, N., Green, A., & Günther, T. (2010): The borehole-fluid effect in electrical resistivity imaging. Geophysics, F107-F114.

Elter M. and Pandeli E., 1990. Alpine and Hercynian orogenic phases in the basement rocks of the Northern Apennines (Larderello geothermal field, Southern Tuscany, Italy). Eclogae Geologicae Helveticae, 83, 241-264.

Fiordelisi A., Mackie R., Manzella A., Zaja A., 1998. Electrical features of deep structures in Southern Tuscany (Italy), Annals of Geophysics, 41(3), 333-341.

Flóvenz, Ó.G., Spangenberg, E., Kulenkampff, J., Árnason, K., Karlsdóttir, R., and Huenges, E., 2005. The role of electrical conduction in geothermal exploration. Proceedings World Geothermal Congress 2005, Antalya, Turkey, CD, 9 pp.

Flóvenz, Ó.G., Hersir, G.P., Saemundsson, K., Ármannsson, H and Fridriksson, Th., 2012: Geothermal energy exploration techniques. In: Syigh, A., (ed.) Comprehensive renewable energy, Vol. 7. Elsevier, Oxford, 51-95.

Foley, lE, Toksoz, M.N., Batini, F., 1992. Inversion of teleseismic traveltime residuals for velocity structure in the Larderello geothermal field. Italy. Geophys. Res. Lett. 19, 5–8.

Furche M., Weller A., 2002. Sensitivity distributions of different borehole electrode configurations considering a model with a cylindrical coaxial boundary. Geophysical Journal International, 149, 2, 338–348.

Gianelli G., Puxeddu M., Squarci P. (1978). Structural setting of the Larderello-Travale geothermal region. Mem.Soc. Geol. It., 19, 469-476

Gianelli G.,1994. Condizioni di pressione e temperatura del termometamorfismo nel sistema geotermico di Larderello. Atti Soc. tosc. Sci. nat., Mem., Serie A, 105, 17-35.

Gianelli, G., and M. A. Laurenzi, Age and cooling rate of the geothermal system of Larderello, Trans. Geotherm. Res. Counc., 25, 731 – 735, 2001.

Gianelli, G., Manzella, A. & Puxeddu, M. 1997. Crustal models of the geothermal areas of southern Tuscany (Italy). Tectonophysics, 281, 221 – 239.

Giocoli, A, Magrì, C., Vannoli, P., Piscitelli, S., Rizzo, E., Siniscalchi, A., Burrato, P., Basso, C., Di Nocera, C., 2008, Electrical resistivity tomography investigations in the Ufita Valley (southern Italy): Annals of Geophysics, 51(1), 213-223.

Gresse M., Vandemeulebrouck J., Byrdina S., Chiodini G., Revil A., Johnson T.C., Ricci T., Vilardo G., Mangiacapra A., Lebourg T., Grangeon J., Bascou P., Metral L., 2017. Three-Dimensional Electrical Resistivity Tomography of the Solfatara Crater (Italy): Implication for the

Multiphase Flow Structure of the Shallow Hydrothermal System. Journal of Geophysical Research: Solid Earth, 122, 8749–8768.

Griffiths, D.H., Barker, R.D., 1993. Two-dimensional resistivity imaging and modelling in areas of complex geology. Journal of Applied Geophysics, 29, 211–226.

Goes, B.J.M., Meekes, J.A.C., 2004. An effective electrode configuration for the detection of DNAPLs with electrical resistivity tomography. Journal of Environmental and Engineering Geophysics 9, 127–141.

Gola G., Bertini G., Bonini M., Botteghi S., Brogi A., De Franco R., Dini A., Donato A., Gianelli G., Liotta D., Manzella A., Montanari D., Montegrossi G., Petracchini L., Ruggieri G., Santilano A., Scrocca D., Trumpy E., 2017. Data integration and conceptual modelling of the Larderello geothermal area, Italy. Energy Procedia, 125, 300-309.

Guglielmetti, L., Comina, C., Abdelfettah, Y., Schill, E. & Mandrone, G., 2013. Integration of 3d geological modeling and gravity surveys for geothermal prospection in an alpine region, Tectonophysics, 608, 1025–1036.

Hermans, T.; Wildemeersch, S.; Jamin, P.; Orban, P.; Brouyère, S.; Dassargues, A.; Nguyen, F. Quantitative temperature monitoring of a heat tracing experiment using cross-borehole ERT. Geothermics 2015, 53, 14–26.

Irons, T.P., McPhserson, B.J.O.L., Moodie, N., Krahenbuhl, R., Li, Y., 2018. Integrating geophysical monitoring data into multiphase fluid flow reservoir simulation. AEGC 2018: Sydney, Australia.

Irving, J., and K. Singha (2010), Stochastic inversion of tracer test and electrical geophysical data to estimate hydraulic conductivities, Water Resour. Res., 46(11), W11514, doi:10.1029/2009WR008340.

ISPRA, 2002. Geological map of Italy at scale 1:50.000. http://www.isprambiente.gov.it/Media/carg/306_MASSA_MARITTIMA/Foglio.html.

Kana, J.D., Djongyang,N., Raïdandi, D., Nouck, P.N., Dadjé, A., 2015. A review of geophysical methods for geothermal exploration. Renewable and Sustainable Energy Reviews, 44 (2015), 87–95.

Kästner, F., Giese, R., Planke, S., Millett, J.M., Flóvenz, O.G., 2020. Seismic imaging in the Krafla high-temperature geothermal field, NE Iceland, using zero- and far-offset vertical seismic profiling (VSP) data. Journal of Volcanology and Geothermal Research, 391, 106315.

Kiessling, D., Schmidt-Hattenberger, C., Schuett, H., Schilling, F., Krueger, K., Schoebel, B., Danckwardt, E., Kummerow, J. and the CO2SINK group, 2010: Geoelectrical methods for monitoring geological CO2 storage, First results from crosshole and surface-downhole measurements from the CO2SINK test site at Ketzin (Germany). – International Journal of Greenhouse Gas Control, 4, 816-826.

Kosinski, W. K., Kelly, W. E. 1981. Geoelectric soundings for predicting aquifer properties. Ground Water 19, 163-171.

LaBrecque, D. J., G. Heath, R. Sharpe, and R. Versteeg, 2004, Autonomous monitoring of fluid movement using 3D electrical resistivity tomography: Journal of Environmental and Engineering Geophysics, 9, no. 3, 167–176.

LaBrecque, D., G. Morelli, W. Daily, A. Ramirez, and P. Lundegard (1999), Occam’s inversion of 3D electrical resistivity tomography, in ThreeDimensional Eelectromagnetics, edited by M. Oristaglio, B. Spies, and M. R. Cooper, pp. 575 – 590, Soc. of Explor. Geophys., Tulsa, Okla.

Leontarakis K., Apostolopoulos G. V., 2012. Laboratory study of the cross-hole resistivity tomography: The Model Stacking (MOST) Technique, Journal of Applied Geophysics, 80, 67-82.

Lesparre, N., Robert, T., Nguyen, F., Boyle, A., Hermans, T., 2019. 4D electrical resistivity tomography (ERT) for aquifer thermal energy storage monitoring. Geothermics, 77, 368-382.

Liotta D and Brogi A.: 2020. Pliocene-Quaternary fault kinematics in the Larderello geothermal area (Italy): Insights for the interpretation of the present stress field. Geothermics, 83, 101714.

Manzella A.: 2004 Resistivity and heterogeneity of Earth crust in an active tectonic region, southern Tuscany, Italy. Annals of Geophysics, 47, 107-118.

Manzella A., Bonciani R., Allansdottir A., Botteghi S., Donato A., Giamberini S., Lenzi A., Paci b M., Pellizzone A., Scrocca D., 2018. Environmental and social aspects of geothermal energy in Italy. Geothermics, 72, March 2018, Pages 232-248.

Majer, E. (2003). 3-D Seismic Methods for Geothermal Reservoir Exploration and Assessment--Summary. Lawrence Berkeley National Laboratory, 1-33.

Morelli, G. and LaBrecque, D.J. 1996. Advances in ERT inverse modeling. European Journal of EEGS 1, 171–186

Muñoz, G.: Exploring for Geothermal Resources with Electromagnetic Methods. Surveys in Geophysics 35.1 (2014), 101-122.

Musumeci G., Bocini L., Corsi R., 2002. Alpine tectonothermal evolution of the Tuscan Metamorphic Complex in the Larderello geothermal field (northern Apennines, Italy). Journal of the Geological Society, London, Vol. 159, 443–456.

Orlando L. 2005. Interpretation of Tuscan gravity data. Bull. Soc. Geol. It., Special Issue n. 3., 179-186.

Palacios A., Ledo J.J., Linde N., Luquot L., Bellmunt F., Folch A., Marcuello A., Queralt P., Pezard P.A., Martínez L., del Val L., Bosch D., Carrera J., 2020. Time-lapse cross-hole electrical resistivity tomography (CHERT) for monitoring seawater intrusion dynamics in a Mediterranean aquifer. Hydrol. Earth Syst. Sci., 24, 2121–2139.

Pandeli, E., Bertini G., Castellucci, P. (1991). The tectonic wedge complex of the Larderello area (Southern Tuscany, Italy). Boll. Soc. Geol. It., 110, 621-629

Pandeli, E., Gianelli, G., Puxeddu, M. and Elter, F.M. (1994). The Paleozoic Basement of the Northern Apennines: stratigraphy, tectono-metamorphic evolution and alpine hydrothermal processes. Memorie Società geologica italiana, Vol. 48, pp. 627-654.

Pechnig R., Niederau J., Rabbel W., 2018. Petrophysical Characteristics of Basement Rocks –Results of Log and Core Data Interpretation. In Manzella A., Botteghi S., Trumpy E., D6.3 Proceedings of the DESCRAMBLE project Final Conference, 25-28.Pucci S., R. Civico, F. Villani, T. Ricci, E. Delcher, A. Finizola, V. Sapia, P. M. De Martini, D. Pantosti, S. Barde-Cabusson, E. Brothelande, R. Gusset, C. Mezon, S. Orefice, A. Peltier, M. Poret, L. Torres, B. Suski. Deep electrical resistivity tomography along the tectonically active Middle Aterno Valley (2009 L'Aquila earthquake area, central Italy). Geophys J Int (2016) 207 (2): 967-982.

Pucci S., R. Civico, F. Villani, T. Ricci, E. Delcher, A. Finizola, V. Sapia, P. M. De Martini, D. Pantosti, S. Barde- Cabusson, E. Brothelande, R. Gusset, C. Mezon, S. Orefice, A. Peltier, M. Poret, L. Torres, B. Suski. Deep electrical resistivity tomography along the tectonically active Middle Aterno Valley (2009 L'Aquila earthquake area, central Italy). Geophys J Int, 207 (2), 967-982.

Rizzo, E., Colella, A., Lapenna, V. and Piscitelli, S. 2004. High-resolution images of the fault controlled High Agri Valley basin (Southern Italy) with deep and shallow Electrical Resistivity Tomographies. Physics and Chemistry of the Earth, 29, 321-327.

Rizzo E. and Giampaolo V., 2019. New Deep Electrical Resistivity Tomography in the High Agri Valley basin (Basilicata, Southern Italy). Geomatics Natural Hazards and Risk, doi: 10.1080/19475705.2018.1520150, in press.

Rizzo E., Giampaolo V., Capozzoli L., Grimaldi S., 2019a. Deep Electrical Resistivity Tomography for the Hydrogeological Setting of Muro Lucano Mounts Aquifer (Basilicata, Southern Italy). Geofluids, Volume 2019, Article ID 6594983, 11 pages.

Rizzo E., S. Piscitelli, J. Bellanova, L. Capozzoli, G. De Martino, M. Guerriero, G. Morelli, F. Fischanger, R. Caputo e V. Lapenna (2019b). Tomografie Geoelettriche Profonde (DERT) per lo studio geologico-idrogeologico di Ferrara. Bollettino di Geofisica Teorica e Applicata, 60, n.Suppl. 2, s100-s105.

Rochira, F., Caggianelli, A., de Lorenzo, S., 2018. Regional thermo-rheological field related to granite emplacement in the upper crust: implications for the Larderello area (Tuscany, Italy). Geodin. Acta 30, 225–240.

Romagnoli, P., Arias, A., Barelli, A., Cei, M. and Casini, M., 2010. An updated numerical model of the Larderello–Travale geothermal system, Italy. Geothermics, 39, 292-313.

Rosenkjær K., Karlsdóttir R., Botteghi S., Calvi E., Donato A., Gola G., Manzella A., Montegrossi G., Santilano A., Trumpy E., Trifirò S., Capozzoli L., De Martino G., Giampaolo V., Perciante F., Rizzo E., Romano G., Godio A., 2017. MT-Inversion techniques with external constraints. IMAGE-D5.6, 65 pages.

Rücher C. and Günther T., 2011. The simulation of finite ERT electrodes using the complete electrode model. Geophysics, 76 (4), F227-F238.

Saccorotti, G., Piccinini, D. Zupo, M., Mazzarini, F., Chiarabba, C., Piana Agostinetti, N. Licciardi, A. and Bagaglia, M. 2014. The deep structure of the Larderello-Travale geothermal field (Italy) from integrated, passive seismic investigations. Energy Procedia 59 (2014) 227 – 234.

Santilano, A., 2017. Deep geothermal exploration by means of electromagnetic methods: new insights from the Larderello geothermal field (Italy). Doctoral dissertation, Politecnico di Torino

Santilano, A., Manzella, A., Gianelli, G., Donato, A., Gola, G., Nardini, I., Trumpy E., Botteghi, S. 2015a. Convective, intrusive geothermal plays: What about tectonics?. Geothermal Energy Science, 3, 51–59.

Santilano A., Godio A., Manzella A., Menghini A., Rizzo E, Romano G., 2015b. Electromagnetic and DC methods for geothermal exploration in Italy, state-of-the-art, case studies and future developments. First Break, 33 (8), 81-86.

Santilano A., Godio A., Manzella A., Dini I., 2015. Electrical resistivity structures and their relation to geological features at the Larderello geothermal field (Italy). Near Surface Geoscience, Turin, Italy, 6-10 September 2015.

Schmelzbach, C., Greenhalgh, S., Reiser, F., Girard, J., Bretaudeau, F., Capar, L., Bitri, A., 2016. Advanced seismic processing/imaging techniques and their potential for geothermal exploration. Interpretation, 4:4, SR1-SR18.

Schmidt-Hattenberger, C., P. Bergmann, D. Kiessling, K. Krüger, C. Rücker, and H. Schütt, CO2SINK Group, 2011, Application of a vertical electrical resistivity array (VERA) for monitoring CO2 migration at the Ketzin site: First performance evaluation: Energy Procedia, 4, 3363–3370.

Slater, L., Binley, A., 2003. Evaluation of permeable reactive barrier (PRB) integrity using electrical imaging methods. Geophysics 68, 911–921.

Slater, L., M. D. Zaidman, A. M. Binley and L. J. West, Electrical imaging of saline tracer migration for the investigation of unsaturated zone transport mechanisms, Hydrology and Earth System Sciences, 1(2): 291-302, 1997.

Spichak V., Manzella A.: *Electromagnetic sounding of geothermal zones*. Journal of Applied Geophysics, 68, 459–478, 2009.

Spichak, V.V., Zakharova, O.K., 2015. Electromagnetic Geothermometry. Elsevier, 1-183.

Storz, H., W. Storz and F. Jacobs (2000): Electrical resistivity tomography to investigate geological structures of the earth's upper crust, Geophysical Prospecting, 48, 455-471.

Suzuki, K., Toda, S., Kusunoki, K., Fujimitsu, Y., Mogi, T., Jomori, A., 2000. Case studies of electrical and electromagnetic methods applied to mapping active faults beneath the thick quaternary, Engineering Geology, 56, 29-45.

Tamburriello G., Balasco M., Rizzo E., Harabaglia P., Lapenna V., Siniscalchi A., 2008. Deep electrical resistivity tomography and geothermal analysis of Bradano foredeep deposits in Venosa area (Southern Italy): preliminary results, Annals of Geophysics, Vol 51, N. 1.

Thompson S., B. Kulessa, D. I. Benn, J. R. Mertes, 2017. Anatomy of terminal moraine segments and implied lake stability on Ngozumpa Glacier, Nepal, from electrical resistivity tomography (ERT). Scientific Reports, 7:46766.

Tietze, K., Ritter, O., Veeken, P., 2015. Controlled-source electromagnetic monitoring of reservoir oil saturation using a novel borehole-to-surface configuration. Geophysical Prospecting, , 63, 1468–1490.

Tietze, K., Ritter, O. Veeken, P., 2017. Erratum/Corrigendum: Controlled-source electromagnetic monitoring of reservoir oil-saturation using a novel borehole-to-surface configuration. Geophysical Prospecting, 65: 317-321.

Troiano A., R. Isaia, M. G. Di Giuseppe, F. D. A. Tramparulo, S. Vitale, 2019. Deep Electrical Resistivity Tomography for a 3D picture of the most active sector of Campi Flegrei caldera. Scientific Reports, 9:15124.

Truesdell, A.H., Haizlip, J.R., Armannsson, H., D'Amore, F., 1989. Origin and transport of chloride in superheated geothermal steam. Geothermics, 18, 295-304.

Trumpy, E. and Manzella, A., 2017 Geothopica and the interactive analysis and visualization of the updated Italian National Geothermal Database. International Journal of Applied Earth Observation and Geoinformation, 54,28-37.

Tsourlos P., Ogilvy R., Papazachos C., Meldrum P., 2011. Measurement and inversion schemes for single borehole-to-surface electrical resistivity tomography surveys. Journal of Geophysics and Engineering, 8, 4, 487–497.

Tuscan Region web site, 2015. Continuum Geologico at scale 1:10000. http://www502.regione.toscana.it/geoscopio/geologia.html

Villa M. and Puxeddu M., 1994. Geochronology of the Larderello geothermal field: new data and the «closure temperature» issue. Contrib. Mineral. Petrol., 315, 4 15-426.

Wagner, F. M., Bergmann, P., Rücker, C., Wiese, B., Labitzke, T., Schmidt-Hattenberger, C., Maurer, H., 2015. Impact and mitigation of borehole related effects in permanent crosshole resistivity imaging: An example from the Ketzin CO2 storage site. Journal of Applied Geophysics, 123, 102-111.

Wilkinson, P.B., Chambers, J.E., Meldrum, P.I., Ogilvy, R.D., Caunt, S., 2006. Optimization of array configurations and panel combinations for the detection and imaging of abandoned mineshafts using 3D cross-hole electrical resistivity tomography. Journal of Environmental and Engineering Geophysics 11, 213–221.

Witter, J.B., Siler, D.L., Faulds, J.E., Hinz, N.H., 2016. 3D geophysical inversion modeling of gravity data to test the 3D geologic model of the bradys geothermal area, Nevada, USA. Geother. Ener., 4(1), 14.

Table 1 – Venelle2 well stratigraphy.

m (from ground level)	**Stratigraphy**
0 ÷ 260	Neogenic and Quaternary deposits
260 ÷ 640	Clayey-marly units in flysch facies of the Ligurian l.s. Complex
640 ÷ 1020	Tectonic Wedge Complex
1020 ÷ 2234	Phyllitic–Quartzitic Group

Table 2 – Material used for the assemblage of the ad-hoc multipolar geoelectrical in-hole cable.

N.	Type	Length	Diameter	Function and characteristics
1	Steel cable	2000 m	4 mm	To increase the traction resistance of the entire cable.
12	Sheathed monopolar copper electric cables	1500 ÷ 2000 m	2 mm	To connect the electrodes to the surface acquisition system. They are resistant to temperatures up to 250° C.
12	Cylindrical steel electrodes	1.5 m	20 mm	To inject current (A) and measures electric potential values (V) in the borehole. They are flexible, to allow a better descent in the borehole, and resistant to high temperatures. They were mechanically connected to copper cables and coupled to the entire cable by hardening foam.
3	Heat shrinks tubing	1500 ÷ 2000 m	16, 19, and 33 mm	To increase the traction and rub resistance of the entire cable.
1	Tape	-	-	It is resistant to medium temperatures.

Figures

Figure 1 – (a) Geological map and geological cross sections of the study area (modified form Liotta and Brogi, 2020). The red dot is Venelle2 well, the red square represents the 3D DERT survey area. (b) Schematic crustal section below Larderello-Travale Geothermal Area and magma emplacement conceptual model, (c) structural stratigraphic framework and the modelled geological surfaces, (d) Temperature evidence from the mineral assemblage of the Plio-Quaternary HT-LP metamorphism (Bt: Biotite, Crd: Cordierite, Chl: Chlorite, Mus: Muscovite, Cor: Corindum), modified from Gola et al. (2017).

Figure 2 – a) Lithology results of multi mineral and standard approach. (Pechnig et al., 2018); b) Temperature data collected in the Venelle-2 well during DESCRAMBLE project (Bertani et al., 2018).

Figure 3 – Realization of ad-hoc multiconductor geoelectrical cable for down-hole electrical resistivity measurements: a) electrical cables assembling, b) steel electrodes placements, c) cylindrical weight; d) heat shrink tubing; e) final packaged cable.

Figure 4 – Position of surface electrodes in an area of about 4 x 5 km surrounding the Venelle2 well.

Figure 5 – Disposition of the multi-conductor in the Venelle2 well: a) installation of the pulley on the top of the hole; b) installation of the stuffing box; c) installation of the pulley close the hole; d) winch system; e) final distribution of the 12 steel electrodes in the hole.

Figure 6 – Data analysis: a) an example of the injected current square waves (A); b) the amplitude of the current signal after FFT; c) an example of the original potential difference (mV) data set with spikes; d) the potential difference (mV) data after the spike removing with polynomial fit (red line);

e) the potential difference (mV) data after the de-trending approach; f) the amplitude of the potential difference signal after FFT.

Figure 7 – (a) 3D distribution of the surface-borehole apparent electrical resistivity data acquired; (b) 3D distribution of all apparent electrical resistivity data acquired.

Figure 8 – a) 3D S-DERT and b) resistivity isosurfaces obtained using only surface electrodes.

Figure 9 – a) 3D Full data DERT and b) resistivity isosurfaces obtained using both surface and borehole electrodes.

Figure 10 – Available geological and lithostratigraphic information of the investigated area near Venelle2 well along A-A’ (c) and B-B’ (d) profiles. Temperature logs of geothermal wells along A-A’ and B-B’ profiles (b). In brackets, the year in which temperature log were acquired

Figure 11 - 2D deep electrical resistivity tomography along profiles SE-NW direction (a, c) and NE-SW direction (b, d) delineated in A-A’ and B-B’ lines in figure 10. They are extracted from 3D S-DERT (a, b) and 3D full data DERT (c, d). The resistivity is in Ωm and the red dots are surface and borehole electrodes.

Figure 12 - 2D sections extracted from the full 3D DERT image along profiles A-A’ and B-B’ compared with the lithostratigraphic information (a, c) and the porosity and temperature dataset (b, d).

Figure 13. Resistivity data extracted from the 3D resistivity inverted model plotted vs temperature data (a) and the fit correlation (b) taking in account the equation 4 (without the previous outliers).

Figure 14 – 2D MT profiles in the Lago basin area (modified from Santilano, 2017). 1) Quaternary deposits; 2) Neoautochthonous terrigenous deposits (Miocene-Pliocene); 3) Ligurian and sub-Ligurian Flysch complex (Jurassic-Eocene); 4) Tuscan Nappe formations (Upper Trias-Miocene); 5) Calcare Cavernoso and anhydrites; 6) Metamorphic Units (Paleozoic); 7) area investigated by MT surveys; 8) area investigated by the new 3D deep electrical resistivity survey. The red squares on the MT profiles (P1 and P3) are the coverage area by DERT survey.

1086 Figure 1

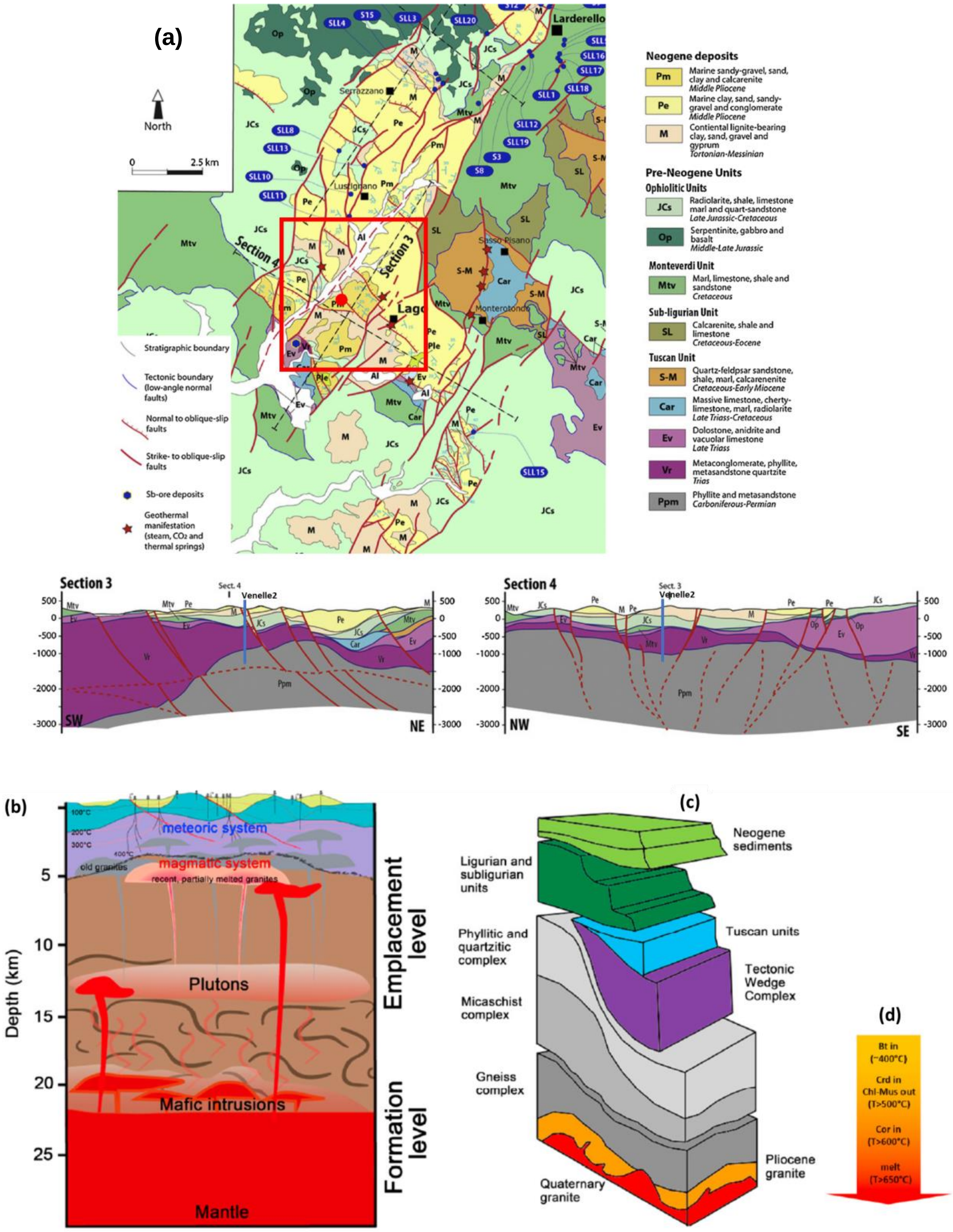

1087

1088

1089

Figure 2

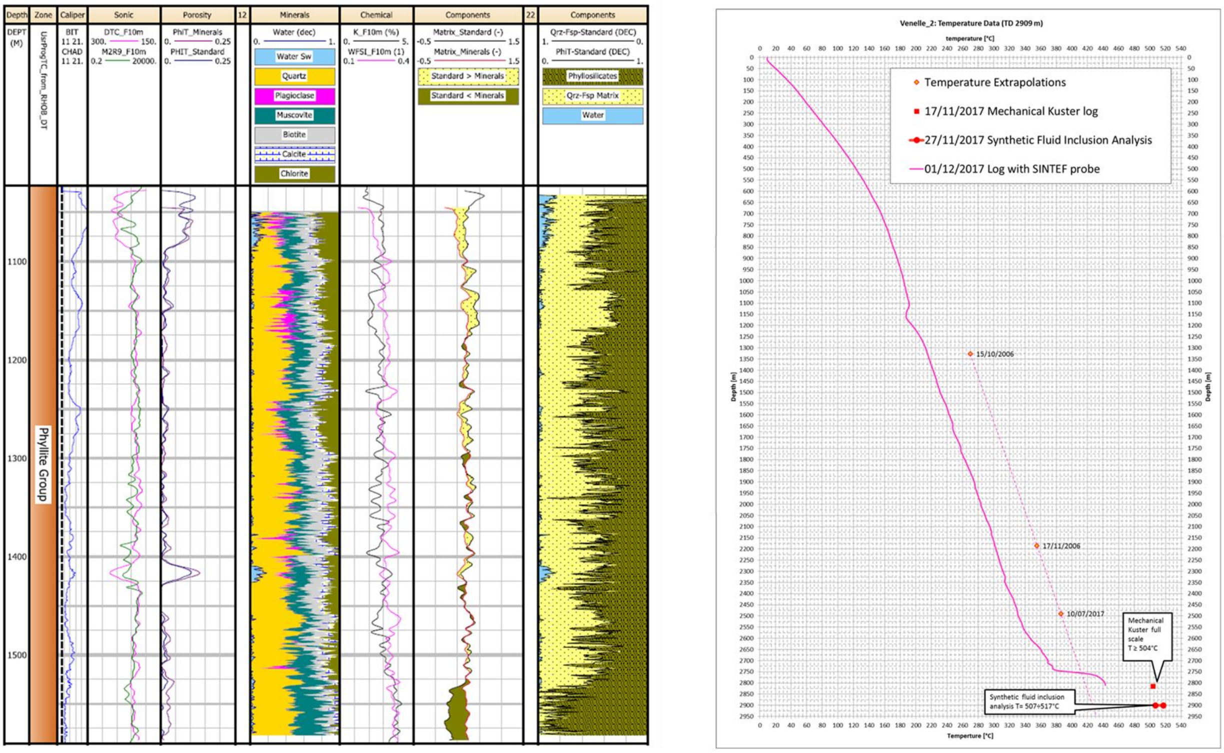

Depth
Zone
Caliper
Sonic
Porosity
Minerals
Chemical
Components
Components
Phyllite Group
Water Sw
Quartz
Plagioclase
Muscovite
Biotite
Calcite
Chlorite
Standard > Minerals
Standard < Minerals
Phyllosilicates
Qrz-Fsp Matrix
Water
Venelle_2: Temperature Data (TD 2909 m)
Temperature Extrapolations
17/11/2017 Mechanical Kuster log
27/11/2017 Synthetic Fluid Inclusion Analysis
01/12/2017 Log with SINTEF probe
15/10/2006
17/11/2006
10/07/2017
Mechanical Kuster full scale T ≥ 504°C
Synthetic fluid inclusion analysis T= 507÷517°C
Depth [m]
Temperture [°C]

a

b

Figure 3

Figure 4

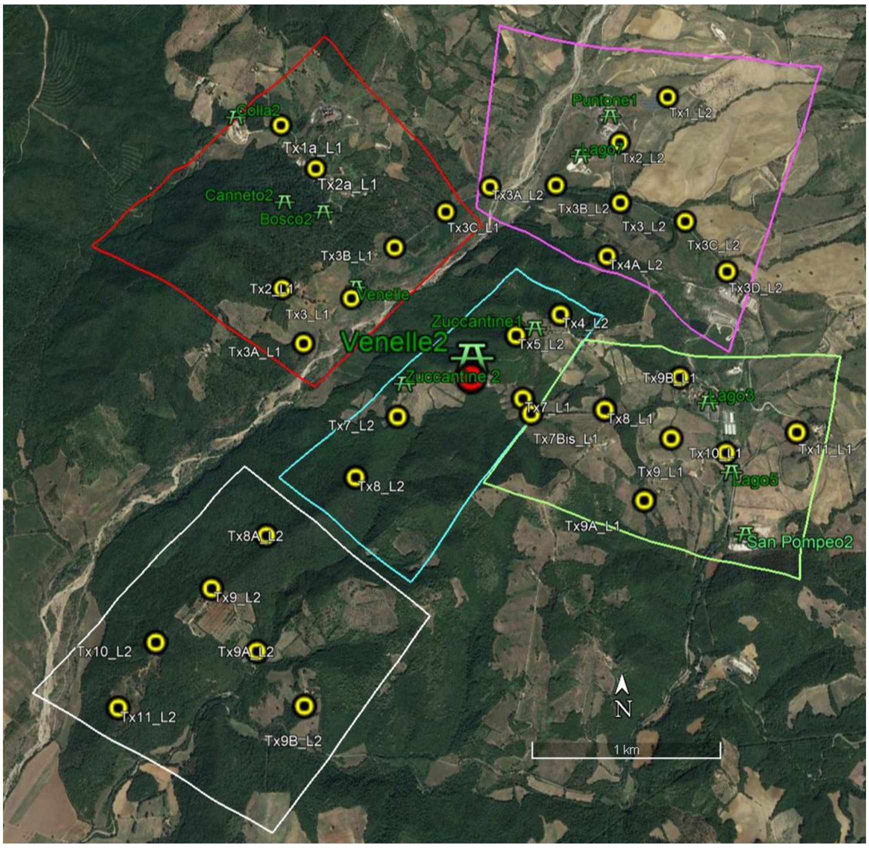
Tx1a_L1
Tx2a_L1
Canneto2
Bosco2
Tx3B_L1
Tx3C_L1
Tx2_L1
Tx3_L1
Venelle
Tx3A_L1
Venelle2
Zuccantine1
Zuccantine 2
Tx5_L2
Tx4_L2
Tx3A_L2
Tx3B_L2
Tx1_L2
Tx2_L2
Tx3_L2
Tx3C_L2
Tx4A_L2
Tx3D_L2
Tx7_L2
Tx8_L2
Tx7_L1
Tx7Bis_L1
Tx8_L1
Tx9B_L1
Tx10_L1
Tx11_L1
Tx9_L1
Tx9A_L1
San Pompeo2
Tx8A_L2
Tx9_L2
Tx10_L2
Tx9A_L2
Tx11_L2
Tx9B_L2
N
1 km

Figure 5

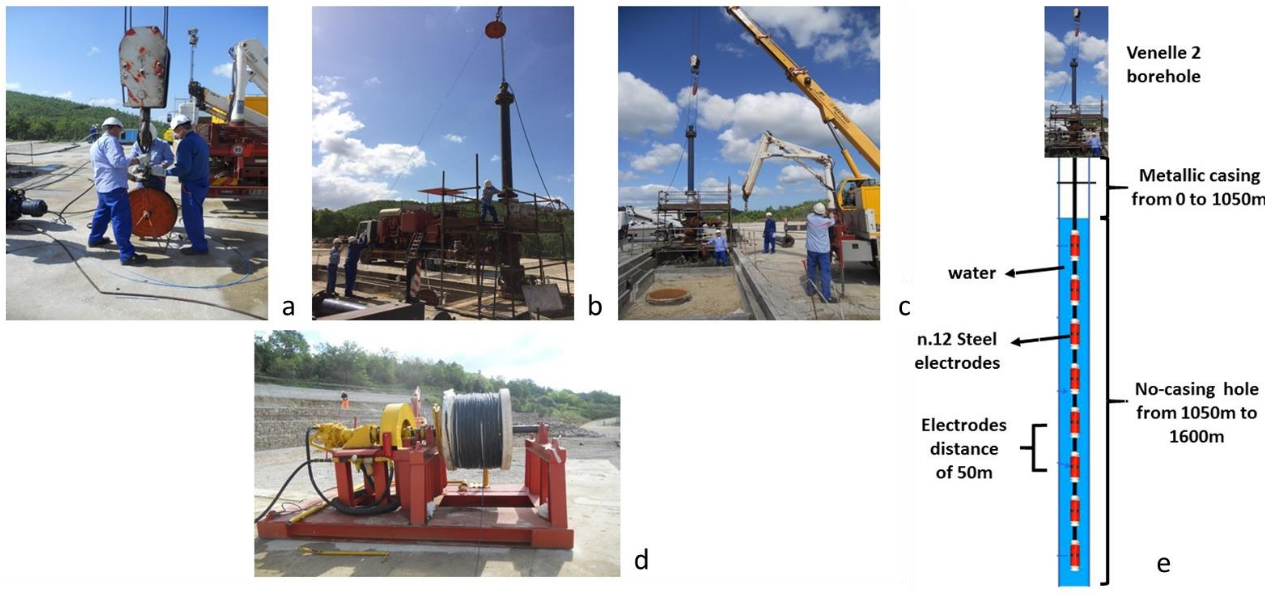
a
b
c
d
e
Venelle 2 borehole
Metallic casing from 0 to 1050m
water
n.12 Steel electrodes
No-casing hole from 1050m to 1600m
Electrodes distance of 50m

Figure 6

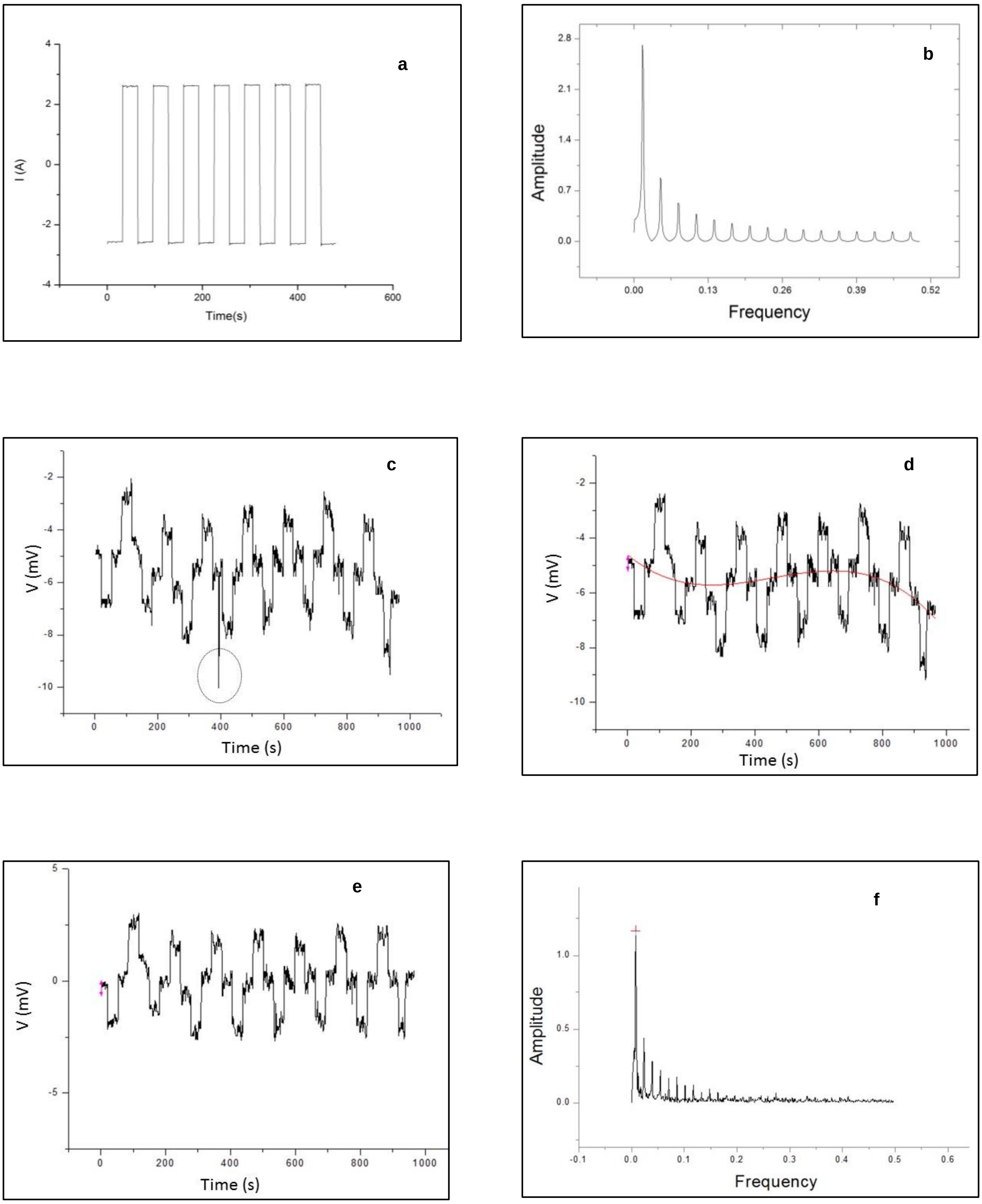

a
I (A)
Time(s)
b
Amplitude
Frequency
c
V (mV)
Time (s)
d
V (mV)
Time (s)
e
V (mV)
Time (s)
f
Amplitude
Frequency

Figure 7

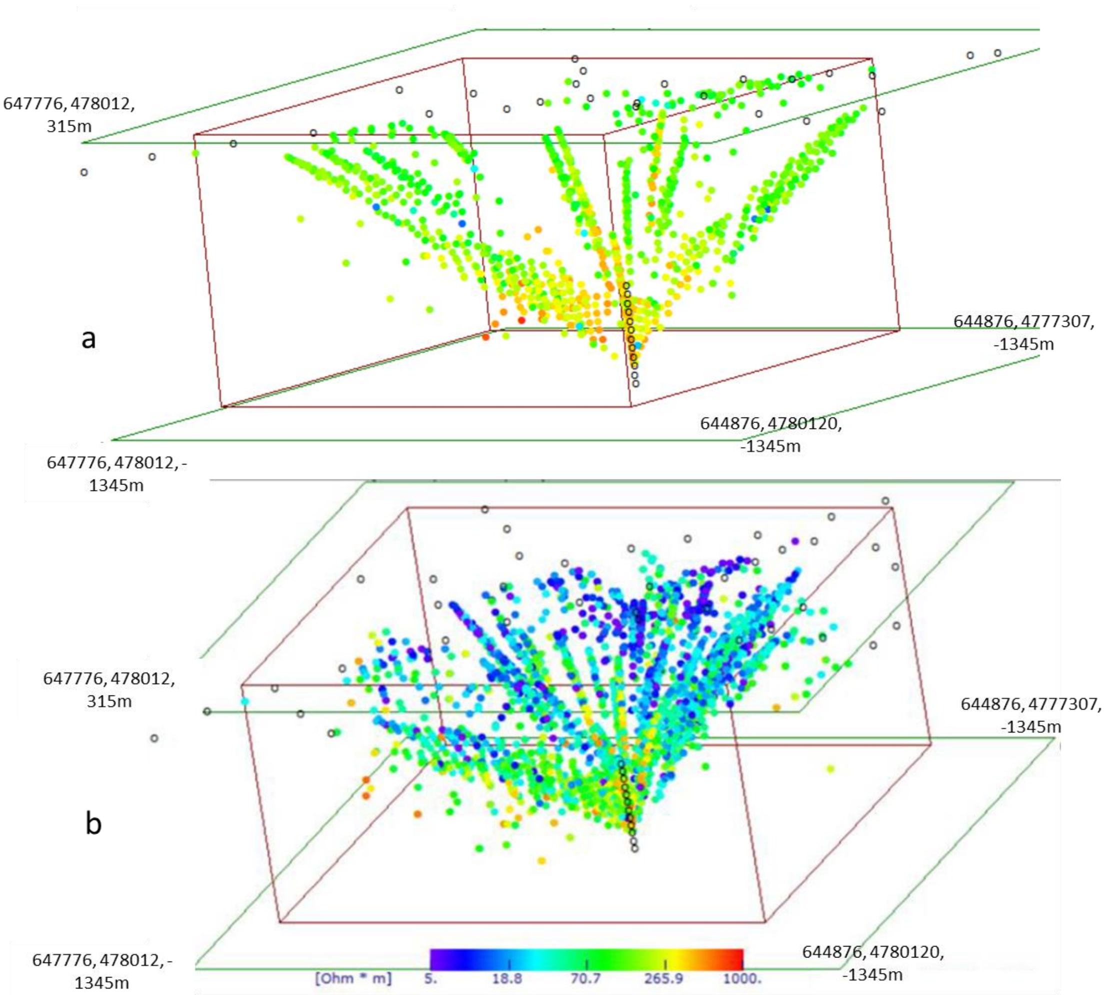

647776, 478012,
315m
644876, 4777307,
-1345m
644876, 4780120,
-1345m
647776, 478012, -
1345m
a
647776, 478012,
315m
644876, 4777307,
-1345m
b
647776, 478012, -
1345m
644876, 4780120,
-1345m
[Ohm * m]
5.
18.8
70.7
265.9
1000.

Figure 8

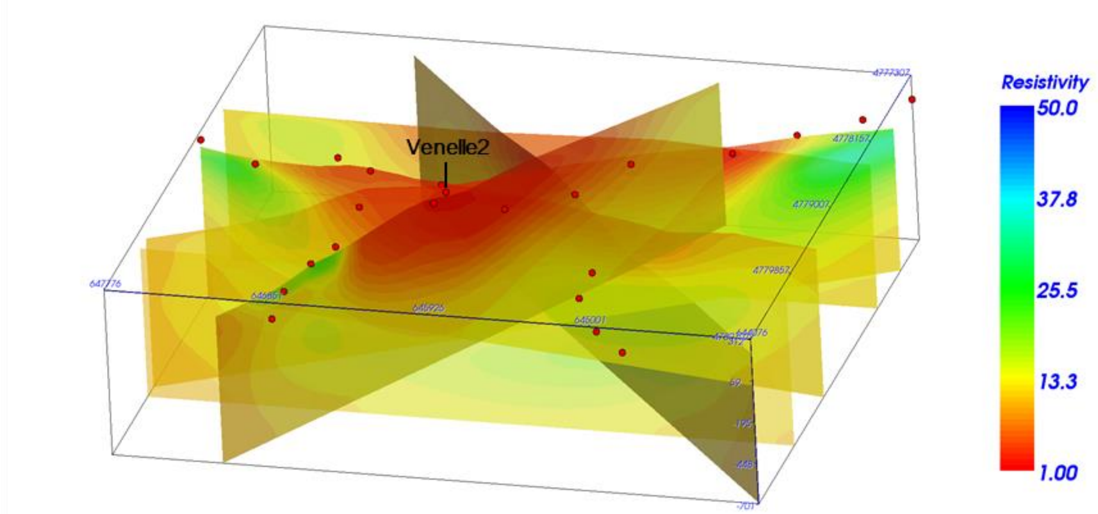

Venelle2
Resistivity
50.0
37.8
25.5
13.3
1.00

(a)

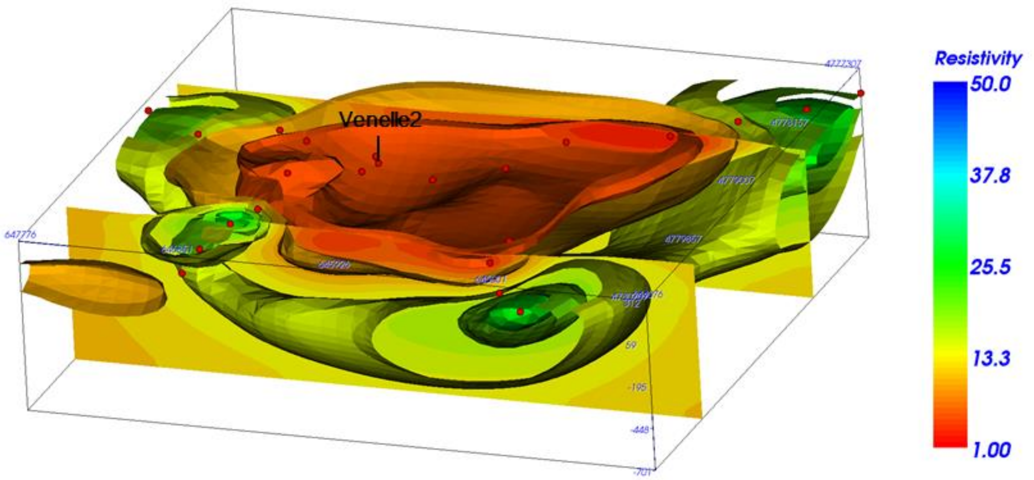

Venelle2
Resistivity
50.0
37.8
25.5
13.3
1.00

(b)

Figure 9

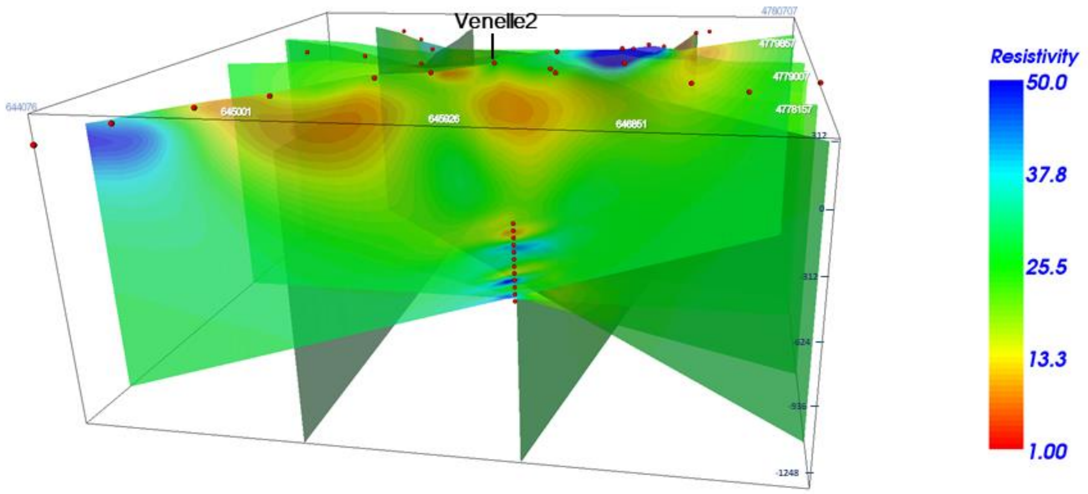
Venelle2
Resistivity
50.0
37.8
25.5
13.3
1.00
645001
645926
646851
4779857
4779007
4778157

(a)

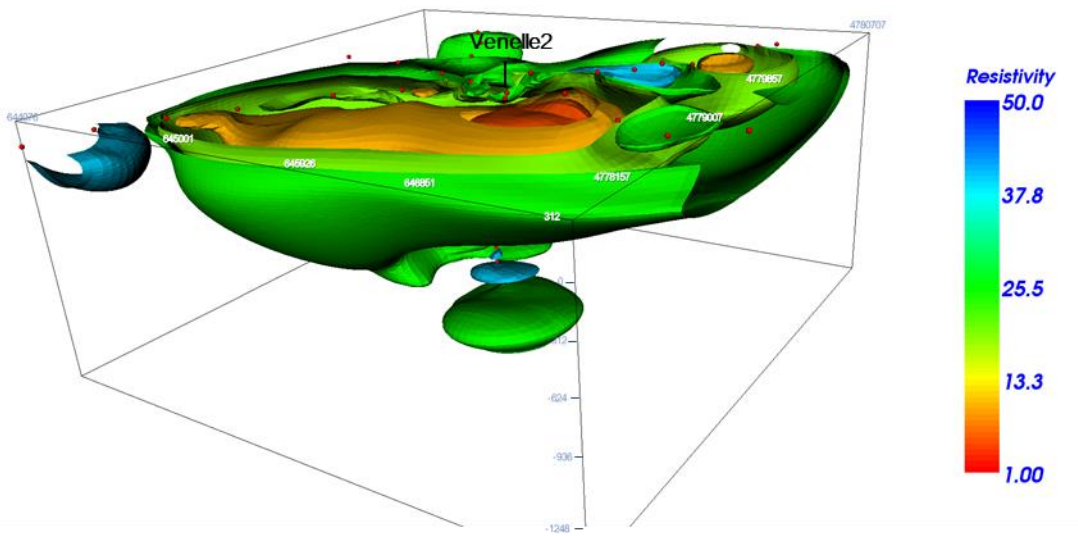
Venelle2
Resistivity
50.0
37.8
25.5
13.3
1.00
645001
645926
646851
4779857
4779007
4778157
312

(b)

Figure 10

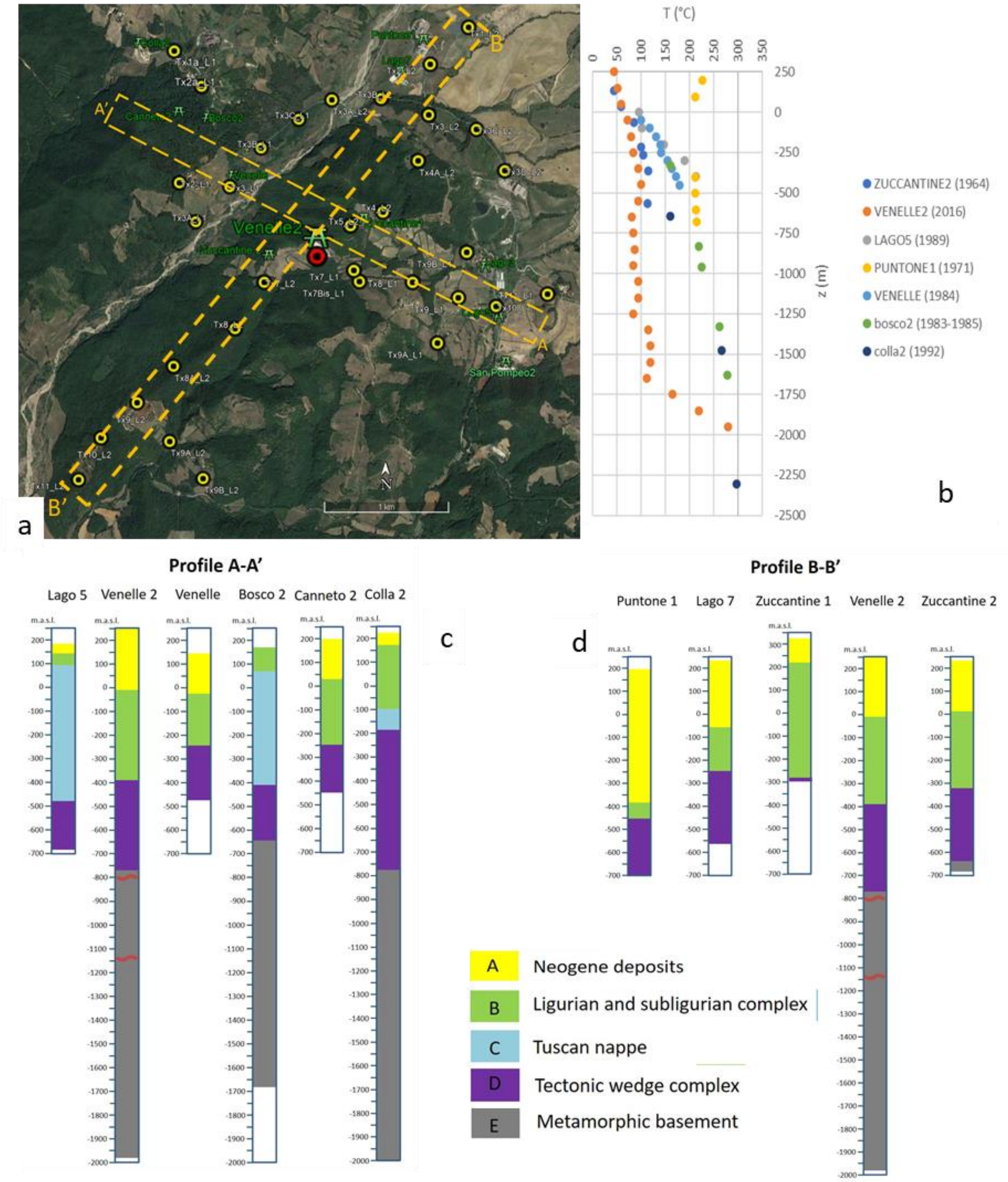
a
A'
A
B
B'
Venelle2
1 km
N
b
T (°C)
z (m)
ZUCCANTINE2 (1964)
VENELLE2 (2016)
LAGO5 (1989)
PUNTONE1 (1971)
VENELLE (1984)
bosco2 (1983-1985)
colla2 (1992)
c
Profile A-A'
Lago 5
Venelle 2
Venelle
Bosco 2
Canneto 2
Colla 2
d
Profile B-B'
Puntone 1
Lago 7
Zuccantine 1
Venelle 2
Zuccantine 2
m.a.s.l.
A Neogene deposits
B Ligurian and subligurian complex
C Tuscan nappe
D Tectonic wedge complex
E Metamorphic basement

Figure 11

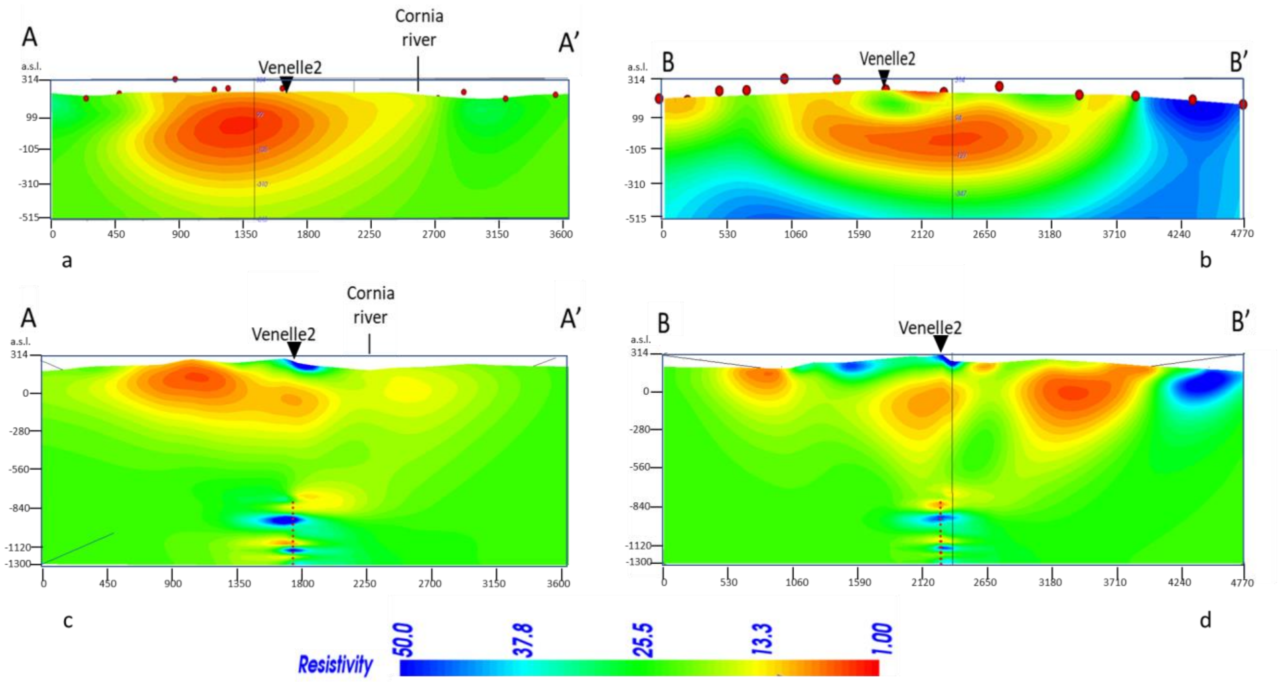
A
A'
Cornia
river
Venelle2
a.s.l.
314
99
-105
-310
-515
0
450
900
1350
1800
2250
2700
3150
3600
a
B
B'
Venelle2
530
1060
1590
2120
2650
3180
3710
4240
4770
b
-280
-560
-840
-1120
-1300
c
d
Resistivity
50.0
37.8
25.5
13.3
1.00

Figure 12

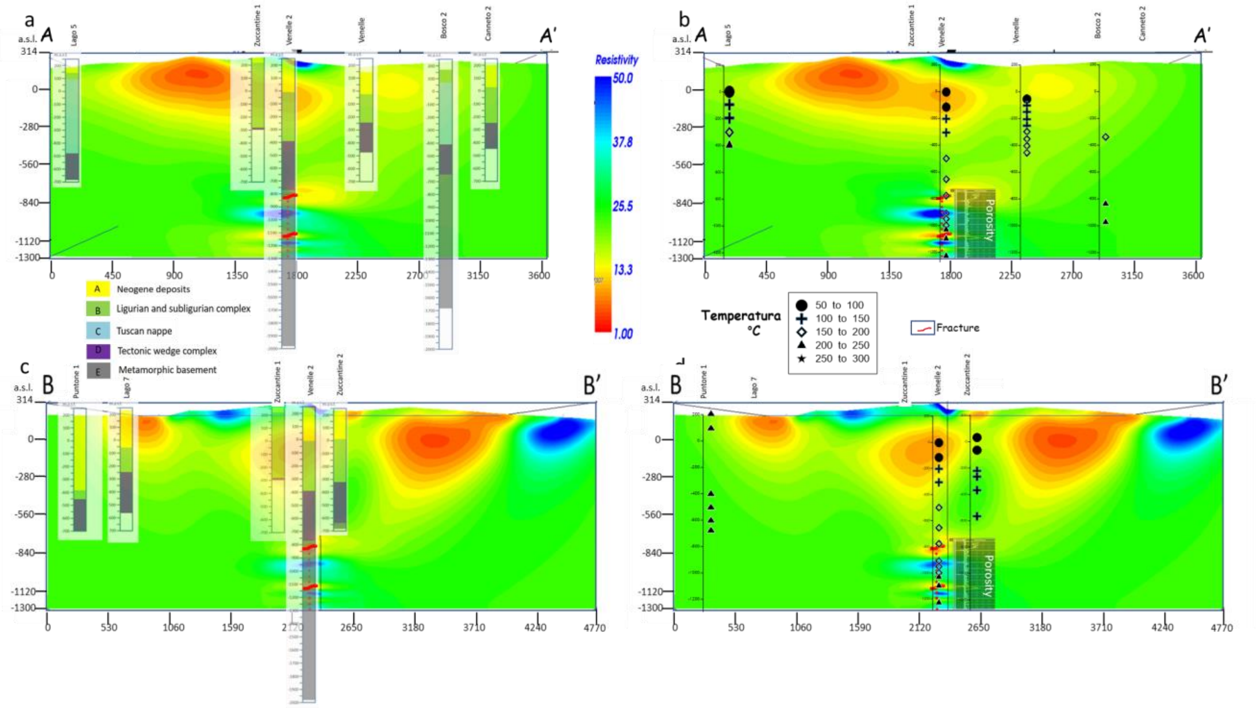
a
b
c
A
A′
B
B′
a.s.l.
Lago 5
Zuccantine 1
Venelle 2
Venelle
Bosco 2
Canneto 2
Puntone 1
Lago 7
Zuccantine 2
Resistivity
50.0
37.8
25.5
13.3
1.00
A Neogene deposits
B Ligurian and subligurian complex
C Tuscan nappe
D Tectonic wedge complex
E Metamorphic basement
Temperatura °C
50 to 100
100 to 150
150 to 200
200 to 250
250 to 300
Fracture
Porosity

Figure 13

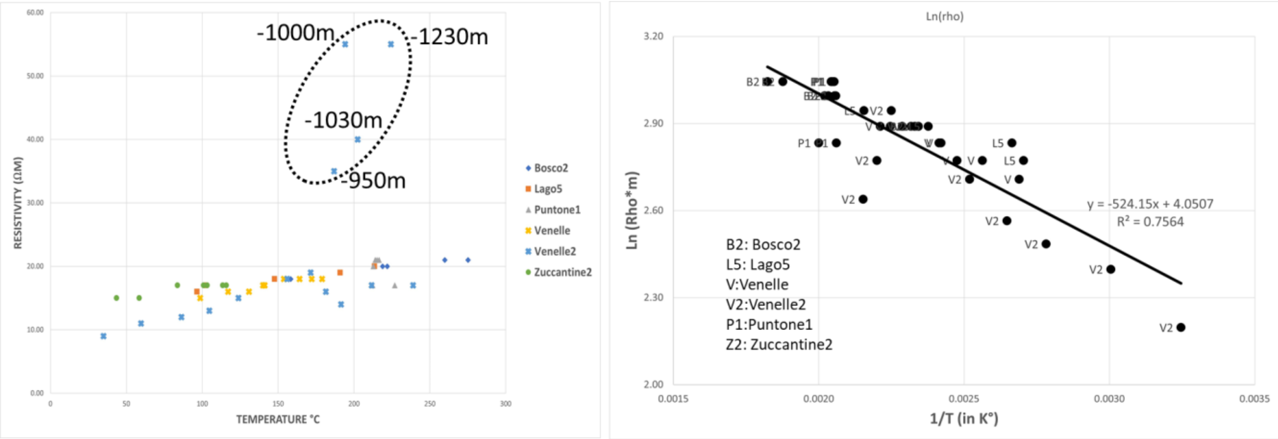

-1000m
-1230m
-1030m
-950m
RESISTIVITY (ΩM)
TEMPERATURE °C
Bosco2
Lago5
Puntone1
Venelle
Venelle2
Zuccantine2
Ln(rho)
Ln (Rho*m)
1/T (in K°)
y = -524.15x + 4.0507
R² = 0.7564
B2: Bosco2
L5: Lago5
V:Venelle
V2:Venelle2
P1:Puntone1
Z2: Zuccantine2

a b

Figure 14

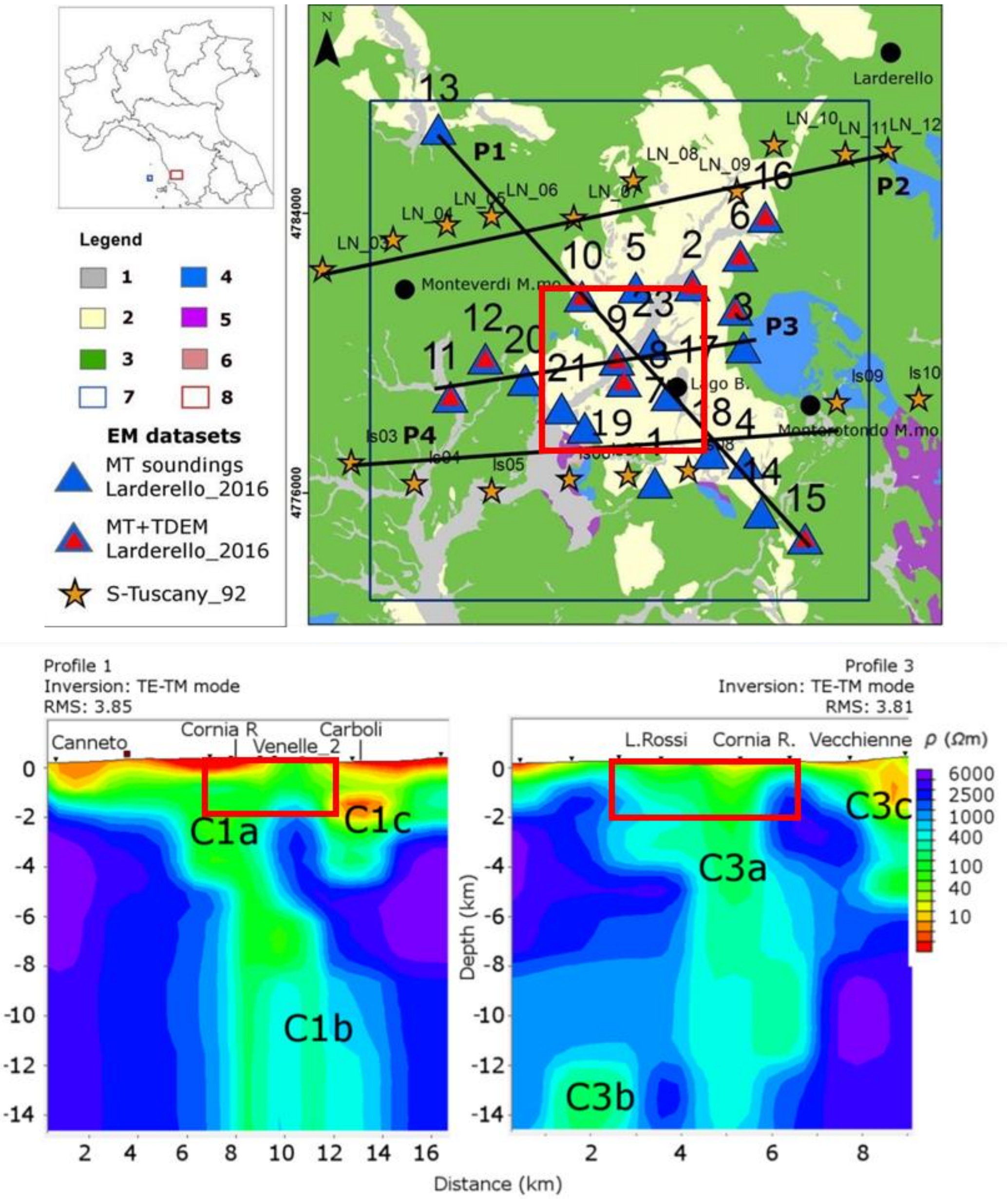
Legend
1
2
3
4
5
6
7
8
EM datasets
MT soundings Larderello_2016
MT+TDEM Larderello_2016
S-Tuscany_92
Larderello
Monteverdi M.mo
Monterotondo M.mo
Lago B.
P1
P2
P3
P4
4784000
4776000
Profile 1
Inversion: TE-TM mode
RMS: 3.85
Canneto
Cornia R
Venelle_2
Carboli
C1a
C1b
C1c
Profile 3
Inversion: TE-TM mode
RMS: 3.81
L.Rossi
Cornia R.
Vecchienne
C3a
C3b
C3c
ρ (Ωm)
Depth (km)
Distance (km)

Declaration of interests

☒ The authors declare that they have no known competing financial interests or personal relationships that could have appeared to influence the work reported in this paper.

☐The authors declare the following financial interests/personal relationships which may be considered as potential competing interests:

AUTHORSHIP STATEMENT

Manuscript title: 3D Deep Geoelectrical Exploration in the Larderello geothermal sites (Italy)

All persons who meet authorship criteria are listed as authors, and all authors certify that they have participated sufficiently in the work to take public responsibility for the content, including participation in the concept, design, analysis, writing, or revision of the manuscript. Furthermore, each author certifies that this material or similar material has not been and will not be submitted to or published in any other publication before its appearance in the *Hong Kong Journal of Occupational Therapy*.

Authorship contributions

Please indicate the specific contributions made by each author (list the authors' initials followed by their surnames, e.g., Y.L. Cheung). The name of each author must appear at least once in each of the three categories below.

Category 1

Conception and design of study: ER, ______, ______, ______;

acquisition of data: ER, LC VG, GDM GR, ______;

analysis and/or interpretation of data: ER, VG, LC, GR AS.

Category 2

Drafting the manuscript: ER, VG, LC, AS;

revising the manuscript critically for important intellectual content: ER VG, AS,

______, ______.

Category 3

Approval of the version of the manuscript to be published (the names of all authors must be listed):

Enzo Rizzo, Valeria Giampaolo, Luigi Capozzoli, Gregory De MArtino,

Gerardo Romano, Alessandro Santilano, Adele Manzella.

Acknowledgements

All persons who have made substantial contributions to the work reported in the manuscript (e.g., technical help, writing and editing assistance, general support), but who do not meet the criteria for authorship, are named in the Acknowledgements and have given us their written permission to be named. If we have not included an Acknowledgements, then that indicates that we have not received substantial contributions from non-authors.

This statement is signed by all the authors (*a photocopy of this form may be used if there are more than 10 authors***):**

Author's name (typed)	Author's signature	Date
Enzo Rizzo	[signature]	30/01/2022
Valeria Giampaolo		
Luigi Capozzoli		
Gregory De MArtino		
Gerardo Romano		
Alessandro Santilano		
Adele Manzella		